UNIVERSITY OF CAPE TOWN
IYUNIVESITHI YASEKAPA • UNIVERSITEIT VAN KAAPSTAD

BLAST IMPACT & SURVIVABILITY RESEARCH UNIT

BISRU

An experimental investigation of interspecies variation in mechanical properties of cortical bone

Lee-Anne Welgemoed

Supervisor:
Mr Trevor Cloete

This dissertation is presented to the University of Cape Town in partial fulfilment of the requirements for the degree of Master of Science in Mechanical Engineering

The financial assistance of the National Research Foundation (NRF) towards this research is hereby acknowledged. Opinions expressed and conclusions arrived at, are those of the author and are not necessarily to be attributed to the NRF.

Abstract

Cortical bone has been found to display properties that vary greatly, with most previous work focused on human or bovine bone. The main aim of this research was to investigate mechanical properties of cortical bone from various species of animal (ostrich, baboon, crocodile and sheep) to allow for comparison of mechanical properties across species, as well as investigate the relationship of material properties to strain rate within each species. This information is valuable for use in modelling. Testing was performed quasistatically and at the high end of the intermediate strain rate regime. These higher rate tests were performed on a modified Split Hopkinson bar setup. A Cone-in-Tube striker was used to provide a near constant strain rate during testing. The use of a momentum trapping system was investigated, but was not practically useful for the scale of specimens and strain rates investigated. It was found that properties of bone from all species displayed a clear dependence on strain rate. The relationship between the properties and strain rate were very similar across all species investigated, although the ultimate values differed. The apparent modulus showed a distinct increase when testing at a higher strain rate than when testing quasistatically. The compressive strength (both yield and ultimate) displayed an increase over the quasistatic range tested and then levelled out at the higher rate. There was greater difference seen in the values of apparent modulus than in the compressive strengths for all species tested. Baboon bone consistently displayed the greatest properties for both apparent modulus and compressive strength, and crocodile the weakest. It was also found that, despite whole bones and specimens being frozen at -32°C, with the specimens frozen in normal saline, a change in the material properties of the bone occurred over time. Apparent moduli decreased, and compressive strengths stayed constant or increased slightly. Less change was seen in the strength than in the apparent modulus.

Declaration

I hereby acknowledge that:

1. I know the meaning of plagiarism and declare that all the work in the document, save for that which is properly acknowledged, is my own.
2. This dissertation has been submitted to the Turnitin module and I confirm that my supervisor has seen my report and any concerns revealed by such have been resolved with my supervisor.

Lee-Anne Welgemoed

Signed by candidate

Acknowledgements

I would like to thank the following people, whose input was invaluable to the completion of this dissertation.

- Mr Trevor Cloete, for many hours of conversation, guidance and supervision.
- Mr Pierre Smith, for manufacturing of all machine parts required.
- Mr Charles Harris, for giving generously of his time to perform the manufacturing of all specimens used.
- The staff and students of BISRU, for their support and advice.
- Mr Clive Welgemoed, for his assistance, and for providing the large amounts of coffee that facilitated the completion of this dissertation.
- Mrs Danaé Welgemoed, for her unending support, encouragement, motivation and advice.
- Mr Keryn Seyffert, for his encouragement, and for proofreading this dissertation on rather short notice.

Contents

Abstract i

Declaration ii

Acknowledgements iii

List of Figures ix

List of Tables xvi

Nomenclature xvii

1 Introduction 1

1.1 Plan of development 3

2 Literature Review 5

2.1 Hierarchical structure of bone 5

2.1.1 Bone physiology 6

2.1.2 Bone structures in different species 10
2.2 Intrinsic factors affecting response to stress 16
2.2.1 Age 16
2.2.2 Sex 18
2.2.3 Mineral content 19
2.2.4 Location and anisotropy 20
2.2.5 Porosity & Density 23
2.3 Storage conditions 25
2.4 Testing conditions 26
2.5 Effect of bone structure on response 28
2.6 Strain rate dependence 30
2.7 Species specific responses 36
2.7.1 Baboon 36
2.7.2 Crocodile 38
2.7.3 Sheep 38
2.7.4 Ostrich 39
2.8 Equipment and testing methods 40
2.8.1 Cone-in-tube striker 40
2.8.2 Momentum trapping 43
2.9 Theory used in data processing and analysis 46

2.9.1 Wave theory 46

2.9.2 Lognormal analysis 49

3 Methodology **50**

3.1 Specimen preparation 50

3.1.1 First machining series 51

3.1.2 Second machining series 54

3.2 Quasistatic testing 56

3.2.1 Test rig setup 56

3.2.2 Testing procedure for the first series of quasistatic tests . . . 57

3.2.3 Testing procedure for the second series of quasistatic tests . 60

3.2.4 Quasistatic processing 61

3.3 High intermediate strain rate testing 68

3.3.1 The design of the specialized equipment 68

3.3.1.1 The design of the Cone-in-Tube striker 68

3.3.1.2 The design of the momentum trapping system . . . 71

3.3.2 Assembly and alignment of the full SHB system 75

3.3.3 Calibration factor calculation 77

3.3.4 Performance of high strain rate tests 80

3.3.5 Higher strain rate processing 82

3.4 Lognormal analysis of each data set 87

4 Results **89**

5 Discussion **115**

5.1 A comparison of the first and second series of data 115

5.1.1 A comparison of the apparent moduli from the first and second quasistatic data series 116

5.1.2 A comparison of the compressive strength from the first and second quasistatic data series 117

5.2 The assessment of the apparent moduli across all species tested . . 118

5.2.1 The interspecies relationships displayed in the first series of data 119

5.2.2 A comparison with the data found in literature 120

5.2.3 The interspecies relationships displayed in the second series of data 125

5.3 The assessment of the compressive strength across all species tested 128

5.3.1 The interspecies relationships displayed in the first series of data 128

5.3.2 A comparison with the data found in literature 129

5.3.3 The interspecies relationships displayed in the second series of data 134

6 Conclusions & Recommendations **137**

6.1 Conclusions 137

6.2 Recommendations 140

Bibliography **141**

Appendix A All measured data **151**

Appendix B Demonstration of the validity of the use of a lognormal distribution for small sample sizes **156**

List of Figures

2.1 The anatomy of a long bone [1]. 6

2.2 A figure depicting (A) lamellar bone and (B) woven bone [2]. 7

2.3 A figure depicting fibrolamellar or plexiform bone [3]. 8

2.4 A figure depicting Haversian bone [4]. 8

2.5 An image of sheep bone at x100 magnification from Brits et al. [5]. 11

2.6 An image of non-human primate bone at x100 magnification from Brits et al. [5]. 12

2.7 An example of lamellar zonal bone tissue seen in crocodylians [6]. . 13

2.8 An example of fibrolamellar bone seen in crocodylians [6]. 13

2.9 An image of ostrich bone showing clear fibrolamellar layers [7]. . . . 14

2.10 A depiction of how transverse and longitudinal specimens relate to a portion of a long bone shaft [8]. 20

2.11 An example of the descriptive terms used when discussing bone position, shown on a full skeleton [9]. 21

2.12 A comparison of cortical bone data from multiple studies over a range of strain rates from Johnson et al. [10]. 33

2.13 The square shaped pulse from a standard uniform striker and the decreasing strain rate seen over a test from Cloete et al. [11]. 41

2.14 The increasing pulse from a conical striker, with tail highlighted, with the more constant strain rate seen over the test from Cloete et al. [11]. 42

2.15 A schematic of a CiT striker in a practical setup as designed by Paul [12]. 43

2.16 A pulse with a "tail" generated by a conical striker and a pulse generated by a CiT striker with no "tail", from Paul [12]. 43

2.17 The original design for nested momentum traps by Prot and Cloete [13]. 44

2.18 A schematic of how a wave propagates through a tandem momentum trap as depicted by Prot and Cloete [13]. 45

3.1 A section of sheep bone cut from the mid-diaphysis, and a small portion cut from the end of the diaphysis. 53

3.2 A strip of bone removed from a mid-diaphysis section, before shaping. 53

3.3 A smooth cylinder of machined bone in the lathe, with the specimen almost cut free. 53

3.4 Photographs of the positional markings made on a baboon bone. . . 55

3.5 A photograph of the quasistatic test rig setup. 57

3.6 An example of the standard output of the compliance tests performed in a single day. 58

3.7 An example of the photographs taken of the first series of quasistatic specimens. 60

3.8 The full progression of refinements made to the quasistatic data. . . 63

3.9 A graph showing the general method used to obtain the 0.2% offset stress. 65

3.10 A graph showing a case in which the 0.2% offset stress is after the failure region. 66

3.11 A graph showing a case in which the maximum strength is not apparent, with the 1% offset strength marked. 67

3.12 An example of a cone used in a CiT striker. 69

3.13 An assembled CiT striker with a shortened steel tube and an aluminium cone. 70

3.14 The inner support in a CiT striker keeping the cone centred. 71

3.15 The momentum trap collars showing the inner connections. 72

3.16 The momentum trap collars showing the outer connections. 73

3.17 The full system of nested momentum traps. 74

3.18 The pulse generated by the incident bar calibration test. 78

3.19 The pulses generated by the transmitter bar calibration test. 79

3.20 The pulse generated for the final calibration test to determine voltage-to-stress coefficient. 80

3.21 An example of the stress data output from the SHB tests. 83

3.22 An example of the stress and strain rate versus strain data within a specimen. 86

4.1 A selection of curves showing an example of the shapes of the stress versus strain curves at each strain rate tested for baboon bone. . . . 90

4.2 A selection of curves showing an example of the shapes of the stress versus strain curves at each strain rate tested for crocodile bone. . . 91

4.3 A selection of curves showing an example of the shapes of the stress versus strain curves at each strain rate tested for sheep bone. 92

4.4 A selection of curves showing an example of the shapes of the stress versus strain curves at each strain rate tested for ostrich bone. . . . 93

4.5 A histogram of the apparent modulus data measured for crocodile bone in the high intermediate strain rate regime with a normal and lognormal distribution superimposed. 94

4.6 The apparent modulus data enclosures and data points for cortical baboon bone. 96

4.7 The apparent modulus data enclosures and data points for cortical crocodile bone. 97

4.8 The apparent modulus data enclosures and data points for cortical sheep bone. 98

4.9 The apparent modulus data enclosures and data points for cortical ostrich bone. 99

4.10 The 0.2% offset compressive yield strength data enclosures and data points for cortical baboon bone. 100

4.11 The 0.2% offset compressive yield strength data enclosures and data points for cortical crocodile bone. 101

4.12 The 0.2% offset compressive yield strength data enclosures and data points for cortical sheep bone. 102

4.13 The 0.2% offset compressive yield strength data enclosures and data points for cortical ostrich bone. 103

4.14 The maximum compressive strength data enclosures and data points for cortical baboon bone. 104

4.15 The maximum compressive strength data enclosures and data points for cortical crocodile bone. 105

4.16 The maximum compressive strength data enclosures and data points for cortical sheep bone. 106

4.17 The maximum compressive strength data enclosures and data points for cortical ostrich bone. 107

4.18 The apparent moduli across all species from the first series of quasistatic testing. 108

4.19 The 0.2% offset compressive yield strengths across all species from the first series of quasistatic testing. 109

4.20 The maximum compressive strengths across all species from the first series of quasistatic testing. 110

4.21 The apparent moduli across all species, for both the second series of quasistatic and the high intermediate strain rate tests. 111

4.22 The 0.2% offset compressive yield strengths across all species, for both the second series of quasistatic and the high intermediate strain rate tests. 112

4.23 The maximum compressive strengths across all species, for both the second series of quasistatic and the high intermediate strain rate tests. 113

5.1 A comparison of the apparent modulus data in the literature and the first and second series of data for baboon bone. 121

5.2 A comparison of the apparent modulus data in the literature and the first and second series of data for crocodile bone. 122

5.3 A comparison of the apparent modulus data in the literature and the first and second series of data for sheep bone. 123

5.4 A comparison of the apparent modulus data in the literature and the first and second series of data for ostrich bone. 124

5.5 A comparison of the maximum compressive strength data in the literature and the maximum compressive strengths from the first and second series of tests for baboon bone. 130

5.6 A comparison of the compressive yield strength data in the literature and the 0.2% offset yield strengths from the first and second series of tests for crocodile bone. 131

5.7 A comparison of the maximum compressive strength data in the literature and the maximum compressive strengths from the first and second series of tests for sheep bone. 132

5.8 A comparison of the maximum compressive strength data in the literature and the maximum compressive strengths from the first and second series of tests for ostrich bone. 133

A.1 The baboon bone data pertaining to the first series of tests. 152

A.2 The crocodile bone data pertaining to the first series of tests. 152

A.3 The sheep bone data pertaining to the first series of tests. 153

A.4 The ostrich bone data pertaining to the first series of tests. 153

A.5 The baboon bone data pertaining to the second series of tests. . . . 154

A.6 The crocodile bone data pertaining to the second series of tests. . . 154

A.7 The sheep bone data pertaining to the second series of tests. 155

A.8 The ostrich bone data pertaining to the second series of tests. . . . 155

B.1 A graph displaying the full set of randomly generated data, separated into bins, with a normal and lognormal distribution plotted on top of the data. 157

B.2 A graph displaying the first 20 data points from the randomly generated set, separated into bins, with a normal and lognormal distribution plotted on top of the data. 158

B.3 A graph displaying the first 5 data points from the randomly generated set, separated into bins, with a normal and lognormal distribution plotted on top of the data. 158

B.4 A graph displaying the first 3 data points from the randomly generated set, separated into bins, with a normal and lognormal distribution plotted on top of the data. 159

List of Tables

2.1 The microstructures reported for relevant species, along with the assessment methods used and criteria assessed for. 15

2.2 The relationship between strain rate and mechanical properties from various studies. 35

2.3 The mechanical properties in literature for various species. 37

3.1 The dimensions used for each cone to accommodate the range of estimated apparent moduli. 70

3.2 The dimensions used for the momentum trap and incident bar setup. 73

3.3 The specifications of the strain gauge and data capture system. . . 77

4.1 Mode of apparent modulus and compressive strengths in each species, at each tested strain rate. 114

Nomenclature

SHB	Split Hopkinson bar
CiT	Cone-in-Tube
BISRU	Blast Impact and Survivability Research Unit
CME	Centre for Materials Engineering
UCT	University of Cape Town
σ	stress
v	velocity
ρ	density
A	area
c	speed of sound of a material
l	instantaneous length
r	reflected
in	incident bar
t	transmitter bar
s	striker
if	at specimen face of incident bar
$diff$	difference across the specimen
$spec$	specimen
$\dot{\epsilon}$	strain rate
ϵ	strain
Δt	time increment at which the data was sampled
X	original data set
Y	lognormally transformed data set
γ	threshold parameter
μ	mean of the lognormally transformed data set
θ^2	variance of the lognormally transformed data set

Chapter 1

Introduction

An extensive body of research exists on the mechanical properties of bone [14–19], with investigations into a wide variety of aspects such as the effects of microstructure on response [20, 21], and the effect of different storage methods on mechanical properties [22–24]. However, the large majority of this research was performed on bovine or human bone, with very little information being available on the responses of other species. What little information is available is either a quasistatically measured property [25, 26], or was tested using a method that does not correlate directly to a strain rate (such as ultrasonic testing) [27–29].

Furthermore, it has been found that the strain rate at which the mechanical properties of bone are tested has a significant effect on the observed response. While it has been shown that strain rate does have an effect on bone properties [8, 17, 30], it was not until work by Adharapurapu et al. [31] that clear effort was made to perform testing at near constant strain rates. This was followed by work by van der Westhuizen [32], who found that ultimate properties were affected by strain rate history during testing, and work by Paul [12] and Cloete et al. [33], who focused specifically on the intermediate strain rate regime, which is an area with very little available information. Again, these studies focused on bovine bone.

To the author's knowledge, there have been no studies that compare the properties of bone across more than two species over a range of strain rates, while keeping variables such as testing methods and strain rate during each test constant. The research to be presented aims to fill this knowledge gap, focusing on consistency in test performance across all species while utilising a near constant strain rate during testing. One of the motivations for this work was to investigate the reason for the wide range of bone properties in the literature. In particular, it is unclear whether the variation is inherent or a result of a variation in testing protocols and specimen storage methods. Hence samples were chosen from four distinct orders of animal in an attempt to maximise the possible variation. These animals have a widely differing developmental histories and modes of ambulation. If there is variation in bone properties across species, it should be seen here, when directly comparing the widest available range of options. If there is not a huge difference seen across the properties of these bones, it would suggest that it may be possible to generate a universal model of bone response.

The goals for this research are:

- To compare the properties of cortical femoral bone across the widest variety of species practically available, while minimising other variables that affect bone response. A wide variety of species was sought so as to allow investigation into differences seen in bone response across different orders of animal, all of which experience different living conditions and different daily stresses applied to the femur.
- To perform all tests with a focus on keeping strain rate near constant, including tests in the intermediate strain rate regime.
- To investigate trends in material response at quasistatic and intermediate strain rates in each species tested.
- To investigate relationships between material responses across different species at quasistatic and intermediate strain rates.

1.1 Plan of development

This dissertation will be structured as follows:

1. Literature review
   The literature review begins with a description of bone and its microstructure, which provides a background on the complexity of bone as a material and the multiple ways in which the microstructure can form. This is followed by information on a variety of factors, both intrinsic and external, that can affect the material response of bone. These factors were important considerations when choosing samples, storage and testing methods. It also includes a review of the available information on the response of multi-species bone relevant to the species tested. This provided information with which to compare the final results obtained in this research. A review was then done on the relevant specialised equipment that could be used to perform constant strain rate testing on bone specimens. This provided a basis for the design of the equipment used in the presented research. Finally, a review of the theory needed to process and analyse the measured data was presented.

2. Methodology
   The methodology begins with a record of how the specimens were prepared, making clear the directionality of the specimens. A description was then given of which equipment was used, how it was set up, as well as how the testing was performed. In the case of the higher rate testing, a description of the equipment design and calibration process was also included. This was followed by a description of how the data was processed to give the necessary final outputs, which makes clear how the results were interpreted to allow for easy understanding. These descriptions were split into quasistatic and high intermediate strain rate subsections for ease of reference. Lastly, a description of how each set of data was analysed was provided, to make clear where the reported results came from. The entire section clarifies exactly how the specimens were prepared, and how the testing and analysis was performed, and includes enough detail to allow repetition of the experiments.

3. Results

   This section presents the results obtained for both series of quasistatic testing and the high intermediate rate testing. Graphs showing the comparison of the first and second series of quasistatic tests with the individual data points overlaid are presented to illustrate the differences between the two series. This is followed by graphs displaying the multi-species comparison, for both series of testing. These graphs illustrate the relationships between the species responses, as well as the changes in response when moving from the quasistatic to higher strain rate regimes. Finally, a table of all the results is presented to allow for ease of comparison with other data, both current and future.

4. Discussion

   The discussion section contains the analysis of the results presented in the previous section. Here, comparisons are made and important features of the data noted. Firstly, a comparison of the first and second series of quasistatic data is presented to examine ageing effects in the specimens. This was then followed by an in-depth assessment of the relationships seen between the species responses for both the first and second series of tests, as assessment of changes in response seen across different strain rates, and a comparison of the measured properties with the available literature values. This assessment was split into two sections, one for the apparent moduli and another for the compressive strengths, to allow for ease of reference.

5. Conclusions and recommendations

   Finally, the important conclusions from this research were summarised, and recommendations for future research were made.

Chapter 2

Literature Review

Reviewed here is the literature relevant to the research to be presented. This includes sections on the hierarchy of bone, the intrinsic factors that affect stress response, as well as the effects of storage and testing conditions, bone structure, and the strain rate tested at on bone response. This is followed by a review of the limited information available on the bone properties of the variety of species investigated, and ends with a review of the specialised equipment needed to test multi-species bone.

2.1 Hierarchical structure of bone

Bone is a highly complex material. Presented here is some basic information on the hierarchical structure of bone, as well as information on how the structure of bone may differ across different species.

2.1.1 Bone physiology

In the human skeleton there are multiple categories of bone, namely short, long, irregular or flat bones [34]. For the presented research, only long bones are considered. Long bones can be defined as bones appearing to be long in shape, with a long hollow shaft of bone (the diaphysis) in the center with rounded ends (the epiphyses) on either side, such as femurs or humeri [34]. The basic anatomy of a long bone is illustrated in Figure 2.1, which shows a typical human femur.

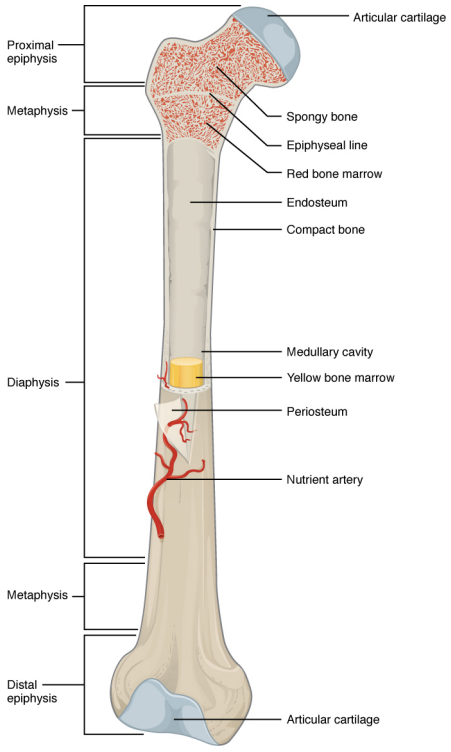

Figure 2.1: The anatomy of a long bone [1].

When observing a long bone in section, two distinct types of bone can be seen. These are cortical bone (also known as compact bone) and cancellous bone (also known as spongy bone). It is also important to keep in mind that the term "bone" can be somewhat ambiguous, as it can refer to both the overall structure (whole bones) and the material (different types of bone such as cancellous or cortical).

Cortical bone, (referred to as compact bone in Figure 2.1), is a densely packed form of bone tissue found primarily in the diaphysis of long bones, where it forms the majority of the bone. It is also found in thin layers on the outsides of the epiphyses of the long bones [34]. If less than 50% of the bone volume is porous space, it is classified as cortical bone [35]. Conversely, if more than 50% of the bone volume is porous space, it is classified as cancellous. Cancellous bone, (referred to as spongy bone in Figure 2.1), is formed from numerous small struts of bone tissue, known as trabeculae. In long bones it can be found mostly in the body of the epiphyses, forming a honeycomb like structure and often with these inter-trabecular spaces being filled with marrow [34].

Cortical bone tissue consists of two main components, namely collagen fibres and hydroxyapatite crystals [36]. At the microstructural scale, there is more than one way in which these components can be arranged. These differences in microstructure are categorized through four broad descriptions. These are woven, lamellar, fibrolamellar (also known as plexiform), and osteonal (also referred to as Haversian). These can be seen in Figures 2.2 through 2.4.

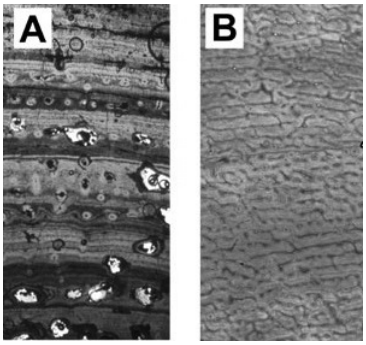

Figure 2.2: A figure depicting (A) lamellar bone and (B) woven bone [2].

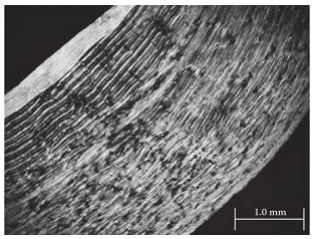

Figure 2.3: A figure depicting fibrolamellar or plexiform bone [3].

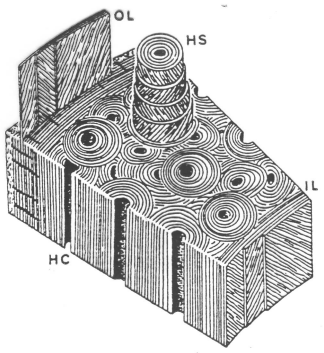

Figure 2.4: A figure depicting Haversian bone [4].

Furthermore, as bone grows, the microstructure will change and adapt. As bone is stressed, microdamage occurs and stimulates remodelling of the bone. Remodelling of bone is the process wherein bone tissue is removed and replaced [37]. Bone remodelling is the main cause of change in bone mass in mature skeletal structures [20]. This affects both the microstructure of the bone and the material content of the bone, both of which have a profound effect on the strength of the bone [20]. It has been suggested that either too much, or too little remodelling of bone can lead to bones more prone to fracture [38]. High levels of remodelling, such as occurs during menopause, increases the porosity of cortical bone [20]. Conversely, if the level of remodelling is too low, there will be a marked increase in the number of microcracks present in the bone [20]. A delicate natural cycle of damage and remodelling is necessary for healthy bones to be optimally fracture resistant [38]. The differences

are clear when comparing newly formed bone found at the outer surface (near the periosteum) with well established bone found closer to the inside of the bone [39].

Woven bone forms very rapidly (such as is found in juveniles with their corresponding high rates of growth) [35], with collagen fibres showing a variety of orientations, having a rather undefined and random structure [21]. It is greatly disorganised, and this widely varying structure results in an isotropic bone response [35]. The bone is not tightly packed, leaving it with a loose structure [21]. Woven bone forms faster, but is weaker than lamellar bone due to the randomness of its orientation [21]. However, the speed at which woven bone can be formed means that it is often found in bones that require rapid growth, such as during growth spurts in young individuals.

Lamellar bone is laid down at a slower rate [21], and is essentially defined as bone created by layers of aligned collagen fibrils (also known as lamellae) laid down on top of one another. These layers may be in different directions to one another, but each layer has its fibres aligned in a particular, distinct, direction [39]. In each of these sublayers of bone, the hydroxyapatite crystals will also be aligned with one another. However, the directionality of the crystals will change from layer to layer [39]. Overall, this gives lamellar bone a "plywood-like" appearance [39].

Fibrolamellar, or plexiform bone, is a combination of woven and lamellar bone that occurs when bone is required to form rapidly. An initial framework of woven bone is rapidly laid down, then replaced with lamellar bone at a more reasonable pace [21]. This type of microstructure also includes the possibility of primary osteons, in a variety of orientations, forming within the woven bone framework [35].

Osteons, formed from circumferential layers of bone, may be either primary or secondary. Primary osteons fill spaces formed when rapid growth of the bone occurs, and are very elongated [39]. Secondary osteons form during remodelling of pre-existing bone, are often cylindrical, and are commonly referred to as Haversian systems [39]. These Haversian systems form through previously formed bone tissue, and have a clear border around the outer edge, known as the cement line [35].

It has been found that an increase in the amount of secondary osteons present causes a decrease in the ultimate compressive strength of the bone [40], the ultimate tensile strength of the bone [17], as well as a decrease in the apparent modulus [17, 40]. Haversian bone displays somewhat transversely isotropic behaviour, due to the symmetry found in the structure of the Haversian systems [41].

2.1.2 Bone structures in different species

Different species have cortical bone with distinctly different microstructures [5,42,43]. The microstructures discussed for various species are summarised in Table 2.1 at the end of this section for convenience. Brits et al. [5] looked at the arrangement of primary vascular canals, as well as primary and secondary osteons, to qualitatively differentiate bone taken from different species. Vascular canals are small open channels in bone through which blood vessels run, and are found both as stand-alone features, and in the centre of primary and secondary osteons. They examined various different species, but of most interest were their findings on sheep, non-human primate and human bone. The sheep bone consisted of primarily vascular longitudinal bone, while still containing osteon bands formed from primary osteons closer to the center of the bone (see Figure 2.5). The non-human primate bone displayed a combination of irregular Haversian bone and avascular bone, as can be seen in Figure 2.6. Avascular bone is bone which contains very few or no vascular canals.

The human bone they studied was split into juvenile and adult. The adult human bone showed a combination of Haversian bone (both dense and irregular) and primary vascular longitudinal bone. The density of the osteons present ranged from scattered to tightly packed. In contrast, the juvenile human bone showed mostly irregular Haversian bone, with scattered secondary osteons and large Haversian canals. This suggests that age of the individual from whence the bone specimens came may have a noticeable effect on the microstructure present.

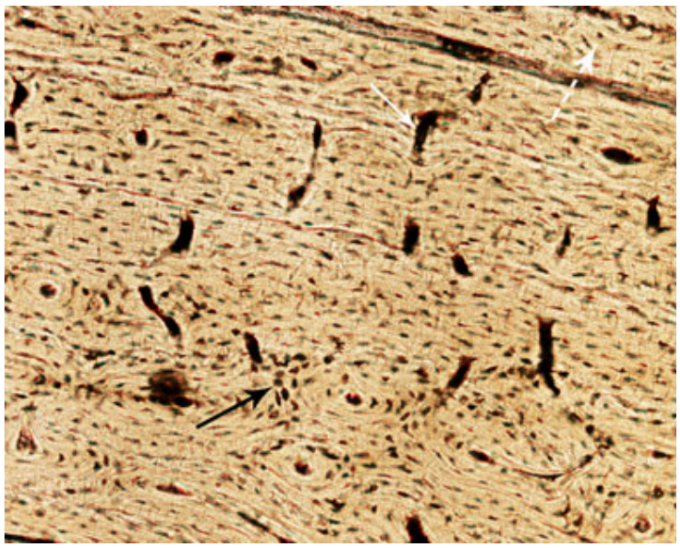

Figure 2.5: An image of sheep bone at x100 magnification from Brits et al. [5]. The black arrow indicates a primary osteon band, the white arrow indicates a vascular canal, and the dotted white arrow points in the direction of outer surface of the bone.

Spatz et al. [25] found that cortical bone from the femur, tibia, and metatarsus of a sheep is mostly fibrolamellar (referred to as laminar, not to be confused with lamellar), with at most a small amount of Haversian bone present, which is in agreement with the findings of Brits et al. [5].

Martiniaková et al. [42] also studied the microstructure of sheep bone, and found mainly primary vascular fibrolamellar bone with few scattered secondary osteons, which is similar to the findings of Brits et al. [5].

Baboons have been found to experience bone remodelling, and hence we can expect to see some Haversian systems in mature baboon bone [44], which is also in agreement with the findings of Brits et al. [5].

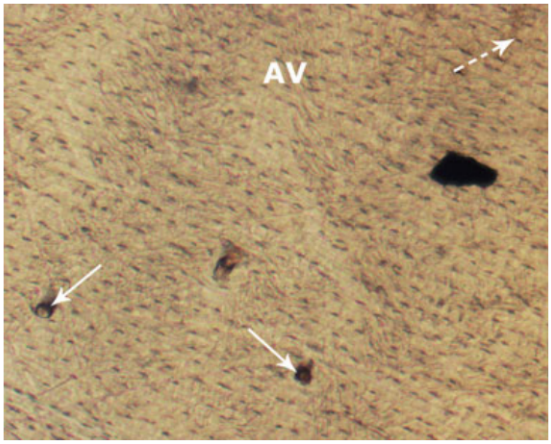

Figure 2.6: An image of non-human primate bone at x100 magnification from Brits et al. [5]. The bone is primarily avascular, with vascular canals indicated by white arrows, and the direction of the outer surface of the bone indicated with the dotted white arrow.

The microstructure found in crocodylians can be split into two main categories. One commonly observed histology is lamellar bone interspersed with longitudinal vascularisation, organized into zones within the bone (known as lamellar zonal bone, seen in Figure 2.7) [6]. The other common histology observed is fibrolamellar bone (seen in Figure 2.8) [6]. It is commonly found in captive crocodylians, and is the most likely configuration to be seen in the specimens collected for the research to be presented.

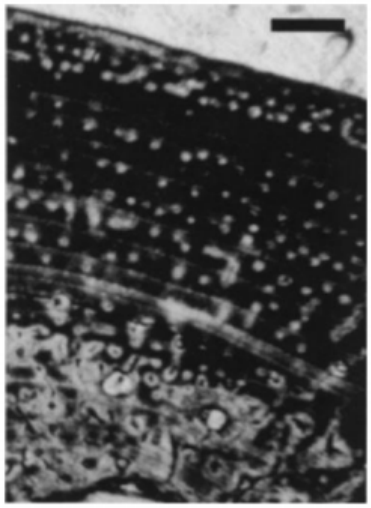

Figure 2.7: An example of lamellar zonal bone tissue seen in crocodylians, with 919 μm scale bar [6].

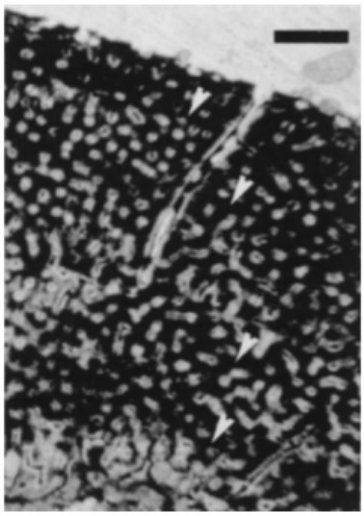

Figure 2.8: An example of fibrolamellar bone seen in crocodylians, with white arrows marking boundaries between areas of fibrolamellar bone (Scale bar 919 μm) [6].

There are conflicting reports on the microstructural organisation of ostrich bone. Spatz et al. [25] found ostrich cortical bone to be mostly fibrolamellar, having little Haversian bone present, which is in agreement with the description given by Castanet et al. [7]. However, Currey [21] reports that there is often extensive Haversian bone present in ostriches. This difference may be due in part to the fact that Spatz et al. [25] were basing their observations solely on the leg bones of the ostrich, and Castanet et al. [7] were basing their observations on long bones from the hind limb, whereas it is unclear where in the skeleton of the ostrich Currey's [21] specimens were taken from. An image of ostrich bone taken from Castanet et al. [7] can be be seen in Figure 2.9.

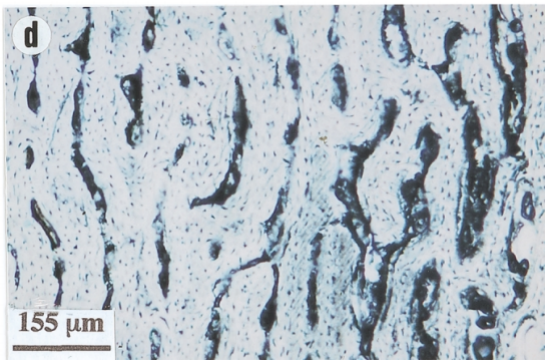

Figure 2.9: An image of ostrich bone showing clear fibrolamellar layers [7].

Furthermore, within a single species, the way in which the femur bears load will affect the specific microstructures present [8]. As each species will stand and move in a different way, it makes sense that the load, and hence the microstructure, will vary across species.

Table 2.1: The microstructures reported for relevant species, along with the assessment methods used and criteria assessed for.

Species	Source	Bones examined	Microstructure	Assessment method	Features assessed for
Sheep	[5]	Femur	Primary vascular longitudinal bone	Sectioned and observed under microscope	Elongated primary. osteons, in osteon bands, as well as short radial canals
Non-human primate	[5]	Femur	Avascular bone sometimes combined with irregular secondary osteons	Sectioned and observed under microscope	Few longitudinal canals as well as bands of secondary osteons with large Haversian canals.
Sheep	[25]	Hind leg metatarsus	Predominately fibrolamellar bone with a few secondary osteons present	Scanning electron microscopy provided images	Secondary osteons were counted and porosities grouped and assessed.
Sheep	[42]	Femur	Primary vascular plexiform bone with few irregular scattered secondary osteons	Sectioned and observed under microscope as well as quantitatively assessed with software	Presence and dimensions of Haversian canals, primary osteons and secondary osteons.
Baboon	[44]	Femur	Showing remodelling and the presence of Haversian systems	Fourier transform infrared microspectroscopy and imaging	Variations in osteons.
Alligator	[6]	Long bones	Lamellar zonal bone or fibrolamellar bone (separate cases)	Sectioned and observed under microscope	Either the presence of lamellae and their relation to present vascular canals or boundaries between zones of fibrolamellar bone respectively.
Ostrich	[25]	Leg metatarsus	Fibrolamellar with few secondary osteons	Scanning electron microscopy provided images	Secondary osteons were counted and porosities grouped and assessed.
Ostrich	[7]	Long bones	Fibrolamellar	Sectioned and observed under microscope	Observation of layering in bone in conjunction with vascular canals and some primary osteons.
Ostrich	[21]	Unknown	Presence of extensive Haversian systems	Unknown	Unknown

2.2 Intrinsic factors affecting response to stress

The factors that determine bone strength are highly interrelated, and so are difficult to assess individually [20]. Discussed presently are intrinsic properties that affect bone response. These are the effects of age and sex of the specimen donor, the porosity and mineral content of the specimens, and the anisotropy inherent in bone. The microstructure also plays a critical role, but is discussed in depth in Section 2.5.

2.2.1 Age

It has been widely demonstrated that the age at death of the individual from which a bone specimen is taken has an effect on the mechanical properties [45–48]. In the literature reviewed, no discussion was seen as to the effect of post-mortem age, that is, the effect of the time between slaughter and testing of bone.

The effects of age are enmeshed with the effects of remodelling and microstructure on bone response, as as an individual ages, more remodelling will occur, and the underlying microstructure may change [43]. As one would expect, as an individual ages, the compressive strength of their bone decreases [46]. However, Martin and Atkinson [47] found that there is actually an initial increase in the material strength of bone up to the age of about 30, at which point the strength begins to decrease again. This makes sense, as bone does not initially form as secondary osteons, but as primary bone, which becomes secondary bone through remodelling as the individual ages. This remodelling will gradually increase the porosity in the bone and number of cement lines present, but this process takes time, as is demonstrated in this rise and fall of material strength.

Augat and Schorlemmer [45] state that with every remodelling of the tissue, the overall porosity of the cortical bone increases, due to the fact that not all of the

previously removed material is fully replaced. This change results in bone that is more porous [45]. In addition to this, as an individual ages, there is more time for microdamage to occur and accumulate, due to repeated loading of the bone, which weakens the bone [45, 49]. This is supported by a study done by Hui et al. [14], who found an increase in fracture occurrence in bones from older individuals. However, it should be noted that this particular study [14] combines information on fractures in the shafts of long bones with fractures in areas such as the head of the femur. This presents information on a combination of cortical and cancellous bone, with no clear way to separate out the response of the cortical bone specifically.

Looking specifically at the mineral content, Ebbesen et al. [46] found that bone mineral density decreases with age, however, their study focused on cancellous bone. In contrast, Currey et al. [48] found that mineral content increases with age. However, they did find that toughness decreases with age, which concurs with the other studies mentioned. One possible cause for this difference in conclusion is the way each researcher assessed mineral content. Ebbesen et al. [46] investigated ash weight and ash density from specimens in which the original volume of each specimen was measured from unprocessed cancellous bone. This means that there would be relatively large spaces present in the samples where the marrow had been. This gives a value of apparent ash density, as a direct measure of the volume of the bone tissue only is difficult to acquire in cancellous bone samples. Currey et al. [48] expressed ash content as the percentage of a dried, defatted sample remaining as ash after the ashing procedure, and all samples were purely cortical. This does not include the porous volume, as is done in the cancellous testing.

It has also been found that the static elastic modulus of cortical bone in children does not differ in a statistically significant way from the static elastic modulus in the elderly [50]. This supports the theory that as an individual ages, their cortical bone develops up to some optimum value, and decreases with further age [50].

2.2.2 Sex

It has been found that females have a bone mineral content (in g) lower than a male of the same age, as well as having a lower mean bone mineral density (g/cm^2) [46].

However, using a variety of measurement methods, it was found that females tend to have a slightly higher bone density in their earlier years, with a faster loss in density than in males, and hence ending up being lower than the bone density of males in later years [46]. The difference in density between sexes is small enough though, as to be considered mostly insignificant [46]. This is supported by a study by Martin and Atkinson [47] which also found that there was no significant difference between the density of bone specimens taken from human males and females.

It was found that specimens from females showed a significantly lower maximum compressive load, due to the difference in overall size of the bone tested, but no significant difference in maximum compressive stress [46].

Also, when investigated by Wu et al. [15], it was found that there were no significant differences in the apparent modulus of bone due to the sex of the specimen donor.

When observing the cross-section of the shaft of a human femur, it has been found that in females the moment of inertia increases until the age of 35, when it sharply drops off [47]. In males it increases throughout life, although the rate at which it increases will slow [47]. This suggests why specimens taken from older females show weaker material strengths, as this decreasing moment of inertia couples with any other factors that would reduce the maximum load the bone is able to carry. In males, the ever increasing moment of inertia helps to counteract the other mechanisms of material weakening [47]. This is coupled with the thinning of the cortical layer of bone in females, while the cortical thickness remains fairly constant in males [47].

This then suggests that while there may be a difference in the frequency of fractures in older human males and females, this may be due to overall physical factors, and

is not due to inherent differences in the bone properties. When looking specifically at the properties of bone, sex is not important.

Crenshaw et al. [51] conducted a study on the effects of sex in swine bone, and found similar differences. They found that there was no difference in withstandable force between the sexes. Much like the study by Martin and Atkinson [47], there was a difference found in the moment of inertia found in males versus females, which is only of concern when testing whole bones and not small bone specimens. This was offset by a slight difference in the mineralisation of the bones, with males having less mineralised bone than females. As is discussed in Section 2.2.3, the degree of mineralisation of bone has a significant effect on the mechanical properties of bone. While there may be a link between mineralisation and sex, it does not appear to be consistent between swine and humans.

2.2.3 Mineral content

Bone mineral content is a measure of the amount of bone tissue that is made up of minerals, mostly calcium and phosphorous, and is generally measured in grams or milligrams. It is often presented as ash weight (g) or as a percentage left of a specimen after ashing (mg/g).

Currey et al. [48] showed that mineral content increases with age in cortical bone. Mineral content has been found to increase regularly and clearly up to the age of 25. Ageing from 25 years upward shows a less clear increase, but when observing the logarithmic relation between ash content and age, it is clear there is a continuation of the increase in mineral content with age in these later years. The increase of mineral content with age can also be found in baboons [44].

Later works by Currey [16, 52] showed an increase in Young's modulus with an increase in mineral content across multiple species, as well as a positive relationship between tensile yield stress and mineral content, although this relationship is looser than that between Young's modulus and mineral content.

Novitskaya et al. [18] performed tests on bovine bone in untreated, demineralized and deproteinized states and found that the untreated bone had the highest compressive strength, meaning whole bone is stronger than the sum of its constituents alone. This further suggests that bone is a complex material that should be assessed as close to its natural state as possible. For cortical bone, lower porosity and higher (but not overly high) mineral content increases strength [20].

2.2.4 Location and anisotropy

The direction in which specimens are cut have a profound effect on their mechanical responses [19, 30, 53] as bone is highly anisotropic [18, 30, 31, 54, 55]. There are three main axes to consider when machining a bone specimen, namely longitudinal, transverse and radial. Pictured in the top left corner of Figure 2.10 is a depiction of how the transverse (referred to as tangential) and radial axes relate to the axis of the long bone, or the longitudinal axis. This is further clarified by the depiction of the longitudinal and transverse specimens on a section of the shaft of a long bone, also shown in Figure 2.10.

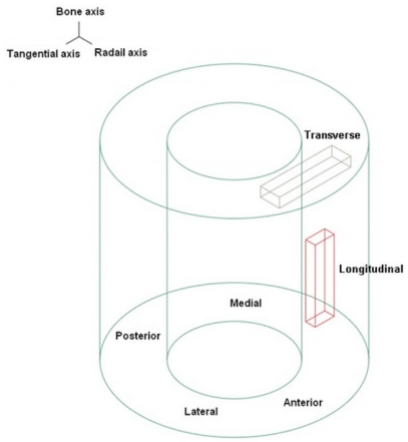

Figure 2.10: A depiction of how transverse and longitudinal specimens relate to a portion of a long bone shaft [8].

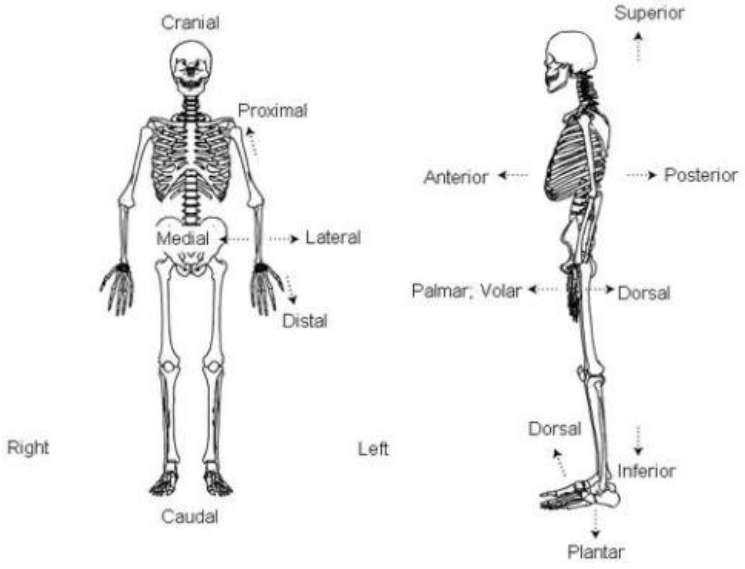

Figure 2.11: An example of the descriptive terms used when discussing bone position, shown on a full skeleton [9].

Depicted in Figures 2.10 and 2.11 are the four "sides" of the bone, namely the medial, lateral, anterior and posterior areas [8]. These terms are pictured on a human skeleton, but apply equally to other animals. The medial area will be closest to the centerline of the skeleton. The lateral area will be the outermost side of the bone, being furthest away from the centerline of the skeleton. The anterior is the front most portion of the bone, and the posterior is the hind side of the bone. Two other important terms are proximal, meaning closer to the head, and distal, meaning further away from the head.

There are clear differences in the ultimate tensile and compressive stress, and ultimate tensile and compressive strain, when comparing tests done in the longitudinal and transverse directions, with longitudinal specimens displaying consistently higher failure stress and lower failure strain values than transverse specimens. [18,19,31,54]. Interestingly, Novitskaya et al. [18] found that the compressive radial strength is higher than the compressive longitudinal strength in bovine bone. This was attributed to differences in microstructure, namely that the radial specimens tested primarily

had a lamellar structure, and the longitudinal had osteons present. The specimens tested were taken from adjacent portions of bone, although where on the bone was not stated.

Further anisotropic behaviour can be observed in cortical bone when observing crack growth resistance, specifically crack growth toughness (which is greatest longitudinally) and initiation toughness (which is greatest transversely) [56].

Anisotropy can also be found when assessing the stiffness of bone. Novitskaya et al. [18] found that in bovine cortical bone, their longitudinal specimens exhibited the highest stiffness, followed by their transverse specimens. The lowest stiffness was measured in radial specimens.

The site on the diaphysis of the femur from where the specimen is cut (i.e. proximally, distally, laterally, anteriorly etc.) can have a noticeable effect on the mechanical properties [57]. Cortical bone has been found not only to be anisotropic, but going so far as to have differing properties around the circumference of the same bone, for example a longitudinal specimen taken from the anterior side of a bone may exhibit properties different to those found on the posterior side of the same bone [8].

A study by Evans and Lebow [58] on the human femur, particularly cortical bone, found that specimens taken from the lateral portion of the diaphysis of bone have displayed the highest ultimate tensile strength, and anterior specimens the lowest, with there being no significant differences in elastic modulus around the circumference of the bone [58]. Further, bone taken from either end of the diaphysis shows different properties to specimens taken from the mid-diaphysis in human bone [58], with the mid-diaphysis showing higher ultimate tensile strength and elastic modulus than either the distal or proximal portions of the diaphysis. In wet specimens, the proximal diaphysis showed a weaker ultimate tensile strength than the distal end, as well as the lowest elastic modulus [58].

How a particular bone responds to stress will be deeply influenced by not only the

mechanical properties of the bone, but also by the spatial arrangement of the bone material, both at the macrostructural and microstructural levels [38]. This results in a complex material, which requires many different properties and failure mechanisms to be investigated to understand fully.

The direction of loading also has an effect on the properties measured. The response of bone to compressive load has been found to be more sensitive to variations in the bone microstructure than in tensile load [59], as well as showing higher values of ultimate strength in compression than in tension, both in the longitudinal and transverse directions [54]. When the Young's modulus is compared between specimens loaded in compression and tension, it has been found that there is a variance of 6%, with the tensile modulus being greater [60].

Wu et al. [15] tested both interstitial (bone tissue existing between osteons, not including cement lines, osteons, or portions thereof) and osteonal human cortical bone. They found the indentation modulus to be greater in the interstitial bone than the osteonal bone. However, this testing was done using nanoindentation, meaning these results are from testing at a microstructural level. It is not certain that this will be an accurate representation of the macroscopic properties as well.

Other factors, such as the cement lines between osteons, may play a role in the macroscopic stress response of bone [61], which may not be accurately represented by nanoindentation testing. This is not to say that understanding the differences in the response of different microstructural components is unimportant, instead emphasizing that understanding their responses when interacting as they would in whole bone is also an important consideration to make.

2.2.5 Porosity & Density

When investigating density effects, and comparing literature, it is important to note which density is being presented, as there are multiple different densities which may

be presented. Areal bone mineral density (aBMD, measured in g/cm^2) is presented when a bone surface is scanned to determine the bone mineral content, and is presented as the surface mineral content in grams divided by the area scanned. Volumetric bone mineral density (vBMD, measured in g/cm^3) is a measure of the bone mineral content throughout a sample, and is equal to the bone mineral content of the entire specimen in grams divided by the sample volume. In practice however, an apparent density (measured in g/cm^3) is often presented, as it is much easier to measure. The apparent density includes both the mineral and organic components of the bone sample, and is the weight of the entire specimen divided by the volume of the entire specimen. Dry apparent density (measured in g/cm^3) may be presented, which is similar to apparent density, but the sample is first dried in an oven to remove as much of the water content as possible. The dry apparent density is then the weight of the dried sample divided by the volume of the dried sample. Lastly, apparent ash density (measured in g/cm^3), which is the density of only the mineral component of the bone, may be presented. The apparent ash density is the ash weight divided by the volume of the sample before ashing. The ash weight of the bone sample is the weight of the ash left over after burning the sample in an oven until only the mineral ash remains.

The porosity and density of bone can have a significant effect on the mechanical properties. As the porosity increases, which comes with a corresponding decrease in apparent density, the elastic modulus and ultimate strength also decreases [40, 62]. Another issue to consider is the effect of inhomogeneities within each specimen itself. Even in small specimens, it has been found that inhomogeneities can have a significant effect on the measured mechanical properties, and can cause large variations between measured properties [60]. Some of these inhomogeneities can be accounted for by differing microstructure, but also include factors such as differing porosity and mineralisation [60]. Porosity is also inextricably linked to the microstructure of the bone. As demonstrated in Section 2.5, different microstructures of bone, for example lamellar versus secondary osteonal bone, will have vastly different amounts of porosity for a given volume of bone. This may contribute to the differences we see in material response of bones with different microstructures. This is supported by the differences reported in studies looking at bone from a single species, such as

Wright and Hayes [40], who found that within their specimen pool, secondary Haversian bone exhibited noticeably lower values for both ultimate strength and elastic modulus.

Seemingly contrary to this, Grimal et al. [57] found that there was a small, insignificant relationship between apparent density and strength, as well as between apparent density and stiffness. However, this was explained by the small range of densities present in the specimens used, and was not found to be contradictory with previous studies showing a relationship between density and strength or stiffness. It simply requires a larger range of densities to show the true relationship. Further data in this may be beneficial. It was also suggested that due to the small range of densities displayed in the specimens, that the differences in response were more likely to be due to the organisational differences possibly present in the bone [57].

2.3 Storage conditions

The storage medium in which the specimens are stored after machining does have an effect on the measured mechanical properties [24, 53]. It has been found that when stored in alcohol, the fracture toughness of bone increases while the work of fracture decreases, i.e. "brittle" behaviour [53]. This is further supported by work by Stefan et al. [24], who found that cortical specimens stored in alcohol-glycerine solution showed a significantly increased Young's modulus and lowered plastic energy absorption. This is thought to be connected to the loss of water within the bone when soaked in alcohol, which can be rectified by rehydration with normal saline [24, 53]. This displays the importance of keeping the bone specimens sufficiently hydrated before testing. Properly hydrated specimens, which represent the natural state of bone, display visco-plastic behaviour, whereas alcohol stored specimens display behaviour more like that of dry bone, which is more brittle [53]. This appears to be consistent across the literature reviewed.

Studies have found conflicting effects when bone is stored in formalin (a buffered formaldehyde solution). Van Haaren et al. [23] found that there was no effect on the mechanical properties of bone, even after a year in formalin storage. In contrast, Stefan et al. [24] found that there was a significant decrease in the energy absorption and ultimate strain in human cortical bone stored in formalin for 6 months. This is in agreement with Goh et al. [63], who found that whole bones stored in formalin for just three weeks showed a significant difference in the energy absorption ability of the bone, causing the bone to respond in a more brittle fashion than fresh bone. However, they also found that there was not a significant change in the stiffness or maximum loading capacity [63]. Finally, and also in agreement, Öhman et al. [64] found that specimens stored for eight weeks in formalin solution showed a significant change in Young's modulus, yield strain and ultimate strain.

Freezing a specimen of "dead bone" i.e. bone that is no longer within a living organism, with reduced enzyme and cellular activity, does not affect the mechanical properties as long as the freezing temperature is above -70°C [22]. It has been found that freezing for up to one year does not influence the mechanical properties of bone [23]. Conversely, Moreno and Forriol [65] found that frozen specimens actually displayed higher strength in bending than fresh bone. However, it should be noted that there was no mention of whether or not they thawed their frozen specimens before testing. They also noted that frozen specimens showed a larger amount of phosphorus than fresh specimens, and theorised this was due to the continued enzyme activity that can occur at a freezing temperature of -20 °C. This makes freezing a suitable method of preservation for bone specimens, although the specimens should be stored at a temperature of less than -20°C and greater than -70°C.

2.4 Testing conditions

The conditions in which bone specimens are tested also have an effect on the measured material properties.

Material properties of bone have been found to be affected by the temperature of the specimen being tested [66]. In cortical bone, the ultimate compressive strength is relatively constant at temperatures of 27°C and above, and increases as temperature decreases below 27°C [66]. Sedlin and Hirsch [67] compared mechanical properties in human femoral cortical bone at temperatures of 21°C and 37°C . They found, in agreement with previous findings, that both the maximum stress and apparent modulus remain generally unchanged in this temperature range. They did, however, find that there was a significant increase in deflection to failure at the higher temperature. Work by Smith and Walmsley [68] somewhat agrees with this, as they found that in a temperature range of 5°C to 43°C, the deflection under a certain load increases as temperature increases. However, they also found that Young's modulus decreases as temperature increases over this range.

Dry bone has been found to display more brittle behaviour than wet bone, with dry bone showing higher failure stresses and lower total strains [31], as well as an increased elastic modulus and hardness [58]. This makes sense, as the collagen component of bone, which affects toughness and elasticity, would be more affected by changes in the water content of bone than the mineral component. When properly hydrated, the collagen component will be most compliant and tough. When dry, it will result in a much less compliant bone material, resulting in the higher failure stresses and lower strains seen.

There is evidence that the size of the specimen being tested may have an effect on the properties measured [55]. Allena et al. [55] found that cylindrical specimens of bovine cortical bone with a small diameter (4mm) displayed higher failure stresses than larger diameter specimens (6, 8, and 10mm) . They theorized that this may be due either to a lack of homogeneity in the stress induced in their specimens, or due to the fact that the smaller a specimen is, the more it correlates with the microstructure present. The smaller the specimen, the more the specimen approaches the dimensions of cement lines, or portions thereof, that may be present. However, Ebacher et al. [59] found that when comparing the response of whole tibia and cortical specimens (with dimensions 35mm x 4mm x 3mm) in bending, they failed similarly with respect to

both the macro-visible fracture pattern and how the microdamage developed.

2.5 Effect of bone structure on response

A study by Weiner et al. [39] sought to assess the function of lamellar bone specifically, and focused only on bone specimens taken from mammals. They concluded that lamellar bone could not be linked to any one particular mechanical function, but rather that it probably fulfilled various functions depending on what conditions the particular bone was being exposed to [39]. It should be noted that they include both circumferential lamellar bone (which correlates with the definition of lamellar bone in other research) and osteonal bone in their definition of lamellar bone. These are referred to as two separate categories in other research, and combining them may have obscured relations between structure and function. In the research to be presented, these two types of bone will be defined as separate categories, due to their clear difference in sub-unit structure (parallel arrays versus cylinders), as well as the fact that these types of sub-units are evident in different portions of the bone (see Section 2.2.4). Furthermore, after comparing data from other studies using microhardness measurements, sonic velocity measurements and testing done on the bone of drug treated baboon tibia, they found no definitive answer as to the link between structure and function, although they did note that osteonal bone was capable of absorbing aspects relating to damage (such as microdamage or fatigue damage) better than lamellar bone. They also noted osteonal specimens held together better after failure than lamellar bone [39].

Novitskaya et al. [18] found that within their specimens, those with lamellar bone and a lack of osteons showed a higher compressive strength than specimens with osteons present.

Haversian bone has displayed some interesting interactions. It has been suggested that the interactions at the cement lines between secondary osteons affects the stress response by allowing the initial formation of cracks, but preventing crack growth [61]. This then provides good fatigue and impact resistance [61], which would clearly be of use in bones or areas of bone bearing a large load, where osteonal bone is often found [39]. Work by Abdel-Wahab et al. [69] agrees, and suggests that cement lines play a role in the prevention of microscale fracture and affect the distribution of maximum stresses within a bone.

It has been found that in compression, Haversian systems are highly prone to microdamage, with cracks both being initiated in and propagating within Haversian systems [59]. Furthermore, the level of sensitivity to cracking found in Haversian bone is dependent on differences in the individual Haversian systems themselves, such as the level of mineralisation and size [59]. It has been found that Haversian bone is both weaker and less stiff than fibrolamellar bone [25, 41, 52]. Ebacher et al. [70] looked at the failure of human cortical bone in compression, and found that longitudinal specimens displayed crack formation oblique to the osteonal direction, with cracks that almost appear step like in places. The majority of the crack travelled along the boundaries of the circular lamellae around the osteons, with the presence of uncracked fibril bundles still connected across the break. The crack was found to consist of many small microcracks, as well as displaying evidence of some small crack interaction with present canaliculi (tiny canals between natural bone cavities), although cracks were much more sensitive to the Haversian canals themselves, and to osteocyte lacunae (small cavities in the bone) [70]. This further displays the importance of the highly hierarchical structure of bone in its response to stress, particularly controlled cracking to allow for high amounts of inelastic strain before failure.

Abdel-Wahab et al. [8] found that lamellar bone with primary osteons present displayed higher elastic moduli and higher ultimate strengths than Haversian bone.

2.6 Strain rate dependence

Under impact conditions, an important aspect of bone response is the effect of strain rate on the material properties. Bone is a complex material, and it has been found to be a highly strain rate dependant material [8, 17, 30, 31, 40, 71].

As strain rate increases, the behaviour of the bone changes from ductile to brittle [40]. While the term "ductile" is used often in literature, it is important to note that bone can never be ductile. What this refers to is a period of incipient failure, followed by a decreasing load bearing capacity, as opposed to short, sharp failure (i.e. "brittle" failure).

Sanborn et al. [19] showed that both longitudinal specimens and transverse specimens are highly strain rate dependant under compression, with greater values for both compressive failure strength and Young's modulus being displayed at higher strain rates. Their testing was performed at approximate strain rates of 10^{-3} per second (s^{-1}), $1s^{-1}$ and $10^{3}s^{-1}$.

Work done by Abdel-Wahab et al. [8] showed that both fracture stress and elastic modulus increases in bovine cortical bone as strain rate increases from $10^{-5}s^{-1}$ to $10^{-3}s^{-1}$. They also found that the fracture stress increases by a much larger amount when the strain rate is varied from $10^{-5}s^{-1}$ to $10^{-3}s^{-1}$ (60%) than when strain rate is varied from $10^{-3}s^{-1}$ to $1s^{-1}$ (only increasing 11%) [8]. They concluded that the elastic modulus does not change significantly when tested at strain rates higher than $1s^{-1}$, which is not in agreement with the other studies reviewed. However, they performed no studies at strain rates higher than $1s^{-1}$. Their conclusions were based solely on extrapolation from the data they generated.

Contrary to other studies, Evans et al. [72] found that ultimate tensile strength increased and then decreased with increasing strain rate in equine bone (over a range of $10^{-4}s^{-1}$ to $1s^{-1}$). However, the sample size was small, and the amount

of scatter high. Their findings on the relationship between strain rate and Young's modulus is consistent with other studies (namely, as strain rate increases, so does Young's modulus).

Evans et al. [72] found evidence that stress changes from pseudo ductile (that is, displaying shearing type failure with a larger "ductile" response region) to brittle (shorter, sharper failure) at some terminal strain rate, somewhere in the range of $10^{-1}s^{-1}$ to $10s^{-1}$. This correlates with the findings of McElhaney and Byars [73], who found that up to strain rates of $1s^{-1}$, bone displayed shearing type failure. Above $1s^{-1}$, bone specimens displayed splintering failure, where many small shards of bone formed. Work by Currey [16] and Paul [12] also found that bone yields at some specific strain, not a particular stress, with lower yield strain in bone with a higher Young's modulus.

Work by McElhaney and Byars [73] showed a clear strain rate dependence of both apparent modulus and compressive strength, for both fresh bovine and embalmed human bone.

Carter and Hayes [71] showed that human cancellous bone under compression, tested in the strain rate region from $10^{-4}s^{-1}$ to $10s^{-1}$, displays an increase in ultimate strength with increase of strain rate. Tensile tests have been done on bovine cortical bone and have also displayed a significant positive correlation between strain rate and yield strength [17] , as well as strain rate and ultimate strength [17, 30, 40]. Wright and Hayes [40] investigated in the range of 5.3 x $10^{-4}s^{-1}$ to $237s^{-1}$, similar to Crowninshield and Pope [30] who tested at strain rates between $10^{-3}s^{-1}$ and $200s^{-1}$. In addition, previous research has found that there is a significant positive correlation between apparent modulus and strain rate [17, 40]. Currey's work [17] demonstrates these same correlations, however it is important to note that the strain rates utilised in his experiments were not constant, and any values for mechanical properties may not be fully accurate (as bone is highly strain rate dependent, which will be discussed further into this section), although the relationships displayed are still valid. This same issue was present in the work of Crowninshield and Pope [30],

where the higher strain rate tests were also not strain rate controlled. In lower strain rates, testing is often done using a displacement controlled servo-hydraulic machine, which provides a constant strain rate, despite this not being focused on before testing.

To the authors knowledge, no study focused on providing a near constant strain rate (that is, a strain rate which is consistent enough to be considered constant for the purposes of testing, see Figure 3.22 for an example), especially in higher strain rate tests, until a study done by Adharapurapu et al. [31]. They performed quasistatic compression tests covering strain rate ranges of $10^{-3}s^{-1}$ to $1s^{-1}$ using servo-hydraulic testers on cortical bovine bone. They also performed high strain rate tests at $10^{3}s^{-1}$ using a modified Split Hopkinson bar (SHB). These tests were performed on both longitudinal and transverse specimens, at a near constant strain rate, and this appears to be the first attempt at such strain rate control. These tests were performed on bovine bone and further showed that cortical bovine bone is indeed strain rate sensitive, with an increase in strain rate causing a corresponding increase in stiffness and strength. The observed decrease in failure strain illustrates the increase in brittle behaviour with increase in strain rate.

Kulin et al. [74] performed a study on equine cortical bone over a range of strain rates. They attempted to account for strain rate by using a pulse shaper, consisting of a small piece of a deformable material between the striker and incident bar, but it was insufficient. There was visible change in the apparent modulus in a graph of the stress versus strain in the specimens. They did, however, consider their strain rate to be sufficiently constant to draw conclusions about the yield strength measured in compression. They found, in agreement with other findings, that compressive yield strength increases with an increase in strain rate.

Johnson et al. [10] did work on creating a model of the behaviour of bone, specifically examining cortical bone. While the modelling aspect of their work isn't relevant to the experimental work to be done in this dissertation, they did perform a highly valuable comparison of available data across a range of strain rates, which is displayed

in Figure 2.12. This serves to show that there is an incredible amount of scatter within bone properties. However, even when that scatter is taken into consideration, there is still a clear rate effect.

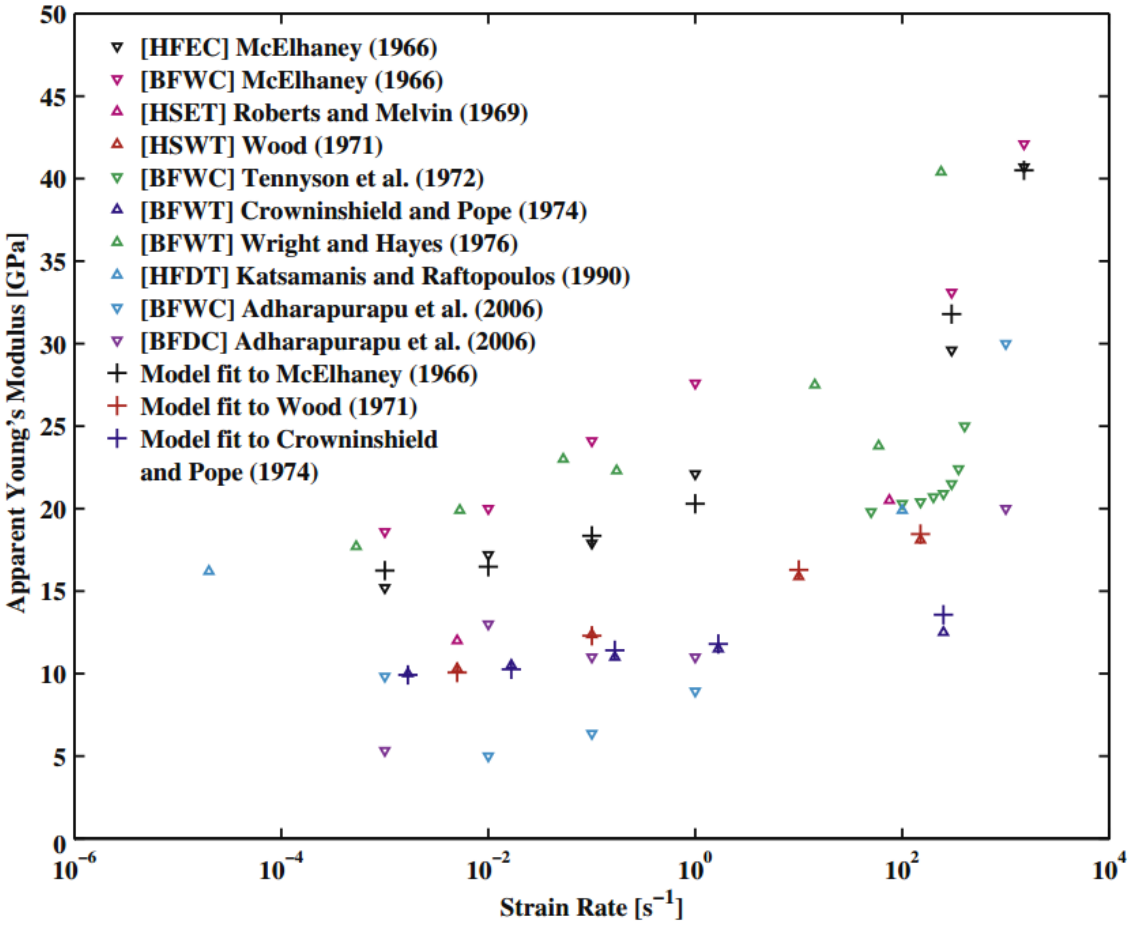

Figure 2.12: A comparison of cortical bone data from multiple studies over a range of strain rates from Johnson et al. [10]. The letters preceding each source indicate testing conditions as follows: H - human bone, B - bovine bone, F - femur, S - skull, E - embalmed, W - hydrated, D - dehydrated, C - compression, T - tension.

Work by van der Westhuizen [32] showed that a conical striker (discussed in more depth in Section 2.8.1) could provide a near constant strain rate in bovine bone specimens tested at dynamic rates. She found that bovine bone has a higher stiffness in the dynamic strain rate regime than in the quasistatic, and that fracture stress increases with strain rate increase. This was further expanded on by Paul [12] and Cloete et al. [33], with the development of the Cone-in-Tube (CiT) striker (again see Section 2.8.1) and further testing of bovine bone, including more data in the intermediate strain rate range. They too found that the compressive strength of longitudinal bone is strain rate dependant. They also showed a clear transition zone between quasistatic and dynamic regions, where the bulk of the increase occurred. This change occurred in the intermediate range, at around $8s^{-1}$. Collected in Table 2.2 is a brief summary of the studies which investigated strain rate dependence of material properties, for ease of comparison.

Table 2.2: The relationship between strain rate and mechanical properties from various studies.

Source & publication date	**Species**	**Cortical or cancellous**	**Compression or tension**	**Strain rate**	**Property and relation**
Carter & Hayes [71] {1976}	human	cancellous	compression	$10^{-4}s^{-1}$ to $10s^{-1}$	ultimate compressive strength increases with increasing strain rate
Currey [17] {1975}	bovine	cortical	tension	1.3 x $10^{-4}s^{-1}$ to $0.16s^{-1}$	tensile yield strength and apparent modulus increase with increasing strain rate
Wright & Hayes [40] {1976}	bovine	cortical	tension	5.3 x $10^{-4}s^{-1}$ to $237s^{-1}$	ultimate tensile strength and apparent modulus increase with increasing strain rate
Crowninshield & Pope [30] {1974}	bovine	cortical	tension	$10^{-3}s^{-1}$ to $200s^{-1}$	ultimate tensile strength increases with increasing strain rate
Adharapurapu et al. [31] {2006}	bovine	cortical	compression	$10^{-3}s^{-1}$ to $10^{3}s^{-1}$	compressive strength and apparent modulus increase with increasing strain rate
Sanborn et al. [19] {2014}	human	cortical	compression	$10^{-3}s^{-1}$ to $10^{3}s^{-1}$	compressive failure strength and apparent modulus increase with increasing strain rate
Abdel-Wahab et al. [8] {2011}	bovine	cortical	tension	$10^{-5}s^{-1}$ to $1s^{-1}$	tensile fracture stress and apparent modulus increase with increasing strain rate
Kulin et al. [74] {2011}	horse	cortical	compression	$10^{-3}s^{-1}$ to $10^{3}s^{-1}$	compressive yield strength increases with increasing strain rate
McElhaney & Byars [73] {1965}	bovine	cortical	compression	$10^{-3}s^{-1}$ to 1,5 x $10^{3}s^{-1}$	compressive strength and apparent modulus increase with increasing strain rate
van der Westhuizen [32] {2008}	bovine	cortical	compression	$10^{-4}s^{-1}$ to $10^{3}s^{-1}$	compressive fracture strength and apparent modulus increase with increasing strain rate
Paul [12] {2014}	bovine	cortical	compression	3 x $10^{-3}s^{-1}$ to $120s^{-1}$	compressive strength and apparent modulus increase with increasing strain rate

2.7 Species specific responses

The literature shows that there is significant variation when comparing the material properties of bones from different species of animal. Showing this most clearly is a study by Currey [16], which showed a marked difference in measured properties between different species when performing tensile testing at a singular strain rate (namely $0.2s^{-1}$). This testing displayed a large range of properties, with Young's moduli ranging between 4.9GPa in a dugong ulna to 31.6GPa in a deer tibia. The yield stress displayed an equally wide range, from 25MPa in a dugong scapula to 192.9MPa in the ossified tendon of a crane.

Gathered here is the information found about previous testing done on the species relevant to the research being presented. Specifically of interest are the reported values of apparent modulus or compressive strength. All values reported are collated in Table 2.3.

2.7.1 Baboon

Through ultrasonic testing, Wang et al. [27] evaluated the apparent modulus of cortical bone at various points on the skull of baboons. They investigated the modulus at three orientations over multiple points of the skull, and found moduli ranging from 9.2GPa to 12.2GPa in the least stiff orientation, and from 17.2GPa to 25.7GPa in the stiffest orientation. While skull bone has a different overall macrostructure than long bones, this at least gives an idea of the range of possibilities. This is comparable to work done on macaque mandibles by Dechow and Hylander [75], who measured apparent moduli ranging from 9GPa in the least stiff direction to 23.9GPa in the most stiff direction. This demonstrates that there may be at least some similarity between baboon bone and bone from other members of the same family. They also measured the stress in the mandible during chewing actions, and found a maximum of 8.84MPa tensile and 16MPa compressive. This is not an accurate representation

Table 2.3: The mechanical properties in literature for various species. For the apparent moduli, multiple sets of numbers indicate testing occurred in multiple orientations. Each set is the range found in a singular direction, with the ranges listed from least stiff to most stiff orientations.

Source	**Species**	**Apparent modulus (GPa)**	**Ultimate strength (MPa)**	**Bone specimens taken from**	**Type of testing or strain rate tested at**
Wang et al. [27]	Baboon	9.2 - 12.2 13.6 - 18 17.2 - 25.7	/	skull	ultrasonic
Dechow & Hylander [75]	Macaque	9 23.9	8.84 - 16 (working stresses not ultimate strengths)	mandible	ultrasonic (apparent modulus) in vivo strain gauge tests (working stresses)
Currey [52]	Crocodile	6 - 8.5	/	/	/
Currey [16]	Alligator	13.0	97.2	femur	$0.2s^{-1}$
Zapata et al. [28]	Alligator	8,8 10.7 20.5	/	mandible	ultrasonic
Moreno & Forriol [65]	Sheep	/	250 (tensile)	femur	quasistatic
Spatz et al. [25]	Sheep	26 - 31.5	/	long bones	quasistatic
Reed and Brown [26]	Emu	13.05	/	femur	$0.000167s^{-1}$
	Emu	14.14	/	femur	$0.00033s^{-1}$
	Emu	15.86	yield 126.54 ultimate 154.6	femur	$0.0005s^{-1}$
Yamada [76]	Ostrich	compressive 5.297 tensile 13.64	compressive 117.72 tensile 69.65	/	/
Cuff et al. [29]	Ostrich	5.03	/	skull	nanoindentation
Spatz et al. [25]	Ostrich	17 - 22.3	/	long bones	quasistatic

of the maximum stresses that may be found in the research to be presented, as they are sustainable working stresses, not ultimate stresses. This does, however, provide a baseline for the minimum stress that would be reasonable to expect in testing.

2.7.2 Crocodile

Currey [52] reported the Young's modulus for crocodile bone ranging from approximately 6GPa to 8.5GPa, although it is unclear exactly how these values were arrived at.

Later work by Currey [16] found that in tension, at a strain rate of approximately $0.2s^{-1}$, alligator femoral bone displayed an apparent modulus of 13.0GPa and a yield stress of 97.2MPa.

Zapata et al. [28] tested alligator crania ultrasonically, and found the apparent modulus to be 8.8GPa in the least stiff direction, 10.7GPa in the intermediately stiff direction, and 20.5GPa in the most stiff direction.

2.7.3 Sheep

Moreno and Forriol [65] performed constant strain rate tests on sheep femora at a quasistatic rate, and found the average ultimate tensile strength of normal, healthy cortical bone to be 250MPa.

Spatz et al. [25] found that cortical bone in sheep displayed a range of Young's modulus from 26GPa to 31.5GPa. These values came mostly from specimens loaded radially through three-point bending, and from a few loaded tangentially through three-point bending. They were all tested at a quasistatic strain rate.

2.7.4 Ostrich

Reed and Brown [26] performed four point bending tests on emu bone, at three strain rates, namely 1.67 x $10^{-4}s^{-1}$, 3.3 x $10^{-4}s^{-1}$ and 5 x $10^{-4}s^{-1}$. They measured the apparent modulus at each of these rates, and found them to be 13.05GPa, 14.14GPa and 15.86GPa respectively. They also measured the yield and ultimate strengths at 5 x $10^{-4}s^{-1}$, and found them to be 126.54MPa and 154.6MPa respectively. This apparent modulus data is comparable to apparent modulus data on ostrich bone in tension, reported by Yamada [76]. Yamada[1] reported values for cortical ostrich bone in both compression and tension. In compression, the ultimate strength was reported as 117.72MPa, and the apparent modulus as 5.297GPa. In tension, the ultimate strength was reported as 69.65MPa, and the apparent modulus as 13.64GPa. Cuff et al. [29] generated other values for the elastic modulus of cortical ostrich bone, using nanoindentation (5.03GPa) and by generating post-hoc values within their model (10GPa and 7GPa). This is a wide range of possible moduli. Cuff et al. also noted that their tests were performed on specimens from the inner region of the bone, which may have differing properties than tough outer surfaces.

Spatz et al. [25] found that cortical ostrich bone (mostly radial specimens tested at a quasistatic strain rate) showed a range of Young's moduli from 17GPa and 22.3GPa. Casinos and Cubo [77] performed tests on whole avian bones, and while these results aren't specifically relevant to the properties of ostrich cortical bone, they did find that ultimate compressive strength and apparent modulus tended to decrease with decreased body mass.

[1]Values reported for ostrich bone by Yamada were taken from Oda, M.: "The strength of a compact bone of an ostrich", J. Kyoto Pref. Med. Univ., 56:892-894, 1954.
An original copy of this paper was unable to be sourced.

2.8 Equipment and testing methods

The research to be presented utilised testing in the intermediate strain rate regime ($1s^{-}1$ to $100s^{-}1$), as well as the lower dynamic strain rate regime ($100s^{-}1$ to $200s^{-}1$). This region was of interest as it was the estimated critical region wherein the change in response was expected to be found, based on literature (see Section 2.6). Furthermore, this region tends to have the sparsest available data, as can be observed in Section 2.6. However, this region can be difficult to test in (hence the sparseness of data), and as such, some specialised equipment was required. A near constant strain rate was also important to the research (again as discussed in Section 2.6), which also required specialised equipment. This section contains a description of this specialised equipment.

2.8.1 Cone-in-tube striker

Due to the complex response of bone to stress, a conventional SHB setup was not sufficient for high intermediate strain rate testing at a near constant strain rate. A conventional SHB consists of two bars (incident and transmitter bars), with the specimen placed between them. A standard uniform striker would be fired at the incident bar (often by means of a gas gun), generating an incident wave that would travel down the bar and into the specimen. Some of this wave would be transmitted into the transmitter bar, and some reflected back into the incident bar. These waves would be captured using strain gauges placed on both bars. Stress wave theory could then be used to interpret these results into stress, strain and strain rate in the specimen (see Section 2.9.1).

This would produce a standard square shaped wave (see Figure 2.13). When used on a strain hardening material, this would produce a decreasing strain rate over the course of the test. To counteract this, the pulse would require shaping [74]. A standard method of pulse shaping would utilise a deformable material placed between

the striker and the incident bar, as was done by Kulin et al. [74]. This shortened rise time and dampened any higher frequencies present in the generated incident pulse. As was found in the research by Kulin et al. [74], this method did not provide a sufficiently stable strain rate to assess apparent modulus at dynamic rates.

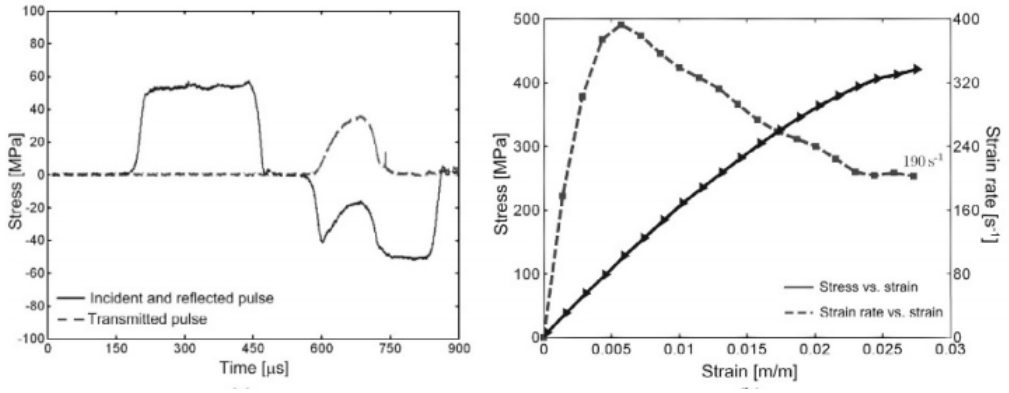

Figure 2.13: The square shaped pulse from a standard uniform striker (shown on the left), and the decreasing strain rate seen over a test (shown on the right) from Cloete et al. [11].

To correctly assess the apparent modulus, the pulse was required to increase at approximately the same slope as the apparent modulus of the strain hardening material being tested. It has been demonstrated that a conical striker can provide this shape, as presented in work by Cloete et al. [11, 33].

The use of a conical striker allows for the induced pulse shape to be controlled, allowing for a more consistent strain rate than the conventionally used uniform strikers in SHB testing [33]. It produced a wave with an increasing slope over the test period, in place of the flatter, more square wave seen in standard testing (see Figure 2.14).

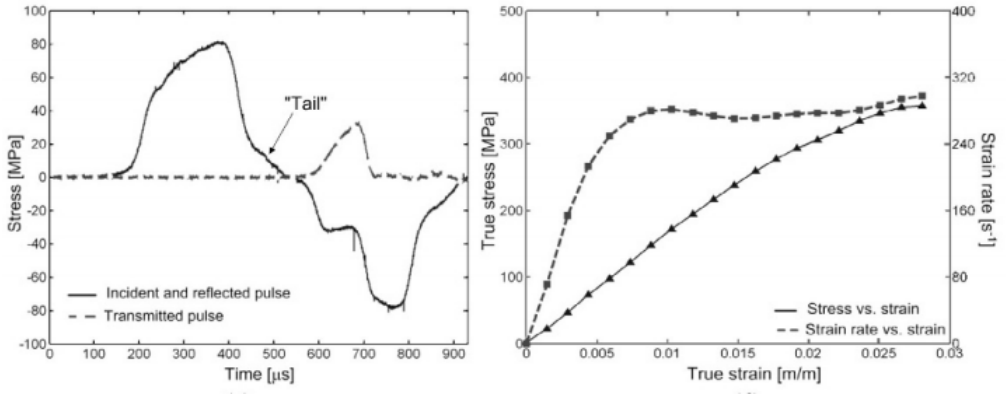

Figure 2.14: The increasing pulse from a conical striker, with tail highlighted (shown on the left), with the more constant strain rate seen over the test (shown on the right) from Cloete et al. [11].

Unfortunately, the conical shape also generates a "tail" on the induced stress wave, which negatively impacts the maximum attainable duration of the test [33]. It also restricts the attainable strain rates, not allowing for the lower range of $40s^{-1}$ that is sought [33]. This led to the development of the CiT striker. The CiT striker combines the shaped pulse attainable with a conical striker with a rapidly removed load. The tube, in which the cone is nested, would strike up against a large reaction mass simultaneously with the cone impacting the incident bar (setup pictured in Figure 2.15). This would cause a stress wave to be generated in both the tube and cone, which travel at the same time back towards the large end of the cone. At best, this would reverse the direction of the CiT, and at worst, simply cause an immediate stoppage of load, which removes the stress "tail "(shown in Figure 2.16) and enables a minimized strain rate and maximized test duration [33].

Ideally the cone and tube would be manufactured from the same material, and the cross-sectional area of the tube would equal that of the large end of the cone, for impedance to be properly matched [33]. The presence of the tube would also allow for easier mounting of the striker within a gas gun barrel than a purely conical striker.

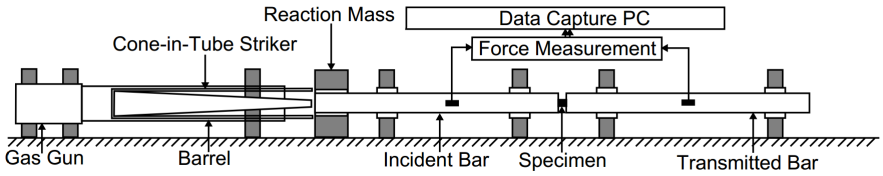

Figure 2.15: A schematic of a CiT striker in a practical setup as designed by Paul [12].

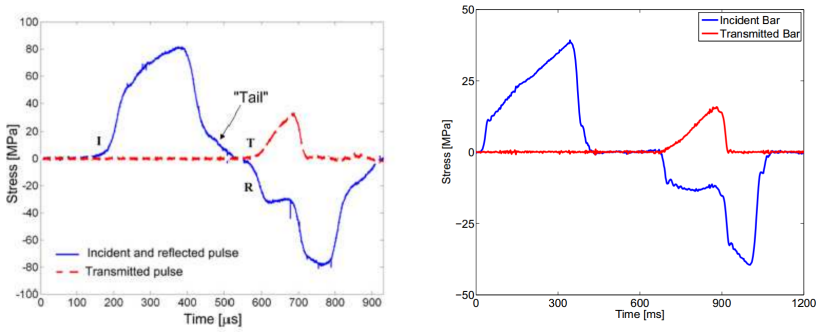

Figure 2.16: A pulse with a "tail" generated by a conical striker (shown on left) and a pulse generated by a CiT striker with no "tail" (shown on right), from Paul [12].

2.8.2 Momentum trapping

The second piece of equipment to be used was based on the tandem momentum traps designed by Prot and Cloete [13]. The purpose of the momentum traps is to limit the loading of the specimen to a single event, preventing reloading and allowing for the specimen to be retrieved intact after testing for further inspection, even when working with relatively delicate specimens such as small specimens of cortical bone. The practical configuration of the design by Prot and Cloete involves two nested tubes, each impedance matched to a bar in the center. This central bar is the incident bar in the SHB setup (see Figure 2.17).

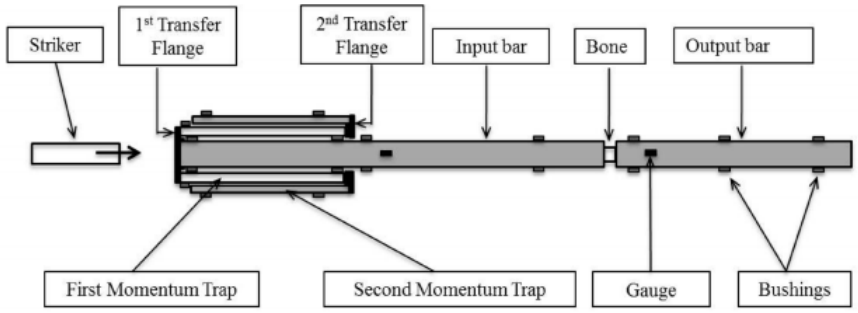

Figure 2.17: The original design for nested momentum traps by Prot and Cloete [13].

The tandem momentum traps work by directing the reflection of stress waves within the bar and traps to prevent secondary loading of the specimen. The progress of the wave through the system can be seen in Figure 2.18. This schematic shows how the waves will propagate through a set of non-nested tandem momentum traps, but the theory still applies in the same way to the nested configuration. The initial compressive loading wave travelled simultaneously along the incident bar and the first momentum trap, which was connected to the incident bar through the use of a flange. The wave reached the end of the first trap and transferred into the second momentum trap. After reaching the end of the second trap, it then reflected as a tensile wave. This caused the second trap to separate from the first trap, as a tensile wave could not be transmitted across the first and second momentum trap boundary, by design. This prevented the first trap from separating from the incident bar before it served its full purpose. At the same time as this was occurring, the wave that passed down the incident bar to the specimen was partially reflected back up the incident bar as a tensile wave. This tensile wave passed down the incident bar, along the flange and into the first trap, leaving the incident bar stationary. This tensile wave caused the inner trap to separate from the incident bar. On the other side of the specimen, the transmitter bar conveyed the compressive pulse that passed through the specimen. This reflected as a tensile pulse when it reached the end of the transmitter bar. The tensile wave then pulled the transmitter bar away from the specimen, preventing reloading and any further damage to the specimen.

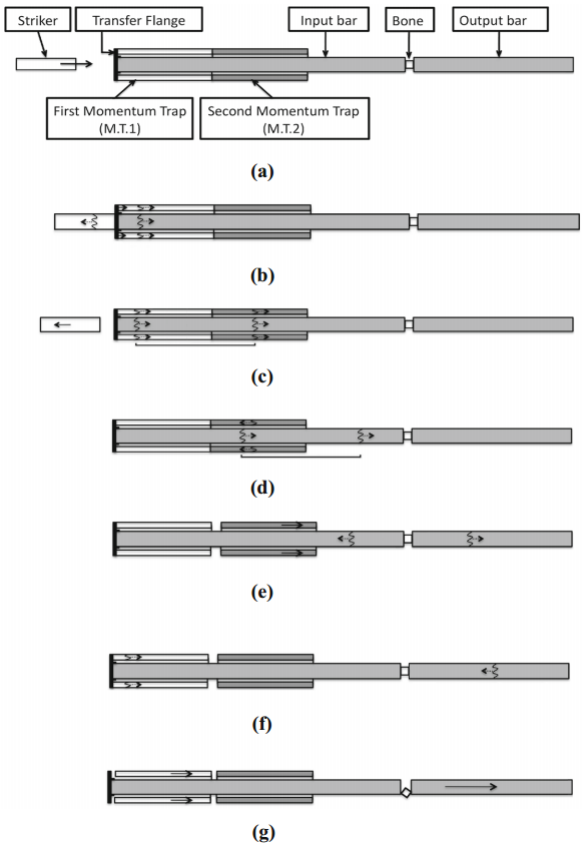

Figure 2.18: A schematic of how a wave propagates through a tandem momentum trap as depicted by Prot and Cloete [13].
(a) The striker just before impacting the system.
(b) The initial compressive wave propagated down the incident bar and into the first trap.
(c) The compressive wave propagated from the first to the second trap, and simultaneously down the incident bar.
(d) The compressive wave continued down the incident bar, and was simultaneously reflected back as a tensile wave at the free end of the second trap.
(e) The second trap separated from the first as the tensile wave reached the trap boundary. The compressive wave was reflected as a tensile pulse from the specimen back into the incident bar. A compressive wave was transferred to the transmitter bar.
(f) The tensile wave in the incident bar transferred through the flange into the first trap. There were no waves left in the incident bar. The compressive wave was reflected as tensile at the end of the transmitter bar.
(g) The tensile wave pulled the first trap away from the incident bar. The tensile wave pulled the transmitter bar away from the specimen.

2.9 Theory used in data processing and analysis

This section contains an overview of the theory needed to process the data that comes from SHB testing (used in Section 3.3.5), as well as information on how a lognormal distribution can be used to analyse data with a skew distribution (used in Section 3.4).

2.9.1 Wave theory

Wave theory describes how stress waves move through bars, and how these waves can be analysed.

When a stress wave is moving through a bar, the stress can be described via equation 2.1 [78]. When such a stress wave moves through one bar and into another, it splits. Some is transferred to the transmitter bar, and some is reflected back into the incident bar. If the reflected wave is compressive, the transmitted stress would be related to the incident and reflected stresses as in equation 2.2 [78]. In the case of a moving striker impacting a stationary incident bar, the stress and hence the velocity transferred to the stationary bar can be described by equations 2.3 [78] and 2.4 [78]. In the case of the striker and incident bar having the same diameter, this can be simplified down to equation 2.5.

Let symbols:
σ = stress
v = velocity
ρ = density
A = area
c = speed of sound of a material
l = instantaneous length

Let subscripts:
r = reflected
in = incident bar
s = striker
t = transmitter bar
if = at specimen face of incident bar
$diff$ = difference across the specimen

$$\sigma = \rho c v \tag{2.1}$$

$$\sigma_t = (\sigma_{in} + \sigma_r)\frac{A_{in}}{A_t} \tag{2.2}$$

$$\sigma_{in} = \rho_{in} c_{in} v_{in} \tag{2.3}$$

$$\rho_{in} c_{in} v_{in} = \frac{\frac{A_s}{A_{in}} \rho_s c_s v_s}{\frac{A_s \rho_s c_s v_s}{A_{in} \rho_{in} c_{in}} + 1} \tag{2.4}$$

$$v_{in} = v_s \frac{1}{1 + \frac{\rho_{in} c_{in}}{\rho_s c_s}} \tag{2.5}$$

Wave theory also states that at a boundary, there can only be one velocity [78]. Therefore, when considering a SHB setup with a specimen between the bars, the velocity of the wave transmitted into the specimen must be the combination of the incident velocity (v_{in}) and the reflected velocity (v_r) at the face of the incident bar in contact with the specimen. The velocity at the specimen face can be calculated via the sum of the incident and reflected velocities when the reflected wave is tensile (see eq 2.6 [79]).

$$v_{if} = v_{in} + v_r \tag{2.6}$$

Again relying on the consistent velocity at a boundary, the velocity at the end of the specimen in contact with the transmitter bar must have the same velocity as that face of the transmitter bar. The values of the velocity at each face of the specimen are then known throughout the duration of the test, and so the difference in velocity over the specimen (v_{diff}) can be calculated (eq 2.7 [79]).

$$v_{diff} = v_{if} - v_t \tag{2.7}$$

Using this velocity difference, the strain rate across a specimen tested via SHB can be calculated by dividing the velocity difference across the specimen by the instantaneous length of the specimen (eq 2.8 [79]).

$$\dot{\epsilon} = \frac{v_{diff}}{l} \tag{2.8}$$

Finally, it is known that the area of the interfaces between two objects through which a pulse is travelling affects the stress transferred [78]. This can be accounted for via equation 2.9 [78].

$$\sigma_1 A_1 = \sigma_2 A_2 \tag{2.9}$$

2.9.2 Lognormal analysis

In the case of a set of data presenting a skew distribution, a common method of analysis is the use of a three-parameter lognormal distribution [80]. If a set of data has a lognormal distribution, then eq 2.10 [80] (where X is a data point in the original set of data) will have a normal distribution.

$$Y = ln(X - \gamma) \tag{2.10}$$

This data set Y will have a mean (μ) and a variance (θ^2). The parameter γ is known as the threshold parameter and is a constant chosen by the person performing the data analysis. From the lognormal data set Y, it is possible to find the mean, median and mode of the original data set X using the values of μ, θ^2 and γ (eq 2.11, eq 2.12 and eq 2.13) [80].

$$Mean(X) = \gamma + exp(\mu + \frac{\theta^2}{2}) \tag{2.11}$$

$$Median(X) = \gamma + exp(\mu) \tag{2.12}$$

$$Mode(X) = \gamma + exp(\mu - \theta^2) \tag{2.13}$$

The mean represents the average value of the data, the median the centre of the data set, and the mode the most common value measured in the data set. In the case of a traditional lognormal distribution, which is skewed right, the mode will always be less than the median, and the median will always be less than the mean [80].

Chapter 3

Methodology

This section details the methods applied in the specimen preparation and the experimental setups. This includes the rig used in quasistatic testing, as well as the design and commissioning of the equipment used for the higher strain rate testing. The calibration of this higher strain rate equipment, and testing procedures for both the quasistatic and higher rate tests are described. Also included is a description of how the data was analysed.

3.1 Specimen preparation

Femurs from four different species were sourced and collected. As is clear in the literature (see Sections 2.2, 2.4 and 2.5), there are multiple factors that can have an effect on the response of bone. For this research, the goal was to find as wide a variation of species as was available, while minimising other factors that may cause differentiation of bone properties. These species were chosen as they come from different classes (aves, reptilia, and mammalia), while still being large enough to provide workable specimens of cortical bone. Also taken into consideration was the

ability to source these materials in Cape Town. Frozen sheep femurs were collected directly from Sacks Butchery in Westlake, Cape Town. These bones came from food animals, and so did not have any diseases. The baboon femurs were sourced from researcher Calvin Mole in the forensics department of University of Cape Town (UCT). These femurs had been retained, untested in any way, in frozen form, and were collected from the freezer in which they had been stored. These bones were stored whole, wrapped in plastic and without any storage medium. The femurs came from baboons that were legally culled, and did not die of any disease. The ostrich bones were delivered from Klein Karoo (a company which specializes in ostrich products), with each bone individually vacuum packed and frozen. These bones were also from food animals and were healthy. The crocodile bone was delivered from Lebonheur crocodile farm, which had had an unexpected death. The animal died due to cold weather conditions, but was otherwise healthy. The refrigeration conditions between the death of the animal and the bones being received is unknown. Once received, the crocodile femurs were stored under the same refrigeration conditions as the other femurs. The gender and exact age of the animals from which the bones came was unknown for all species. Specimens were machined from these bones in two series, described presently.

3.1.1 First machining series

Each bone was removed from the freezer and allowed to gradually defrost to room temperature before machining. One species was worked with at a time to avoid accidental mislabelling. A utility knife was used to scrape off any excess flesh or membrane from the outside surface of the bone. The central portion of the diaphysis (the mid-diaphysis) was cut from the bone, as is shown in Figure 3.1.

In the case of the baboon bone, sections of the diaphysis from further towards the epiphyses were also excised. This was done as the wall of the mid-diaphysis was very thin, making machining specimens very difficult. This was done only in the

first machining series. For each baboon bone specimen it was clearly noted down whether it was from the mid-diaphysis, or from the 'end' of the diaphysis.

The hollow section of bone was then cut longitudinally into strips, as seen in Figure 3.2. Each of these strips was then ground down with a belt-sander to a roughly cylindrical shape on one end. This was done to allow the bone to be held securely in the chuck of a lathe for further machining. This also ensured the bone would run straight when being turned, that is, it would not wobble due to being held off-centre. These bone pieces were then turned on a lathe into smooth cylinders. Once cylindrical, small pieces were sectioned off at the appropriate length to form a small, cylindrical bone specimen (Figure 3.3).

The cortical bone in the majority of species tested was found to be thin in comparison to what was found in bovine bone [12]. This lead to small specimen diameters. In the case of the baboon, crocodile and sheep bone, the general dimensions of each specimen were 2.5mm in diameter, and 3mm in length. The cortical thickness was higher in the ostrich bone, and hence the ostrich specimens had general dimensions of 3mm in diameter, and 4mm in length.

The sectioning process left each specimen with a small protrusion on one face. The specimen was taken and the flawed face sanded using a fine grit sand paper to remove this protuberance. The diameter and the length of the specimen were then measured and recorded. Each specimen was stored in a clearly labelled specimen jar, in normal saline solution. These were transported to the bio-freezer at the Blast Impact and Survivability Research Unit (BISRU) wet lab and stored frozen at -32°C until needed.

Figure 3.1: A section of sheep bone cut from the mid-diaphysis, and a small portion cut from the end of the diaphysis.

Figure 3.2: A strip of bone removed from a mid-diaphysis section, before shaping.

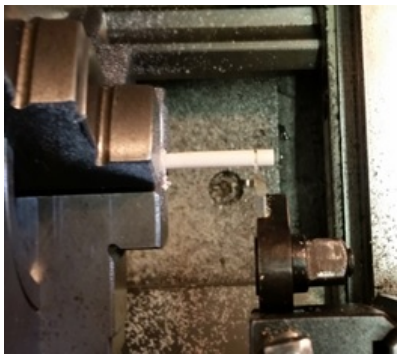

Figure 3.3: A smooth cylinder of machined bone in the lathe, with the specimen almost cut free.

3.1.2 Second machining series

A second series of specimens was machined at a later time to allow for the assessment of degradation within the material due to longer specimen storage times. The whole bones remained frozen, in the same conditions as before machining of the first specimen series. The same machining process was followed as in the first series, and the samples were stored in the same conditions that the first specimen series were exposed to, but were frozen for a longer period of time before testing. This second series of specimens were of the same general dimensions as the first series, and an additional measurement of weight was taken to allow for an apparent density to be calculated. The baboon specimens had an average apparent density of $2.111 \pm 0.043\text{g/cm}^3$, crocodile specimens an average apparent density of $1.970 \pm 0.042\text{g/cm}^3$, sheep specimens an average apparent density of $2.000 \pm 0.058\text{g/cm}^3$, and ostrich specimens an average apparent density of $2.017 \pm 0.035\text{g/cm}^3$. In addition, before machining, the position around the circumference of the bone was marked (shown in Figure 3.4) to provide a record of whether each specimen came from the anterior or posterior of the bone.

After being thoroughly scraped down with a craft knife to allow the marker to stick to the surface of the bone, the diaphysis was divided and clearly marked using different coloured markers. The anterior and posterior borders were marked first. The anterior border was marked as from the center of the front of the knee joint, to the anterior central portion of the anatomical neck of the hip joint (shown in Figure 3.4a). Likewise, the posterior border was marked from the center of the back of the knee joint to the posterior central portion of the neck of the hip joint (shown in Figure 3.4c). The left and right edges were then marked at roughly the center of the corresponding left or right side of the bone (shown in Figures 3.4b and 3.4d). Using these borders, the bone was divided into anterior and posterior sections.

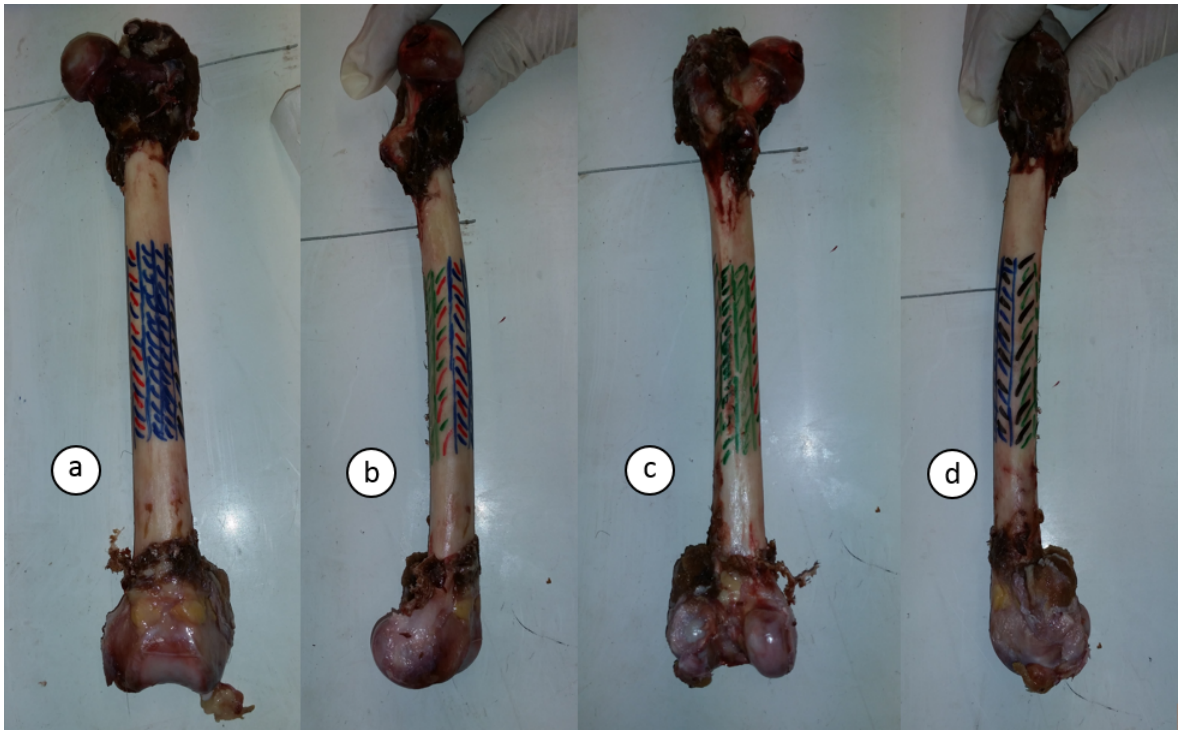

Figure 3.4: Photographs of the positional markings made on a baboon bone.
(a) The markings on the anterior side of the bone, with the anterior border marked by the most central blue line. The anterior surface is shaded in blue.
(b) The markings on the left side of the bone, with the central border marked in blue. The area shaded in red and blue is on the anterior, and the area shaded in red and green is on the posterior.
(c) The markings on the posterior side of the bone, with central green line marking the posterior border, and the posterior surface marked in green.
(d) The markings on the right side of the bone, with the central border marked in blue. The area shaded black and blue is on the anterior, and the area shaded black and green is on the posterior.

3.2 Quasistatic testing

Quasistatic testing was performed in two series. Described presently is the setup of the testing rig used, the procedures used for the first and second series of quasistatic testing, and how this data was processed to output the apparent modulus and compressive strengths of the specimens tested.

3.2.1 Test rig setup

For the first series of quasistatic tests, a Zwick quasistatic testing machine in the Centre for Materials Engineering (CME) at UCT was used. The full setup is pictured in Figure 3.5. The Zwick was set up for compression testing, utilising a 10kN load cell. A small attachment, consisting of a cylindrical, flat ended piece of metal with a pin hole for easy attachment, was connected to the load cell to provide a wide flat surface with which to compress the specimens. A larger, existing cylindrical stand was used to provide a base for the experiments. On top of this was placed a small slab of tungsten carbide, as it would provide a smooth, hard surface that would not yield under the expected stresses. This slab was utilised in calibration, and throughout testing as the base surface on which the specimen was placed. A perspex safety guard was placed around this set-up to ensure that, should a specimen shatter, no person or equipment would be damaged. The space between the perspex safety guard and the base of the set-up was packed with paper towel, so as to prevent any bio-material from accidentally falling into the machinery.

The second series of quasistatic testing was performed on an Instron quasistatic testing machine, which functions in the same way as the Zwick used in the first series of tests. These tests were performed with a 5kN load cell, but as the expected maximum load was 2.5kN, this was not an issue. In actuality, this load cell was more appropriate for the expected loads and would be more sensitive, providing clearer

representation of the material response. There were no other differences in test setup.

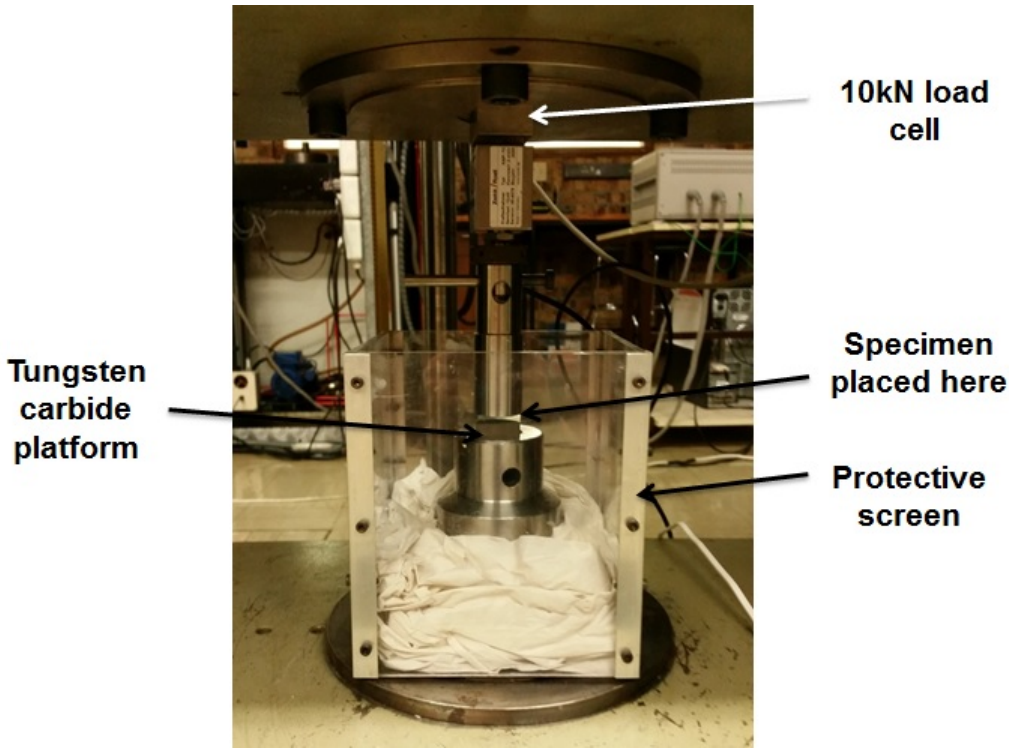

Figure 3.5: A photograph of the quasistatic test rig setup.

3.2.2 Testing procedure for the first series of quasistatic tests

Before any testing was performed on each day, compliance testing was performed on the equipment. This was done to account for the effects of machine compliance, and allow for correction of the data to remove these effects. The test rig was set up as described in Section 3.2.1, but no specimen was placed. This resulted in the compression test being performed solely on the block of tungsten carbide, which does

not yield. Hence, any compliance measured was the compliance between the machine components themselves. This was especially important to take account of when considering the scale of the testing being performed. With such small specimens, and consequently such small displacements required for strain to be experienced, even a low compliance within the machine had a large effect. Five compliance tests were performed on each day of testing at a low strain rate, until a total stress of 2kN or slightly above was reached. This output force (in N) vs travel (in mm) data. For each test, this produced a graph which was roughly linear, an example of which can be seen in Figure 3.6. The average slope of this graph was calculated for each of the five tests, and these five values were averaged to provide a value of compliance in mm/N.

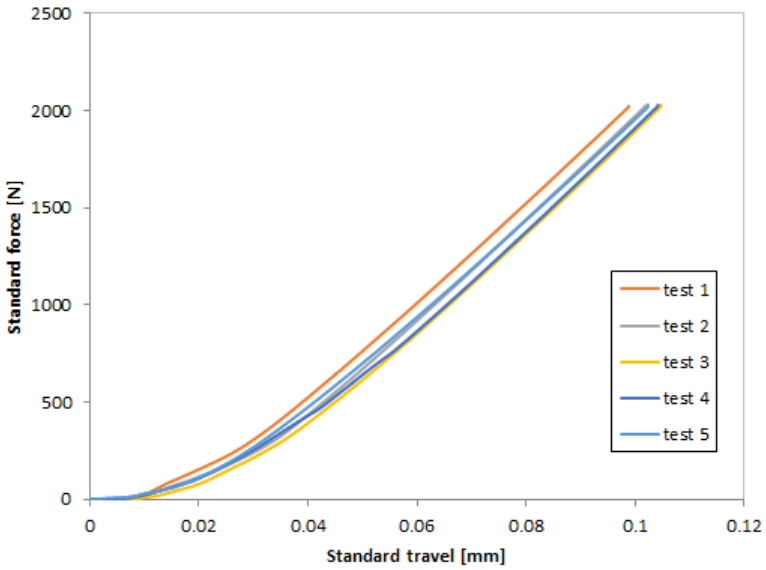

Figure 3.6: An example of the standard output of the compliance tests performed in a single day.

Five specimens from each species per strain rate were selected at random from the first series of specimens machined. The frozen specimens were removed from the freezer and allowed to thaw. They were then removed from their saline solution, and

any excess saline clinging to the specimen was removed by dabbing gently with paper towel. Just before testing, the diameter and length of each specimen was measured a second time. The tungsten carbide platform was removed from the setup to allow for easier placement and alignment of the specimen on the platform, as attempting to place the specimen onto the platform while it was still within the perspex enclosure was awkward and more likely to result in the specimen being dropped. The specimen was placed with one of its flat faces down, such that the cylinder stood upright, on the small slab of tungsten carbide. The platform was placed back into the rig with the specimen positioned at its center. The tungsten carbide platform was placed such that the specimen was also at the center of the upper compressing platform. The upper testing platform was manually lowered to just barely touch the specimen's upper surface. This was done to reduce the amount of time needed before the test started, and to prevent a sudden stress increase when the testing surface suddenly comes into contact with the specimen. The digital readout on the computer was monitored to ensure that no pre-load was being imposed on the specimen.

Compression tests were performed at strain rates of $10^{-1}s^{-1}$, $10^{-2}s^{-1}$ and $10^{-3}s^{-1}$. At each strain rate, specimens were tested in a random order (that is, not testing one species, then the next etc.) so as not to introduce any additional bias into the data. The test was stopped after the specimens began to display non-elastic behaviour, as the primary focus was on the elastic region of the material response. Each strain rate was tested in a day, to minimise any possible differences in testing that may occur over several days. A light microscope connected to a camera and computer was used to observe and photograph the majority of the specimens after testing. An example of these photographs can be seen in Figure 3.7. The analysis of the failure modes observed was outside the scope of this research, but these photographs have been labelled and stored for later use, along with the remains of the tested specimens.

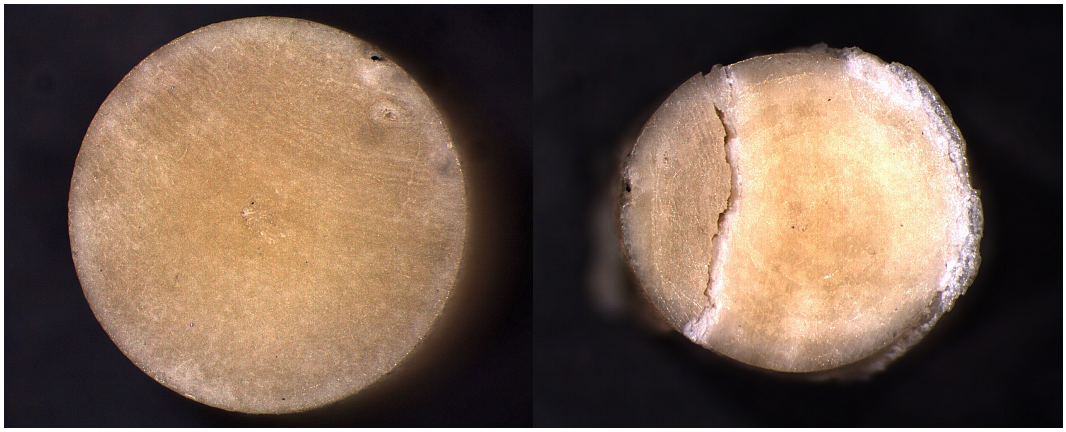

(a) (b)

Figure 3.7: An example of the photographs taken of the first series of quasistatic specimens.
(a) A photograph of a specimen of ostrich bone before testing.
(b) A photograph of the same specimen of ostrich bone after testing.

3.2.3 Testing procedure for the second series of quasistatic tests

In the same manner as in the first series of tests, compliance testing was performed on the equipment each day before testing occurred. However, only three compliance tests were performed each day, as this was deemed sufficient to obtain an accurate average. These compliance tests were performed with the same procedure as described in Section 3.2.2.

The specimens used on each day of testing were selected randomly from the second series of specimens. They were thawed gradually to room temperature. Once removed from their specimen jar, any excess saline was dabbed off with paper towel. At this point, each specimen to be tested that day was weighed and measured. Aside from the addition of weighing the specimens, the test procedure was the same for the first and second series of quasistatic tests (refer to Section 3.2.2).

On the first day of testing, three specimens per species were tested, two at a strain rate of $10^{-2}s^{-1}$, and one at a strain rate of $10^{-1}s^{-1}$. This was done so as to determine whether or not there had been material deterioration (as discussed in more detail in Section 5.1). These strain rates were chosen as they were the quickest to test, and allowed for the quickest determination of deterioration. After this data was analysed and material degradation confirmed, further tests were done to bring the number of tests per strain rate up to three. On the second day of testing, three specimens were tested per species, at a strain rate of $10^{-3}s^{-1}$. On the third and final day of testing, three more specimens were tested per species, this time with one at $10^{-2}s^{-1}$ and two at a strain rate of $10^{-1}s^{-1}$.

3.2.4 Quasistatic processing

This section reviews the processes applied to the data gathered from the quasistatic testing. It aims to make clear how the final data was arrived at.

The data collected from the Zwick software was the force (in N) and displacement (in mm) history over the time taken during the test. The very first correction made was the compliance correction. This was done first so that all further analysis would be on the material response only. The compliance value from the compliance tests (described in Section 3.2.2) gave a value for the amount of displacement taking place in the machine for each newton of force applied. This was subtracted from the measured displacement to provide the actual displacement within the specimen for

the measured force. This can be seen in Figure 3.8 as the change between line one and line two (which largely overlaps with line 3). As is clearly displayed, due to the small scale of the specimens, the effect of machine compliance was significant, and had a large affect on the assessment of the apparent modulus of the material.

The data in the elastic region had small changes in gradient along its length. These changes in gradient could be due to settling between the specimen and the machinery, imperfect specimen alignment, or small partial failures due to porosity or pre-existing microdamage in the specimen being tested. All of these factors would cause a minor decrease of the apparent modulus of the specimen. Therefore, the most accurate representation of the material property would be at the maximum gradient. To give an accurate representation of the gradient, the data was linearised. The gradient of the compliance corrected data was assessed for the entire near-linear portion of the data, and the maximum gradient was pin-pointed. Then, either 100 data points (for testing at strain rates of $10^{-3}s^{-1}$ and $10^{-2}s^{-1}$) or 10 data points (for testing at strain rates of $10^{-1}s^{-1}$) on either side of this maximum point were used for regression analysis to find the most accurate gradient i.e. the apparent modulus. The gradient was then used to remove the take-up region at the beginning of the test (seen in Figure 3.8 as the change between line two and line three). This take-up region was a result of the specimen and machine settling at the beginning of the test as they came into full contact with one another, and was affected by any surface irregularities in the specimen. This take up region is an artefact of testing and does not represent the properties of the material, and was hence removed.

Finally, the displacement was corrected to show the true behaviour of the material by shifting the data such that the x-intercept was zero. This is displayed in Figure 3.8 as the change between line three and line four. This process was repeated for each specimen that was tested. For each specimen, the 0.2% offset yield strength and the maximum compressive strength was also noted.

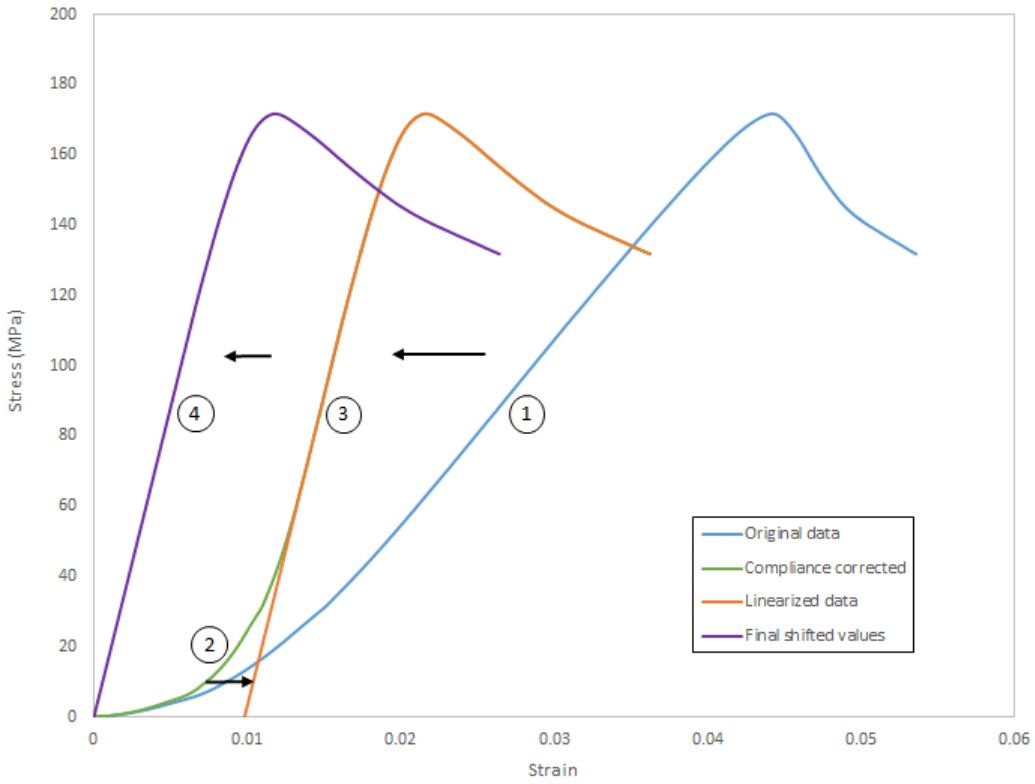

Figure 3.8: The full progression of refinements made to the quasi-static data.

To present the compressive strength of the material examined, it becomes necessary to consider the shape of the failure curves, or the stress-strain curves, displayed in the data. Examples of the curves seen in the data can be seen in Figures 4.1 through 4.4 in Chapter 4. Most commonly, the stress-strain curve increased in a fairly linear manner, followed by a short non-linear portion as failure began, up to some maximum compressive stress. This would be followed by a continuously decreasing load-bearing capability. In the more dynamic strain rate region, the most common curve shape again displayed this linear increase, but this was then followed by a sharp, severe drop at the maximum stress. This was due to the much more abrupt, complete failure frequently found in the higher strain rate tests. Often specimens were crushed entirely, whereas in the quasistatic regime, the specimens

were often collected in a singular piece after testing, or in a few large pieces still held fairly well together.

However, in certain cases, the stress-strain curve displayed an alternate behaviour. In these cases, the specimen displayed the expected initial linear increase, but then continued to sustain load at a gradient that was very shallow compared to the initial linear increase, as seen in Figure 4.2 in the curve representative of the second series of $10^{-1}\mathrm{s}^{-1}$ tests (solid orange line). In these cases, the maximum strength is not clearly defined.

To compare the compressive strength of the specimens, the 0.2% offset stress was calculated (as marked in Figure 3.9). The 0.2% offset method was chosen as in many cases, there was no clear point at which the linear portion of each graph ended, instead showing a fairly smooth transition from linear response to incipient failure region. In a few cases, when specimens displayed a severe drop in load-bearing ability, the 0.2% offset stress was clearly after the failure region (see Figure 3.10). In these cases, the 0.2% offset is not an accurate representation of the material property, and the maximum compressive stress was reported in its place. Also noted was the maximum strength. In the few cases where the maximum strength was not apparent, the 1% offset stress was noted in its place (see Figure 3.11). This percentage was chosen as it seemed to be the percentage that most accurately coincided with the maximum stresses in graphs that did have a maximum stress.

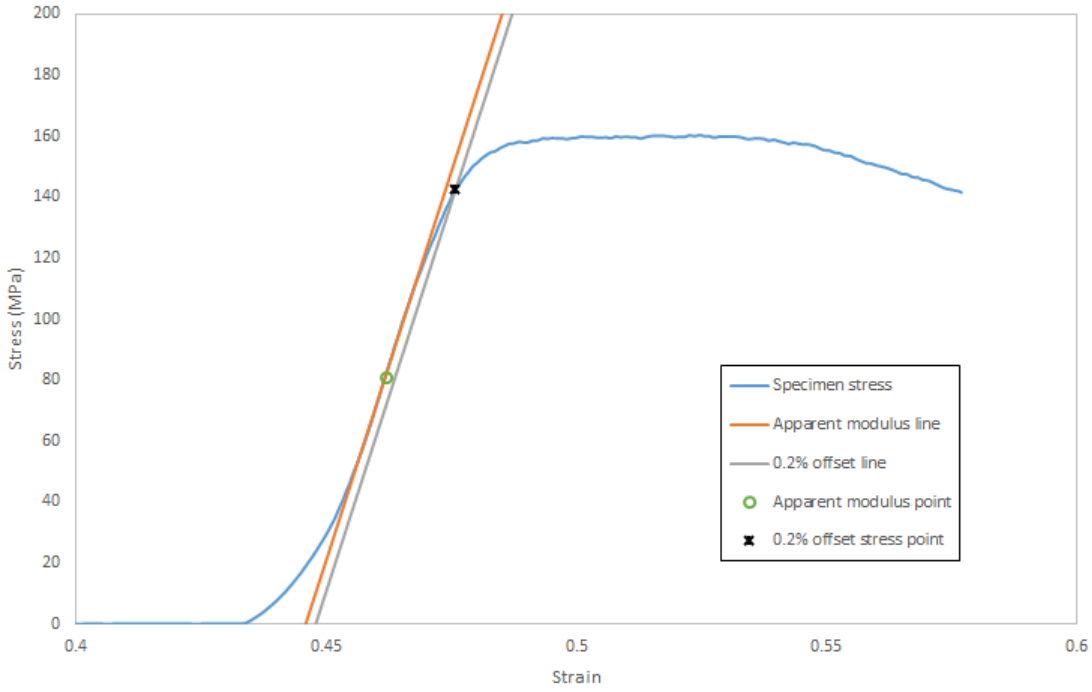

Figure 3.9: A graph showing the general method used to obtain the 0.2% offset stress. Both the point around which the apparent modulus was estimated, and the point at the 0.2% offset stress are marked.

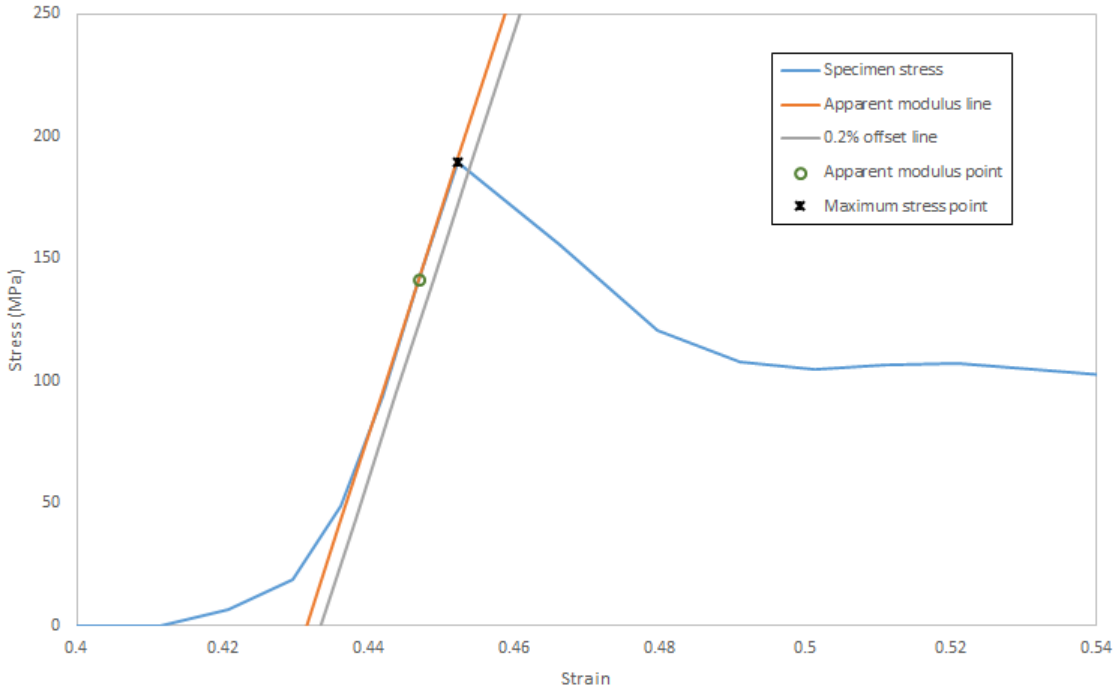

Figure 3.10: A graph showing a case in which the 0.2% offset stress is after the failure region. Both the point around which the apparent modulus was estimated, and the point of maximum stress are marked.

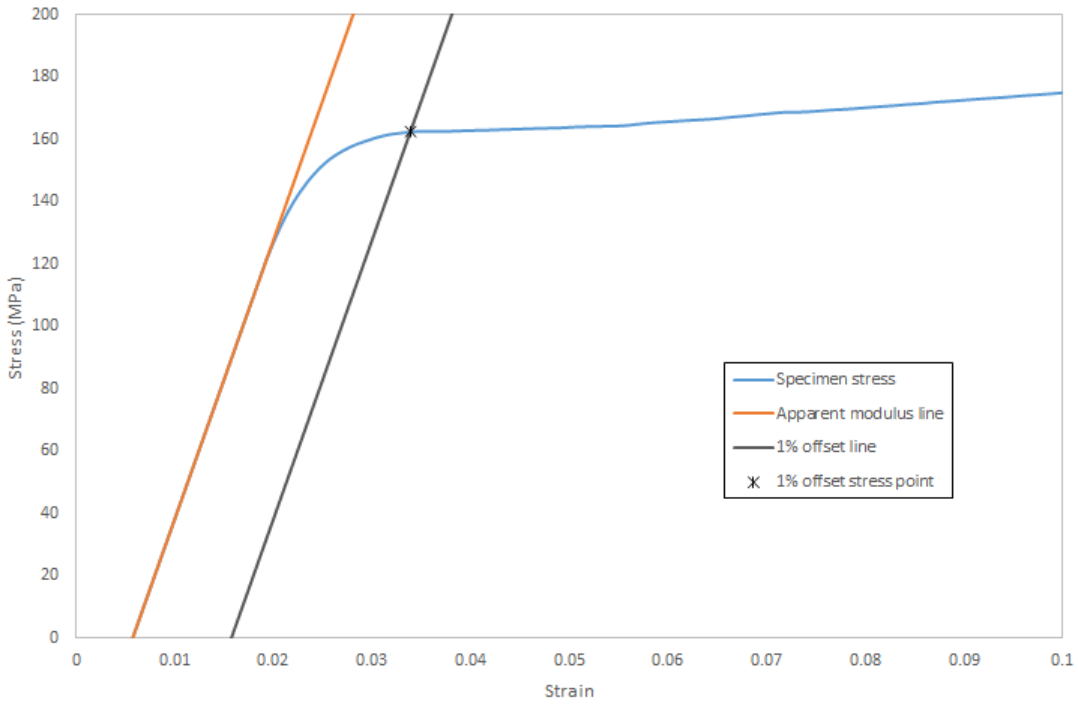

Figure 3.11: A graph showing a case in which the maximum strength is not apparent, with the 1% offset strength marked.

The raw data collected from the Instron software was also in terms of displacement (mm) and load (N) over the length of the test. The same processing was applied as for the first series of quasistatic testing.

3.3 High intermediate strain rate testing

This section describes the design and use of the specialised equipment needed for testing bone at high intermediate strain rates. Also included is a description of how this equipment was assembled and calibrated, and how the data output from this testing was processed.

3.3.1 The design of the specialized equipment

To test small specimens of cortical bone at strain rates between $40s^{-}1$ and $200s^{-}1$, specialized equipment was required. These strain rates cover the upper end of the intermediate range, as well as the lower end of the dynamic range. For ease of reference, the range of investigated strain rates will henceforth be referred to as the upper intermediate or the high intermediate range. Two modifications to a standard SHB setup were investigated, namely the use of a CiT striker (see Section 2.8.1) and the use of a tandem momentum trap (see Section 2.8.2).

3.3.1.1 The design of the Cone-in-Tube striker

The CiT striker design is based on the work done by Cloete et al. [33] and Paul [12]. The purpose of a CiT striker is to provide an increasing stress pulse to allow for a constant strain in the specimen (see Section 2.8.1).

Three cones were designed based on the apparent moduli measured in the first series of quasistatic testing. One was for the lowest estimated average apparent modulus (11 GPa for the crocodile specimens), one was for the mid-range estimated apparent moduli (13-14GPa for the sheep and baboon specimens), and one was for the highest

estimated apparent modulus (17GPa for the ostrich specimens). These estimated slopes were used in conjunction with a numerical model of the wave generated by a conical striker, which was used in previous work done at BISRU and reported on in Cloete et al. [11], to discern the correct dimensions for each cone. In each case, the length, the large diameter of the cone and the small diameter of the cone were adjusted within the model until the gradient of the obtained wave and the estimated apparent moduli were the same. The wide end of the cone was limited by the inner diameter of the available gas gun barrels, as the entire CiT assembly was required to fit within the barrel.

The end diameters determined in the model were used to create a smoothly tapering cone. Extra length was left at the large end and threaded for attachment to the tube, and a lip that abutted the tube edge was also included. This threaded portion was the same for each cone, allowing the tubes to be interchangeable. An example of the striker can be seen in Figure 3.12, and the dimensions of the cones used are recorded in Table 3.1.

Figure 3.12: An example of a cone used in a CiT striker.

Ideally, the tube and the large end of the cone would be impedance matched to allow for the wave in the tube to dominate the reflected pulse in the cone. In practice, exact impedance matching was not possible, as the tubing used needed to be a standard size that could be acquired locally, and the cross-section of the tube was somewhat smaller than required. Testing showed that this was not problematic, and that the smaller diameter tube still worked correctly.

Table 3.1: The dimensions used for each cone to accommodate the range of estimated apparent moduli.

Average apparent modulus for which the cone was designed (GPa)	**Diameter of the wide end of the cone (mm)**	**Diameter of the small end of the cone (mm)**	**Length of the cone (mm)**
11	24	6.5	850
13 - 14	24	7.4	850
17	24	8.3	850

In the original design by Paul [12], the tube was made out of aluminium 6063. However, the incident and transmitter bars used in this research were aluminium, as opposed to the steel bars used by Paul, and the specimens were much smaller here than the bovine specimens used by Paul. To accommodate for this, the striker was further modified. The outer tube was made from steel, and made shorter than the cone. This allowed for an earlier release of the stress wave. It also allowed for easier use of the tandem momentum trapping system, as the cone could be placed up against the incident bar without requiring the momentum trap (which was level with the incident bar when in use, see Section 3.3.1.2, Figure 3.17) to pass through the reaction mass supplied for the tube. The assembled CiT striker is pictured in Figure 3.13. A small internal support was added in the tube at the thin end of the cone to keep it centred within the tube, as seen in Figure 3.14.

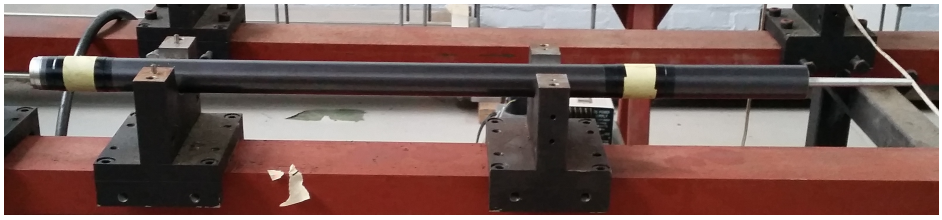

Figure 3.13: An assembled CiT striker with a shortened steel tube and an aluminium cone.

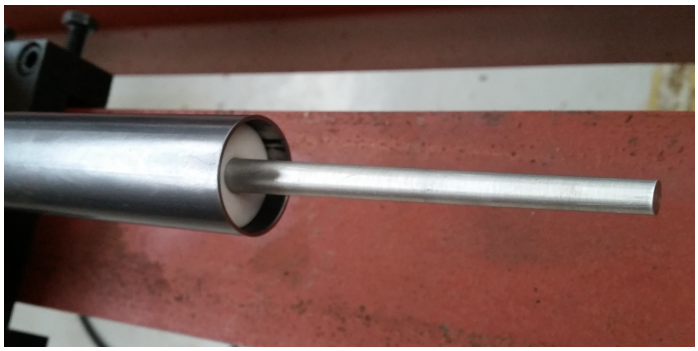

Figure 3.14: The inner support in a CiT striker keeping the cone centred.

3.3.1.2 The design of the momentum trapping system

The momentum trapping system investigated was based on the tandem momentum trapping system presented by Prot and Cloete [13] (see Section 2.8.2). The momentum trapping system was investigated in hopes of preventing reloading of the specimens during testing and allowing the specimens to be recollected post-testing for later assessment. It consisted of two nested aluminium tubes, made from the same material as the incident bar, namely aluminium 6063. These two tubes were size controlled such that the impedance in each tube matched that of the incident bar. The tubing diameters used were chosen as they were the only stock sizes that could be obtained that both matched impedance with one another and the incident bar, as well as nested neatly within one another.

The collars utilised to connect the incident bar, inner and outer traps were designed to specifically allow separation at key points during testing. This collar design is the main difference between the work being presented and the original work by Prot and Cloete (see Section 2.8.2).

The inner collar, which connected the incident bar to the inner trap, screwed onto the incident bar and rested against the inner trap. The interface between collar and inner momentum trap was stepped, as shown in Figure 3.16. The purpose of this stepping was to provide the smoothest path through which the stress waves could travel while minimising the machining needed. It also allowed free motion of the components relative to one another, allowing separation of the inner trap from the collar. The interface between the incident bar and the collar was a shallowly tapered thread (seen in Figure 3.15). This taper was to prevent the loosening of the collar during testing, as well as minimising interference of the transmitted stress waves.

Figure 3.15: The momentum trap collars showing the inner connections (inner collar on left, outer collar on right).

The outer collar, connecting the inner trap and outer trap, was similarly constructed, with the inner trap to outer collar interface being stepped and the outer collar to outer trap interface consisting of a shallowly tapered thread, as seen in Figures 3.15 and 3.16.

Figure 3.16: The momentum trap collars showing the outer connections (inner collar on left, outer collar on right).

Table 3.2: The dimensions used for the momentum trap and incident bar setup.

Part	**Length (mm)**	**Inner diameter (mm)**	**Outer diameter (mm)**
Incident bar	3000	/	20
Inner trap	1450	21.78	29.57
Outer trap	1200	31.5	34.1

The trap lengths were designed so as to allow all components to be sufficiently supported, as well as to allow for strain gauging of the incident bar near its mid point. The dimensions used for this system are as reported in Table 3.2.

Ideally, the collars would be made from the same material as the momentum traps, for impedance matching. However, a shear analysis was performed, and it was found that the inner collar would not survive the expected forces if manufactured from aluminium. The inner collar was therefore made from titanium. The outer collar was large enough that aluminium was sufficient. In practice, it was found that

the outer collar was prone to damage while in use. This occurred after the initial separation of the traps. During use, it was found that the traps were separating and then reconnecting. During this reconnection, the alignment was not ideal, and caused damage to the steps of the outer collar. This was counteracted by adding two alignment collars between the inner and outer traps, with one of them placed as close to the outer collar as possible.

The incident bar within the inner trap was supported by two internal Teflon supports which were press-fit into the ends of the inner trap. The fully supported system can be seen pictured in Figure 3.17.

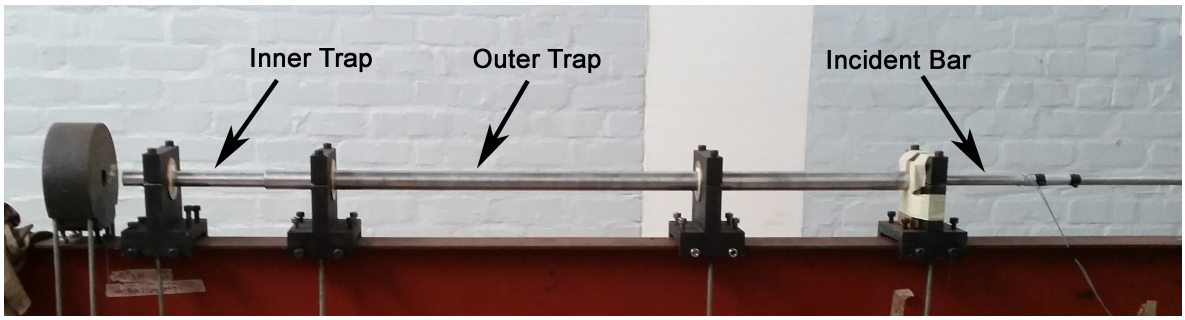

Figure 3.17: The full system of nested momentum traps.

In practice, it was found that the momentum trapping system was not separating correctly. While the original system worked excellently for larger specimens tested with larger stress waves [13], there were two key differences in this testing that proved problematic for a system with these dimensions. Firstly, the size of the specimens used in this research was very small, markedly smaller than bovine specimens. This led to smaller stresses being required during testing. Secondly, an aim of this research was to collect data as far into the intermediate strain rate range as possible. This too led to small stress pulses generated at low velocities. While the momentum traps were made of aluminium, they were still required to be fairly long, to allow for the test durations required. This led to a system where the waves used in testing were not large enough to reverse the momentum of the trapping system itself. Therefore,

the momentum trapping system was disengaged during testing. This meant that the specimens could not be recovered after testing for further evaluation of failure, however it did not affect the measurement of the mechanical properties being assessed, namely the strengths and apparent moduli.

Future iterations may benefit from a reduction of the diameters of the bars used. This would reduce the mass of the trapping system without altering the lengths of the bars, which are necessary to obtain the required test duration. However, this second iteration of design and testing fell outside the scope of the presented research, as the collection of specimens post dynamic testing was not a main goal of the study.

3.3.2 Assembly and alignment of the full SHB system

Once all components were completed, the final step before alignment was to attach the strain gauges. Two strain gauges were placed diametrically opposite one another on the incident bar, at a distance of 1.25m from the specimen face. Another two were placed diametrically opposite on the transmitter bar, at 0.29m from the specimen face. The specifications of these gauges are captured in Table 3.3, and the full specifications of the utilised data capture system are described later in this section.

The alignment was an important and challenging aspect of assembly. First, an appropriate gas gun barrel was selected and installed, with an assembled CiT striker loaded. The barrel was checked with a spirit level, and the supports were assessed with a set square and spirit level to ensure it was properly level and aligned. Two alignment collars were placed around the tube of the CiT striker. This provided a better fit within the barrel, but did not prevent proper motion. The reaction mass was placed next. Both the spirit level and set square were used, as well as ensuring that the striker tube abutted the mass correctly. Next was the outer momentum trap tube. The trap system was aligned one component at a time, from the outside in, as each internal component was partially supported by the structures around

it. For the outer trap, it was ensured that it could move freely within its supports, as well as being both level and correctly radially aligned with the opening of the reaction mass. A protective piece of wood was placed up against the support at the outer trap end furthest away from the reaction mass, to prevent the trap from being damaged should it impact the support. The inner trap was then placed, running freely within the outer trap and its own support, and running through the reaction mass unobstructed. This was followed by the incident bar, which ran through the inner trap as well as its own supports. The challenge was in the fine tuning of each component so that they not only nested correctly, with all components level, but that they also ran freely without binding along the lengths required during the testing. Lastly, the transmitter bar was aligned.

A small, open-topped box was placed underneath the specimen area to catch the specimen during or after testing. A piece of A4 paper was adhered to the side of the nearest support, able to be easily flipped over the test area, as well as easily folded back. This was to prevent any fragments from being projected away from the test area, and instead be redirected down into the specimen collection box. It did not directly interact with the bars, and did not interfere with the test itself.

For the purposes of calibration, a light trap was required. The sensors were already available, and a sleeve with grub screw to secure the device to the gas gun barrel during use was manufactured. This light trap simply fit over the outside of the barrel, which had four pre-existing holes (two sets, diametrically opposed) in the correct configuration for the use of the sensors already present. This light trap was connected to an oscilloscope. As the striker passed through the barrel, it passed through first one set of the opposed light sensors, and then the other. This output two clear waves on the oscilloscope. The distance between these two waves was the time taken for the front of the striker to pass from the first to the second set of light sensors. As the distance between the two sensors was known, the velocity of the striker could then be calculated. The strain gauges were connected to a data capture computer already set up in the workspace. The amplifiers used were custom built, had a gain of 1000, and were operated at a bandwidth of 100kHz. The data capture

Table 3.3: The specifications of the strain gauge and data capture system.

Parameter	Value
Gauge factor	2.14
Gauge resistance	120Ω
Gain in amp	1000
Bridge voltage	4,02V
Number of arms in half Wheatstone bridge	2

computer used an ADLINK PCI-9812 data capture card, sampling at 10MHz and with 12 bit resolution. The specifications of the strain gauge and the specifications of the data capture system needed for calculations is recorded in Table 3.3.

3.3.3 Calibration factor calculation

A SHB setup requires calibration before use. The purpose of this calibration was to determine the correct conversion factor to convert the output voltages from the strain gauges into stresses. To do this, the weight and dimensions of the incident and transmitter bars were measured to calculate the density of each. The distance from the centre of the incident bar strain gauge to the end of the incident bar, and the distance from the beginning of the transmitter bar (that is, the face that interacts with the specimen) and the centre of the transmitter bar strain gauge was measured.

A test with solely the incident bar was performed, using a uniform striker, to generate a clear pulse, as seen in Figure 3.18. A small buffer of deformable material was placed on the striker side of the incident bar before testing, to produce a smooth wave with minimal oscillations. As can be clearly seen in Figure 3.18, the generated pulse

travels through the strain gauge, reaches the end of the bar and is reflected back. The time taken for the pulse to travel this distance can be ascertained by inverting the wave and adjusting the time displacement until the reflected pulse overlaps the initial pass of the pulse entirely. The change in time is then the time taken for the pulse to travel to the end of the bar and back again. This time, in combination with the measured distance from the strain gauge to the end of the bar, was used to calculate the speed of sound in the incident bar.

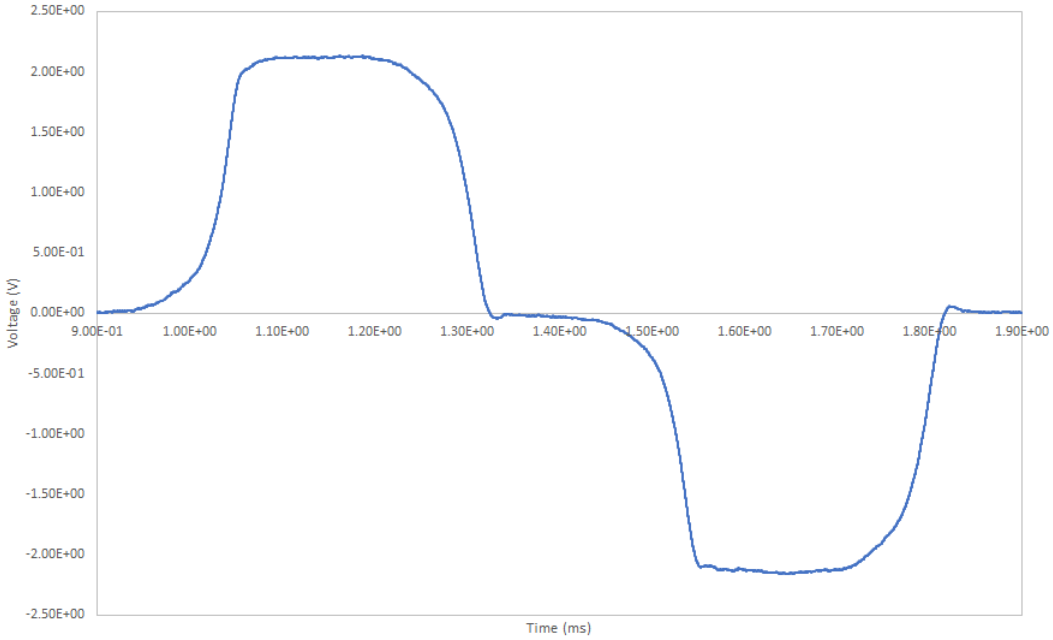

Figure 3.18: The pulse generated by the incident bar calibration test.

A second calibrating test was then performed with both the incident and transmitter bars in place, with no specimen. This generated a wave that passed clearly from the incident bar into the transmitter bar, shown in Figure 3.19. As the time taken to travel to the end of the incident bar was known, it was possible to ascertain the time taken for the wave to transfer from the front face of the transmitter bar to the transmitter bar strain gauge. This was again done by adjusting the time differences. The input wave was shifted forward by half the time determined in

the first calibration test (as we are comparing waves at the ends of the bars, not at the incident bar strain gauge). The output wave was then shifted back until it overlapped with the forward shifted input wave. The amount of time the output wave was shifted by was then the time taken for the wave to travel from the front face to the strain gauge in the transmitter bar. This time, and the measured distance from the front face of the transmitter to the connected strain gauge, was then used to calculate the speed of sound within the transmitter bar.

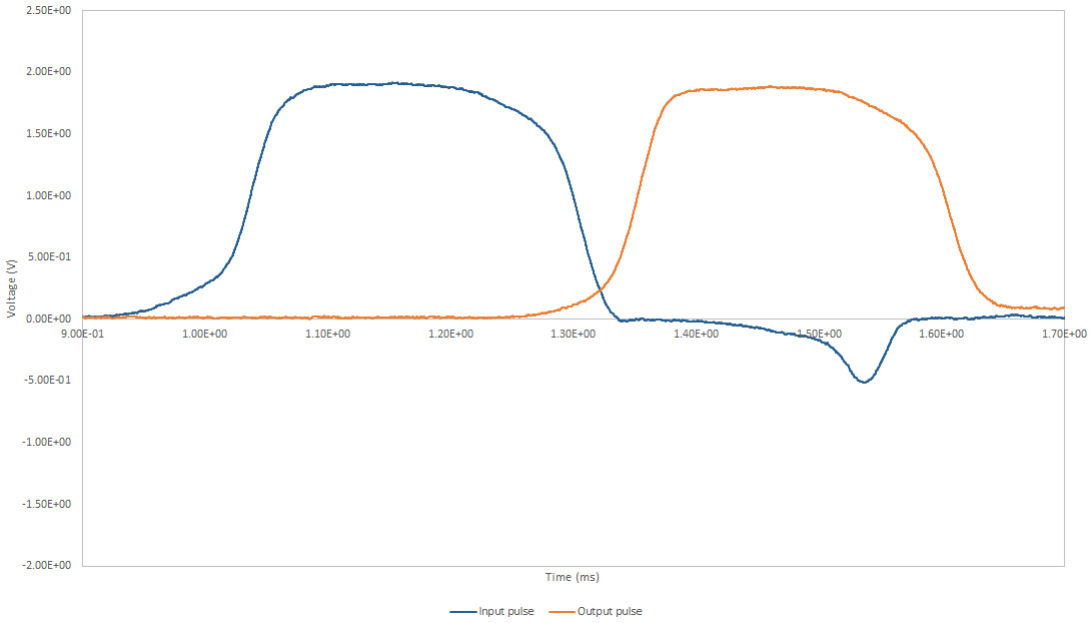

Figure 3.19: The pulses generated by the transmitter bar calibration test.

A third and final calibration test was performed, once again with only the incident bar, but without the deformable buffer in place. This was done to create a more square shaped input pulse (that is, a pulse with a sharp increase and decrease, with a maximum voltage that stays fairly constant) as seen in Figure 3.20. When this test was performed, the velocity of the striker was measured with a light trap device (as described at the end of Section 3.3.2). Knowing the striker velocity (and that the striker had also been measured and weighed, was the same material as the transmitter

bar and had the same diameter as the incident bar), the incident bar velocity was calculated using equation 2.5. Using these values, and the knowledge that stress is the product of the density, speed of sound in the material, and the velocity of the impact wave (as referenced in Section 2.9.1, eq 2.1), the maximum stress in the bar was calculated. This stress correlated to the maximum voltage, seen at the flat top of the wave, and the value of stress per volt (in MPa/V), which is also known as the calibration factor, was obtained.

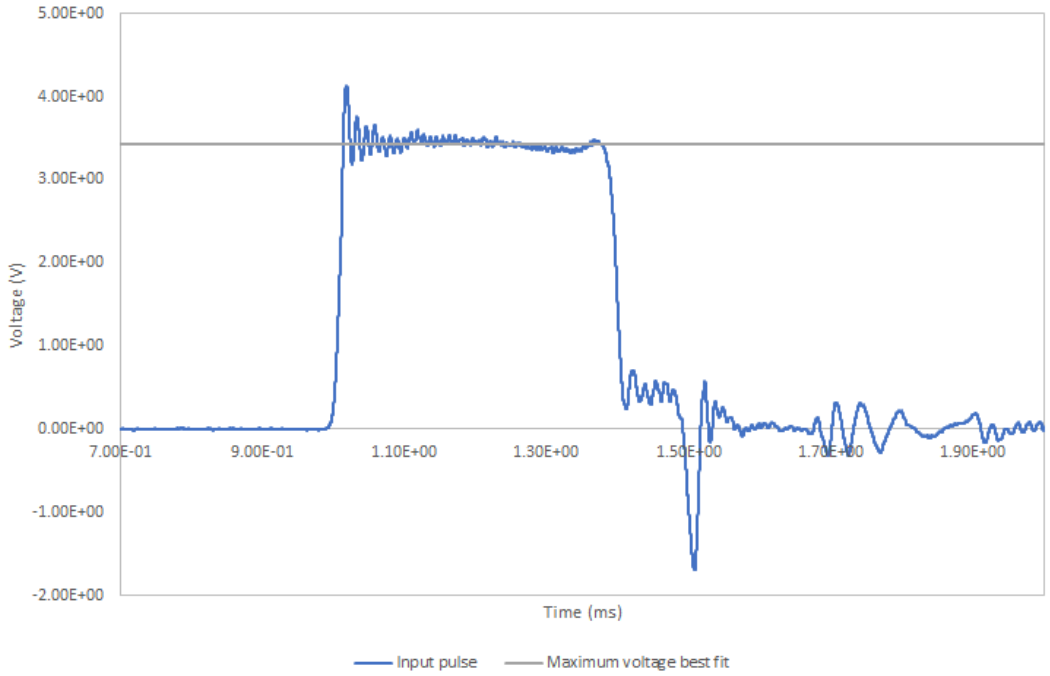

Figure 3.20: The pulse generated for the final calibration test to determine voltage-to-stress coefficient.

3.3.4 Performance of high strain rate tests

As discussed in Section 3.3.1.2, the momentum trapping system that was investigated did not work well with small specimens and low pressures, as are needed for this

testing. Hence, the method outlined herein is for the setup without the momentum traps engaged. The tubes remained in place, as they supported the incident bar, but the collars were removed. This resulted in the majority of specimens being unrecoverable after testing.

Before testing began for a given day, the number of specimens required were allowed to defrost gradually to room temperature. Once removed from the specimen jar, any excess saline was gently dabbed from the specimen with paper towel, as was done in the quasistatic testing. The specimens were weighed. The length and diameter of the specimen were measured. Both the faces of the incident and transmitter bars that would be in contact with the specimen were coated in a thin layer of petroleum jelly. This acted as lubrication and had the added benefit of aiding in the adhesion of the specimen to the bars.

The gas gun utilised for testing was originally designed for use with high pressures. In this research, low pressures were required to attain the sought after strain rates. At these low pressures, there was insufficient pressure to allow for reliable firing of the gun. Hence, to ensure reliable firing at the pressures required, the following method was developed to reduce specimen loss and minimise the time required for testing. Before each test, a loosening shot was fired to loosen the components of gas gun. To do this, the striker was pushed firmly up against the reaction mass, with the incident bar positioned so as to not be in contact with the striker. No specimen was loaded. The gas gun was brought slightly above the pressure required for the test to be performed. This extra pressure was the exact amount that would be released during this loosening shot, such that once completed, the gas gun would contain the correct pressure for the test. The loosening shot was fired. The incident bar was then positioned up against the striker, such that when fired, the tube of the striker would impact the reaction mass at the same time as the cone impacted the incident bar. The specimen was then loaded onto the center of the incident face using tweezers, and held in place on the face by the earlier applied layer of petroleum jelly. The transmitter bar was pulled up against the specimen. It was confirmed that the specimen box was correctly in place, and the paper shield was drawn over the

specimen area. Finally the striker was loaded to a predetermined position within the gas gun barrel. The data capture software was started, the test was fired and the data saved. Everything done between the loosening shot and the actual test was done as quickly as possible, as the longer the gap in time, the more likely it was that a misfire would occur. Once the data was saved, any remaining pressure in the gas gun was released, and the specimen was collected. In the majority of cases, the specimen underwent severe deformation, resulting in multiple distinct bone shards. This further justifies the investigation that was done into the use of momentum trapping (see Section 3.3.1.2), as momentum trapping could prevent some of this destruction. In rare cases the specimen survived. All recovered specimen fragments were placed back into their specimen jar to be frozen and stored. This allows for the possibility of future researchers investigating the failure surfaces of the specimens, which was outside the scope of this research, but may be interesting at a later date.

3.3.5 Higher strain rate processing

Each successful test resulted in two sets of output signals, one from each bar with a set of strain gauges, in voltage versus time. This voltage was multiplied by the calibration constant, as discussed in Section 3.3.3, to provide values of stress in each bar. This was then shifted in time to apply correctly to the ends of the bars and not the strain gauge position, resulting in values for the stress at the face of each bar that was in contact with the specimen, as can be seen in Figure 3.21.

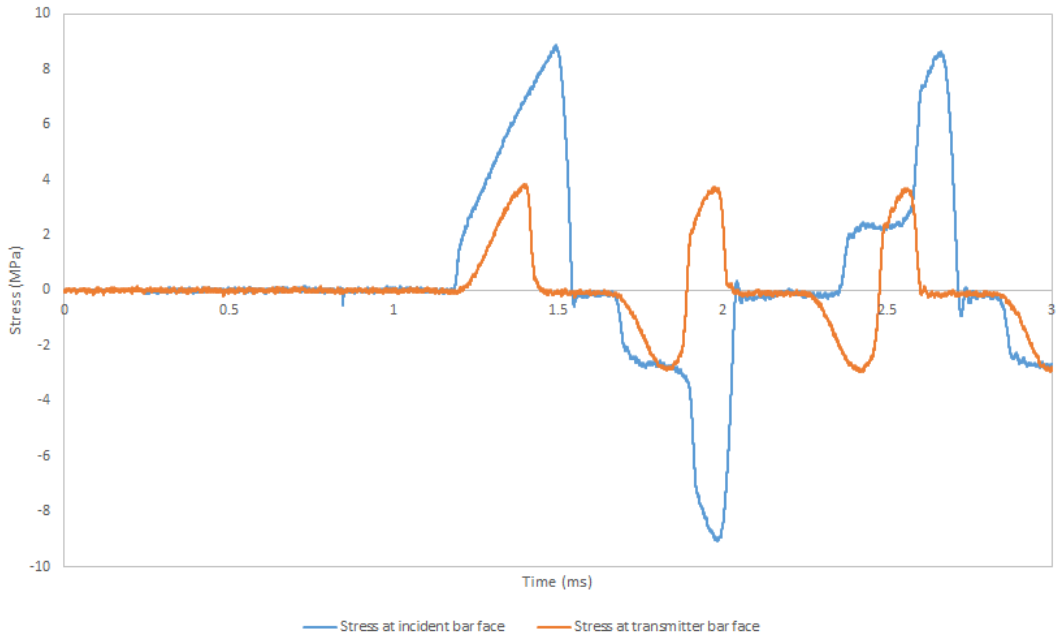

Figure 3.21: An example of the stress data output from the SHB tests.

This data was then analysed using equations 3.1 through 3.10, based on wave theory (Section 2.9.1), as well as equations directly from Section 2.9.1, to show the strain rate, strain, and stress within the specimen.

Let
Δt = time increment at which the data was sampled.

Let subscript:
$spec$ = specimen

From the SHB tests came values for the stresses in the incident and transmitter bar specimen faces throughout the test, as described earlier in this section. There is a value for the stress at each of these bar faces at every time increment Δt. Equation 2.2 in Section 2.9.1 can be rearranged to solve for the reflected stress at each time increment, knowing that the incident and transmitter bars both have the same cross-sectional area, and that the reflected stress is tensile not compressive, seen here as equation 3.1.

$$\sigma_r = \sigma_{in} - \sigma_t \tag{3.1}$$

The values of c and ρ had been measured for both the incident and transmitter bars. With this information, and the stress history from the SHB tests, equation 2.1 (Section 2.9.1) can be rearranged to solve for the velocities of the forward moving wave (v_{in}), reflected wave (v_r) and transmitted wave (v_t) at each moment in time (eq 3.2, eq3.3 and eq3.4).

$$v_{in} = \frac{\sigma_{in}}{\rho_{in} c_{in}} \tag{3.2}$$

$$v_t = \frac{\sigma_t}{\rho_t c_t} \tag{3.3}$$

$$v_r = \frac{\sigma_r}{\rho_{in} c_{in}} \tag{3.4}$$

Using these velocities, the velocity difference over the specimen was calculated (equations 2.6 and 2.7, Section 2.9.1). This value was required to calculate the strain rate at each point in time (equation 2.8, Section 2.9.1). Also required to calculate the strain rate was the instantaneous length, which changed throughout the test. This changing length affected both the strain and strain rate values. Hence to calculate the strain, strain rate and instantaneous length, a stepping method was used. That

is, at each time step, first the instantaneous length was calculated based on the previous value of strain and specimen length (equations 3.5 and eq 3.6).

$$l_1 = initialspecimenlength \tag{3.5}$$

$$l_{i+1} = l_1(1 - \epsilon_i) \tag{3.6}$$

This was followed by the calculation of the strain rate, using the newly calculated instantaneous length (eq 2.8, Section 2.9.1 and equation 3.7). Finally, the cumulative strain was calculated by using this strain rate and the time step, and adding it to the previous strain (eq 3.8 and eq 3.9).

$$\dot{\epsilon}_i = \frac{v_{(diff)i}}{l_i} \tag{3.7}$$

$$\epsilon_1 = \dot{\epsilon}_1 \Delta t \tag{3.8}$$

$$\epsilon_{i+1} = \dot{\epsilon}_{i+1} \Delta t + \epsilon_i \tag{3.9}$$

All stress experienced at the transmitter bar face is stress being experienced by the specimen. There is a significant difference between the area of the specimen and the area of the transmitter bar where they make contact. Therefore, the stress in the specimen itself is calculated by rearranging equation 2.9 (Section 2.9.1) into equation 3.10.

$$\sigma_{spec} = \sigma_t \frac{A_t}{A_{spec}} \tag{3.10}$$

After this analysis, a graph displaying the stress versus strain, and the strain rate versus strain was plotted. An example of this can be seen in Figure 3.22. This allowed for easy assessment of the consistency of the strain rate over the duration of the test. From the stress versus strain data, the apparent modulus was assessed in the same way as the quasistatic data, that is, regression analysis of a number of data points around the point of maximum gradient in the linear region of the data (see Section 3.2.4 for a more detailed description of this method). The 0.2% offset yield strength and maximum compressive strength were also noted for each specimen, again using the same method as in Section 3.2.4.

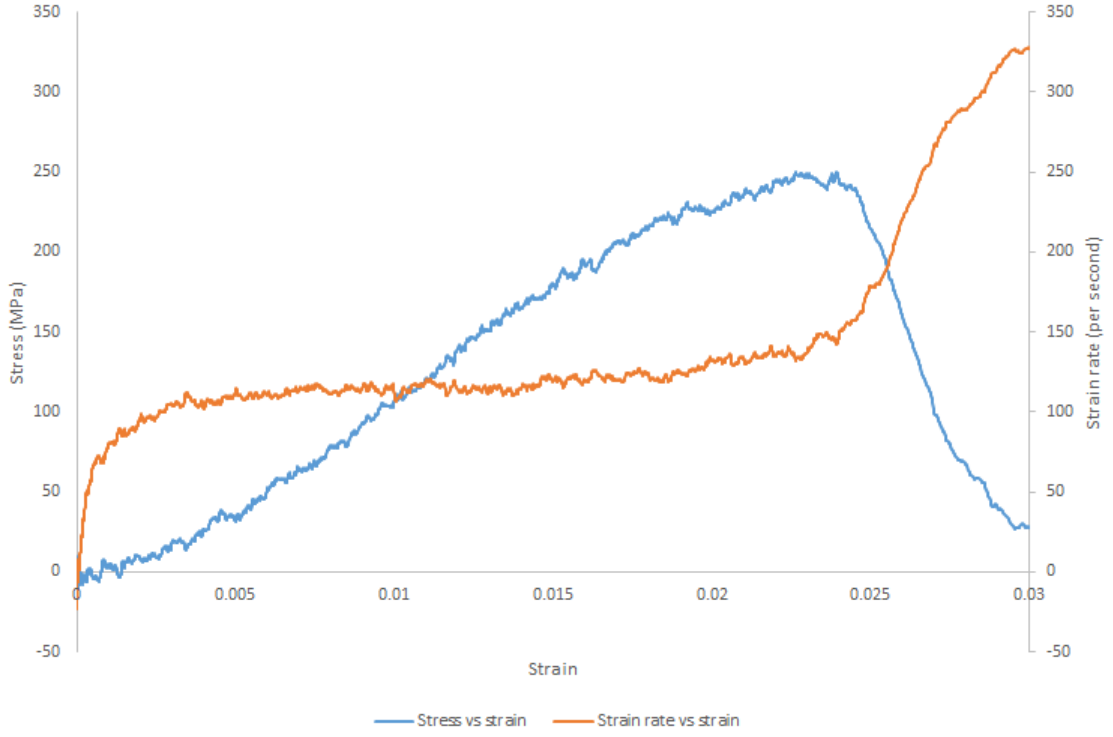

Figure 3.22: An example of the stress and strain rate versus strain data within a specimen.

3.4 Lognormal analysis of each data set

For each set of data, where a set of data was all the values of a particular property, at a particular strain rate, in a single species, the data was analysed using a lognormal distribution (as described in Section 2.9.2).

A lognormal distribution assumed that the data could be represented in such a way that the logarithm of the values, in conjunction with a constant, were normal, or near normal. This indeed described the data better than assuming a normal distribution. This is reasonable, as the data is expected to show a somewhat skew distribution, as is discussed further in Chapter 4.

As reviewed in Section 2.9.2, for data with a skew distribution, a three parameter lognormal distribution is an appropriate assessment tool. In Section 2.9.2, the equations given are for a positively skewed distribution. As the data being assessed in this research is negatively skewed (as would be expected of data clustering around an upper value), a minor change in form was required for the equations. To allow the data cluster at an upper value to be correctly displayed, the data was assessed as in equation 3.11, in place of equation 2.10 in Section 2.9.2.

$$Y = ln(\gamma - X) \tag{3.11}$$

This resulted in the following changes to the equations 2.11, 2.12 and 2.13 (originally discussed in Section 2.9.2), used to calculate mean, median and mode of the data (eq 3.12, eq 3.13 and eq 3.14).

$$Mean(X) = \gamma - exp(\mu + \frac{\theta^2}{2}) \tag{3.12}$$

$$Median(X) = \gamma - exp(\mu) \tag{3.13}$$

$$Mode(X) = \gamma - exp(\mu - \theta^2) \tag{3.14}$$

For each set of data, a value of γ was assigned that was two larger than the minimum value in the set, so as to assure the natural logarithm would not be invalid. The data was converted into the appropriate logarithmic values using eq 3.11. Then the γ value was numerically optimised to minimise skewness of the distribution of the set of log values. This was done using a skewness analysis and a goal seek function in Microsoft Excel. The numerical value of the constant γ does not affect the reading of the material property being examined, as it is removed when converting the values out of the logarithmic space. From the logarithmic set, the value of μ and θ were then calculated. This was done by calculating the average of the logarithmic set (μ) and the standard deviation of the logarithmic set (θ). From these values, the mean, median and mode in the original reference frame were calculated using equations 3.12, 3.13 and 3.14.

Chapter 4

Results

This section contains the data in its final form, after all processing, with the apparent modulus and both the 0.2% offset yield and maximum compressive strengths displayed for all species and strain rates tested.

Displayed here (Figures 4.1 through 4.4) are a selection of curves for each species, to illustrate the general shapes seen in the stress versus strain data.

Once all the data was properly processed into apparent modulus and compressive strength, they were grouped by strain rate within each species. At that point, it was noted that the data tended to cluster together in a skew distribution, not in a standard normal distribution. While the sample sizes used in this research are indeed small (with the smallest being three and the largest being eight) it was, nevertheless, evident in the data and a Monte-Carlo simulation (see Appendix B) that a lognormal fit gave a more representative summary of the data than a simple average would. It would be reasonable to expect that the properties of cortical bone specimens that contain no inherent or manufactured defects would be normally distributed. However, in practice, cortical bone specimens can have material imperfections (such as increased porosity from remodelling or increased vascularity) and manufacturing imperfections (such as asperities or induced microfractures). These imperfections

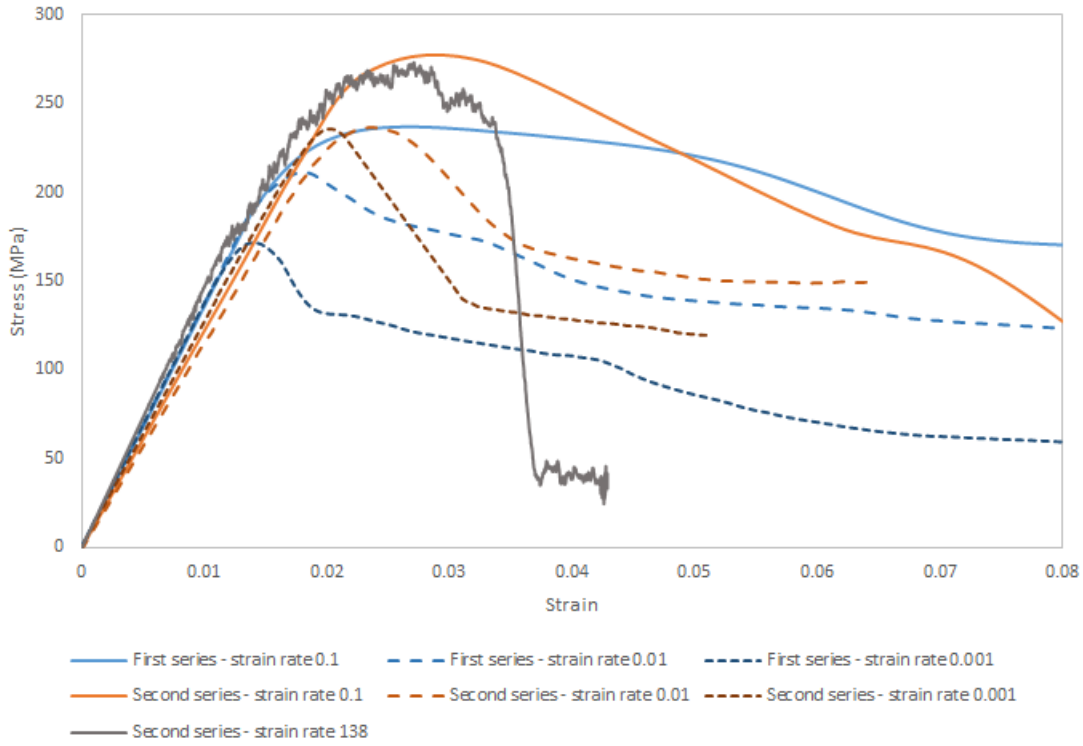

Figure 4.1: A selection of curves showing an example of the shapes of the stress versus strain curves at each strain rate tested for baboon bone.

would be expected to decrease the observed strength and stiffness. Hence, it is likely that a skew distribution would be observed, with the true material property clustered at the upper end of the distribution. If a normal distribution was used to represent this skew data, the low outliers would would be afforded a disproportionate effect on the position of the data mode. As the parameter being assessed is simply the mode of the data, and no deeper statistical analysis was performed, it is not important to attempt to fit a normal distribution. Therefore, to correctly display the data distribution, each set of data was assessed as a lognormal distribution, as described in Sections 2.9.2 and 3.4. Furthermore, should this assumption of a skew data distribution be incorrect, the lognormal analysis would still provide the correct modal position, minimising the risk of misinterpreting the mode of the data.

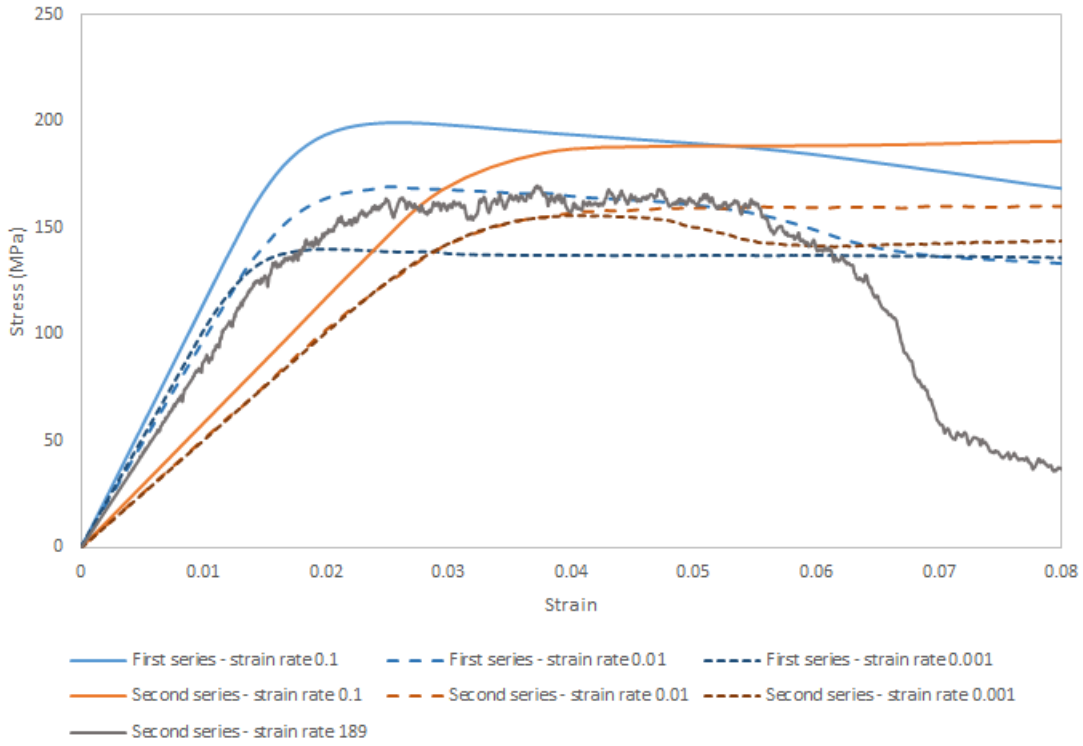

Figure 4.2: A selection of curves showing an example of the shapes of the stress versus strain curves at each strain rate tested for crocodile bone.

Due to the data being skewed left instead of skewed right, it is also expected that the mode will always be larger than the median, and the median will always be larger than the mean (the exact opposite of what occurs when data is skewed right, see Section 2.9.2). The mean represents the average of the data points. In a normal distribution, the mean is generally the value chosen to represent the data. However, as the data in this case is skewed, the mean loses some of its significance. The mean takes all data points into consideration equally, which in the case of skewed data, gives an inaccurate representation of the data concentration. To accurately represent the data, the mode is the most useful value. The mode is the most common value measured in the data set. The median is the value at the middle of the set of data. The mode, as stated, will be the highest value of the three. It represents more clearly

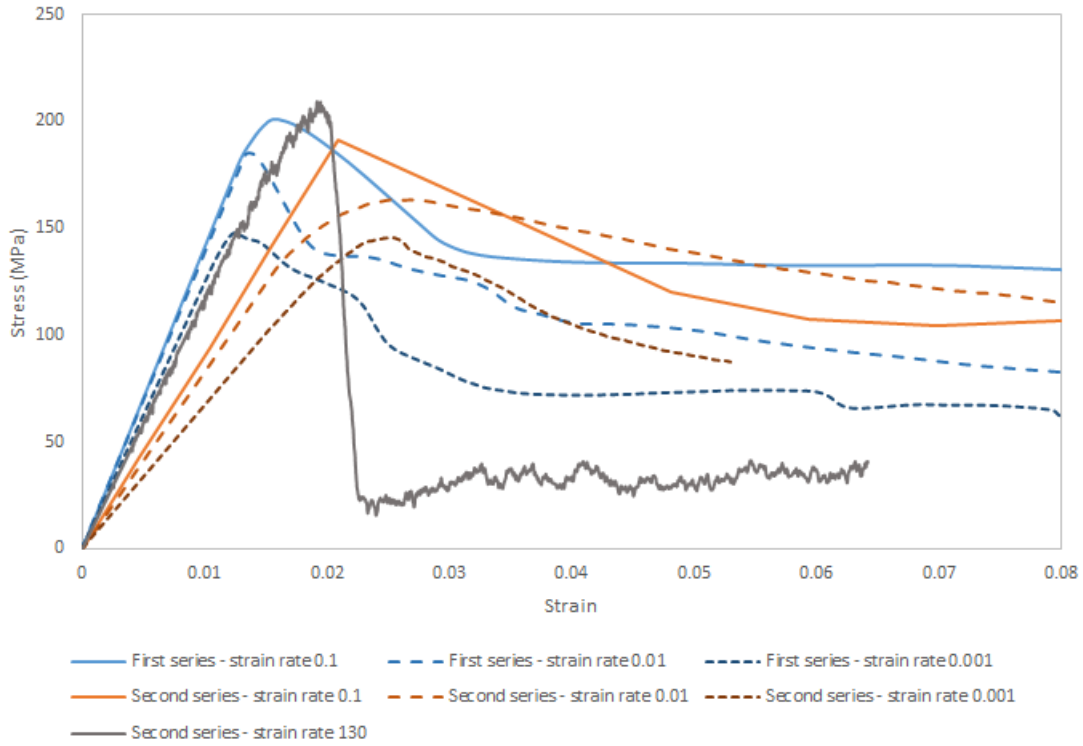

Figure 4.3: A selection of curves showing an example of the shapes of the stress versus strain curves at each strain rate tested for sheep bone.

than either the mean or the median where the peak of the data is, and hence gives the clearest representation of the material response. Therefore, the mode is the most relevant value, and is the value reported for each material property measured.

Figure 4.5 shows an example of a set of data (the apparent modulus of crocodile bone measured in the high intermediate strain rate) with both normal and lognormal distributions displayed. The histogram shows that the data is lightly skewed to the left. As can be seen in Figure 4.5, a normal distribution (denoted by the line with orange triangles) does not accurately represent the peak in the data. A lognormal distribution (denoted by the line with the blue circles) allows for the trailing values to be represented without allowing them to overpower the concentration of data at

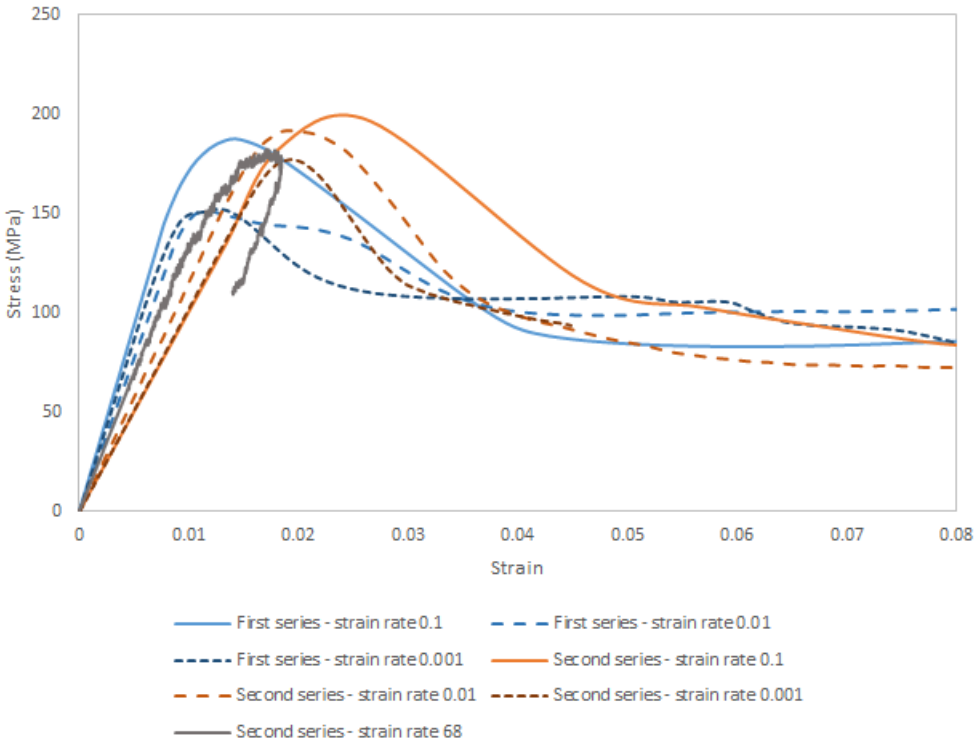

Figure 4.4: A selection of curves showing an example of the shapes of the stress versus strain curves at each strain rate tested for ostrich bone.

the higher end of the spectrum. Displayed in Appendix B are further examples of how a lognormal analysis is more appropriate for a skew data set than a normal distribution.

It was found that when all the data was superimposed on a single graph, it became cluttered. One set of data could not be easily distinguished from another, and it was impossible to draw accurate conclusions about the relationships between the species. Hence, to provide more clarity in the data, a unique way of displaying the data was implemented. At each strain rate, for each set of data within a species, the data spread was plotted as a diamond shaped enclosure. The upper point was plotted at the maximum value measured, the bottom point at the minimum value

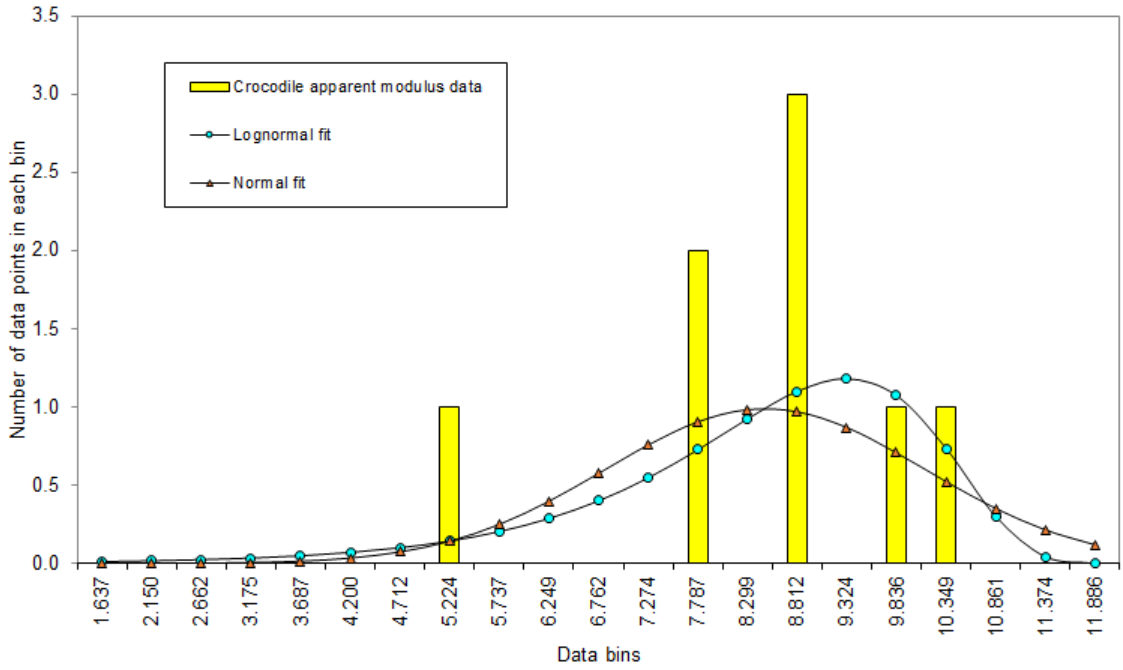

Figure 4.5: A histogram of the apparent modulus data measured for crocodile bone in the high intermediate strain rate regime. A normal distribution and lognormal distribution are superimposed upon the histogram.

measured, and the point on either side plotted at the mode of the data. This again allowed for the lower data points to be included, without attributing more weight to them than the skew distribution requires. The width of the enclosure did not denote variation of strain rate, but was simply meant to be a visual representation of where the majority of data clustered.

To further illustrate why this display method was necessary, in Figures 4.6 through 4.17 all of the data points have been superimposed with the enclosures described.

Displayed in Figures 4.6 through 4.9 are the apparent moduli measured in both the first and second series of quasistatic tests. These values are compared in more detail in Section 5.1.1. Displayed in Figures 4.10 through 4.17 are the compressive strengths from both the first and second series of quasistatic tests. Again, these values are compared in more detail in Section 5.1.2.

As can be seen in some cases, the mode appeared to be outside of the range of measured values. In all these cases, the mode was not significantly outside the range of values measured. This sometimes arises when only a small sample size is used, and of those data points measured, the majority cluster at the upper end of the data set. However, it can be shown that this result is both valid and a better representation of a skew distribution than a simple mean value could be (see Appendix B).

Figures 4.18, 4.19 and 4.20 show the comparison of the apparent modulus and compressive strengths for the first series of quasistatic data, across all species tested. Figures 4.21, 4.22 and 4.23 display the apparent moduli and compressive strengths of the second series of quasistatic data, as well as the higher strain rate data, for all of the species tested. Contained in Table 4.1 are the mode values for the measured properties, at each strain rate tested.

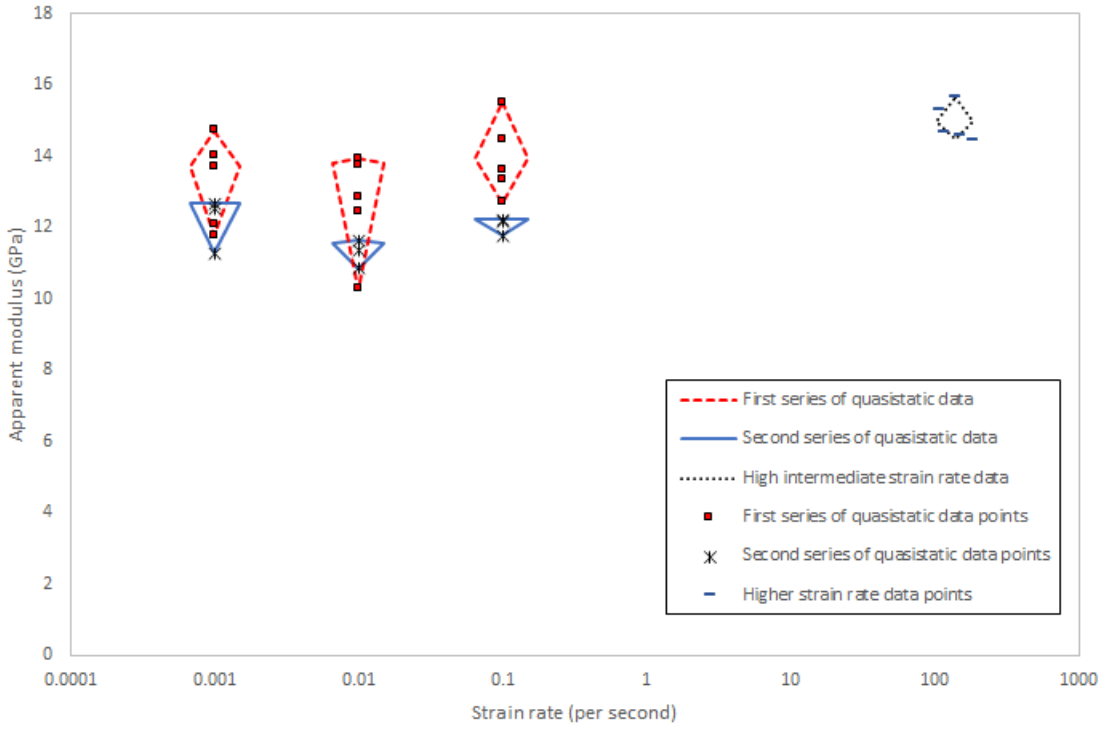

Figure 4.6: The apparent modulus data enclosures and data points for cortical baboon bone.

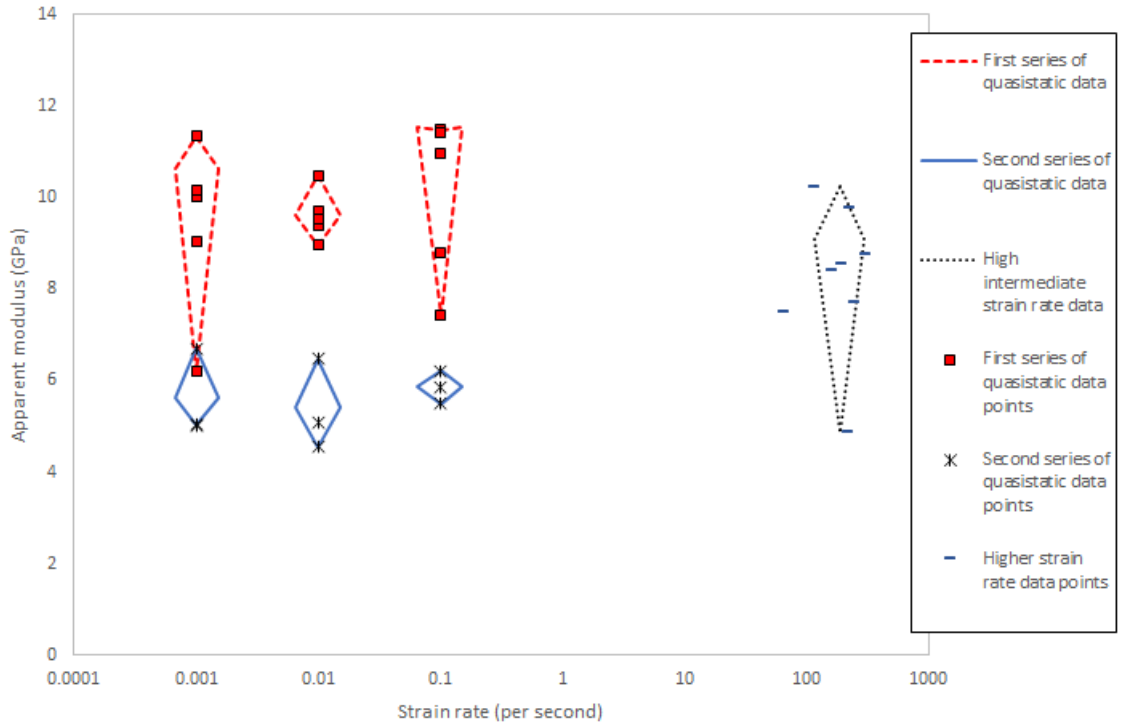

Figure 4.7: The apparent modulus data enclosures and data points for cortical crocodile bone.

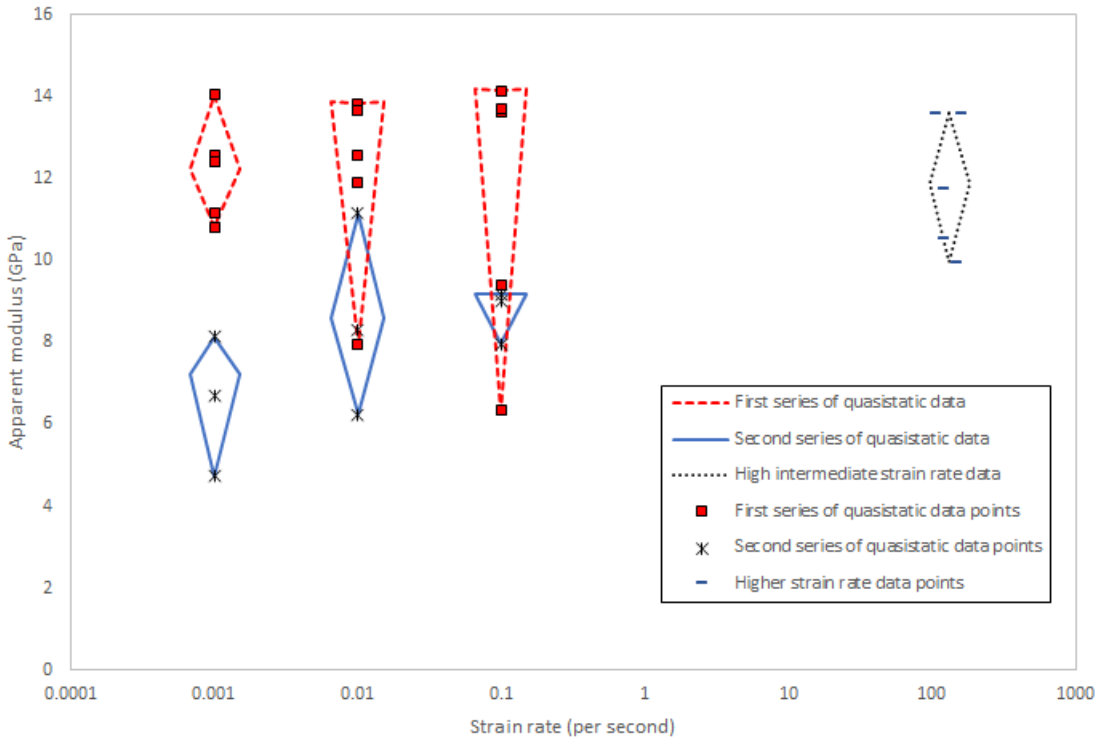

Figure 4.8: The apparent modulus data enclosures and data points for cortical sheep bone.

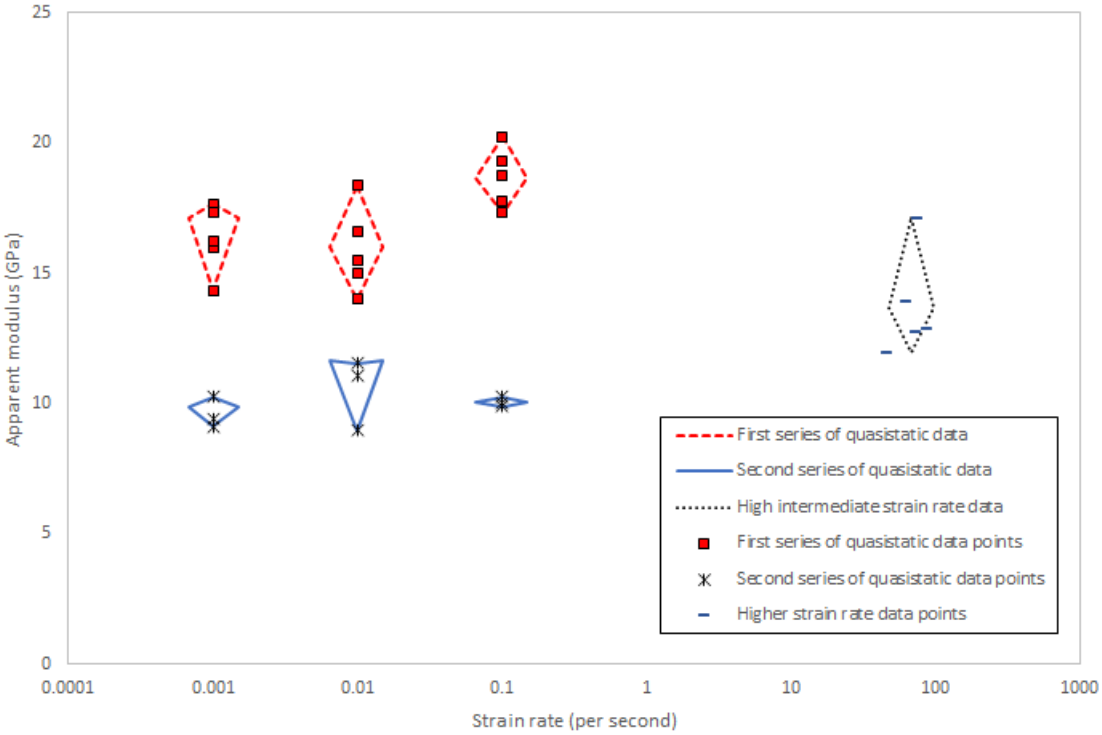

Figure 4.9: The apparent modulus data enclosures and data points for cortical ostrich bone.

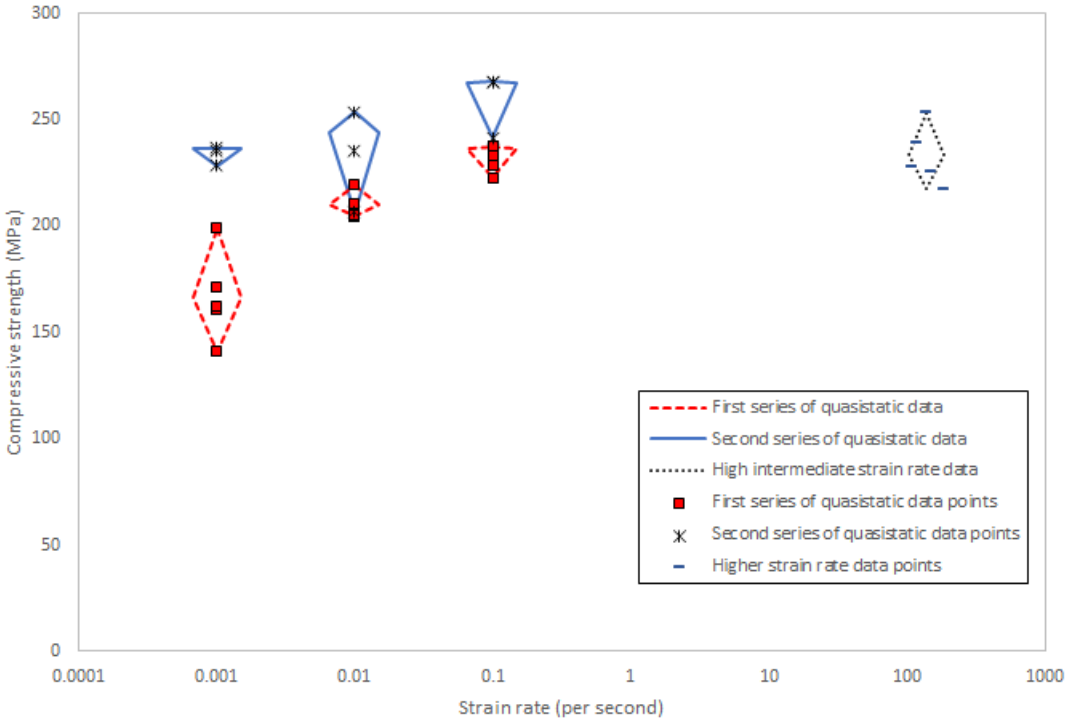

Figure 4.10: The 0.2% offset compressive yield strength data enclosures and data points for cortical baboon bone.

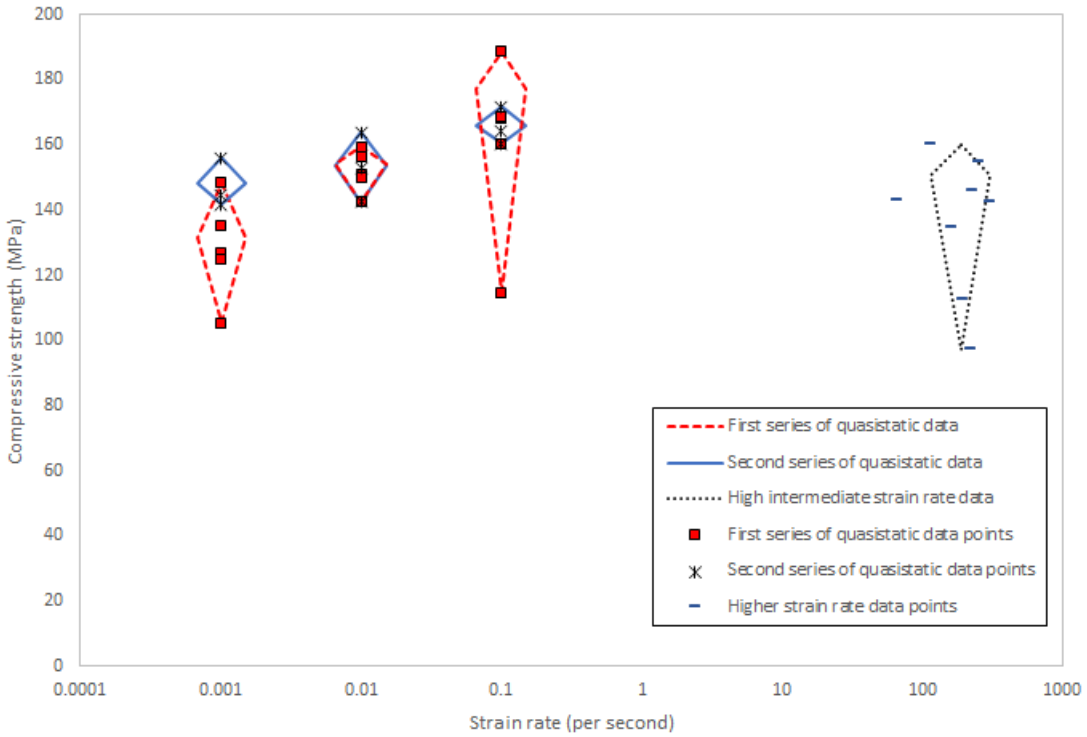

Figure 4.11: The 0.2% offset compressive yield strength data enclosures and data points for cortical crocodile bone.

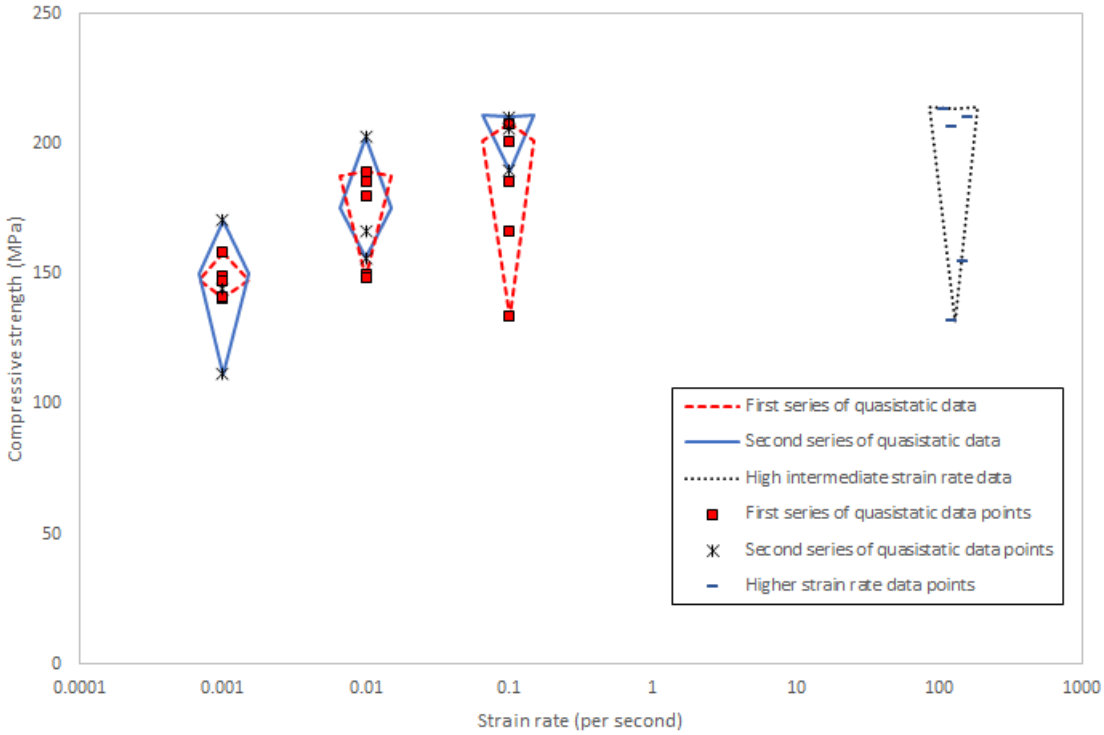

Figure 4.12: The 0.2% offset compressive yield strength data enclosures and data points for cortical sheep bone.

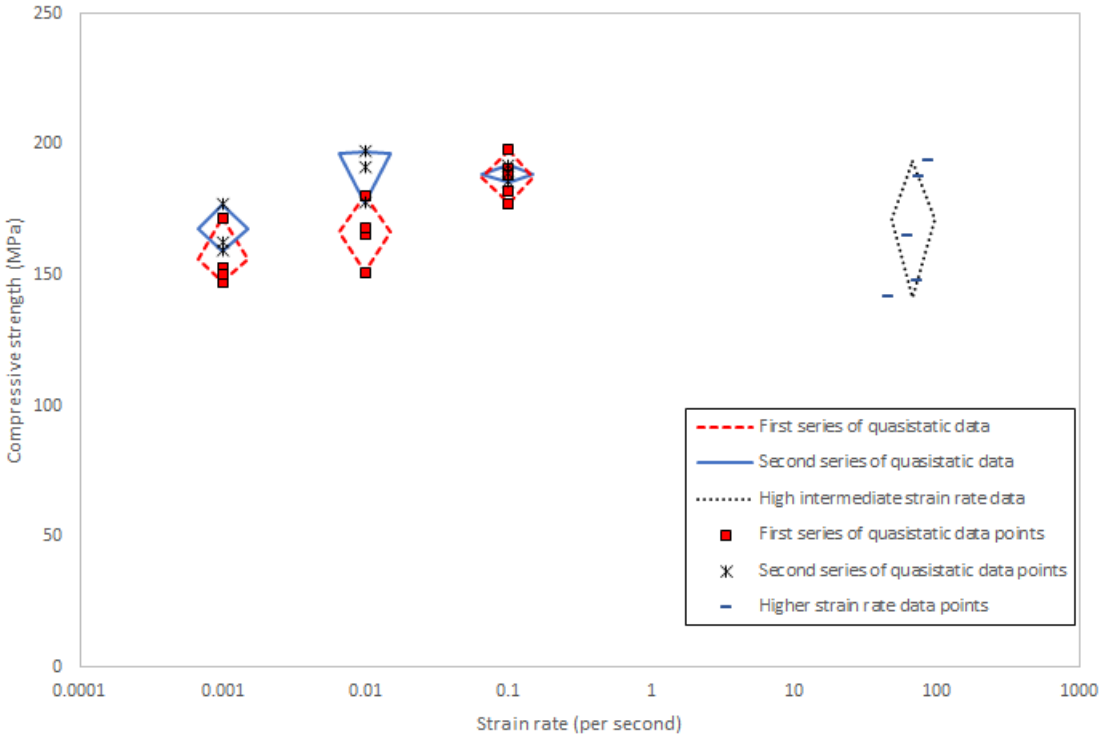

Figure 4.13: The 0.2% offset compressive yield strength data enclosures and data points for cortical ostrich bone.

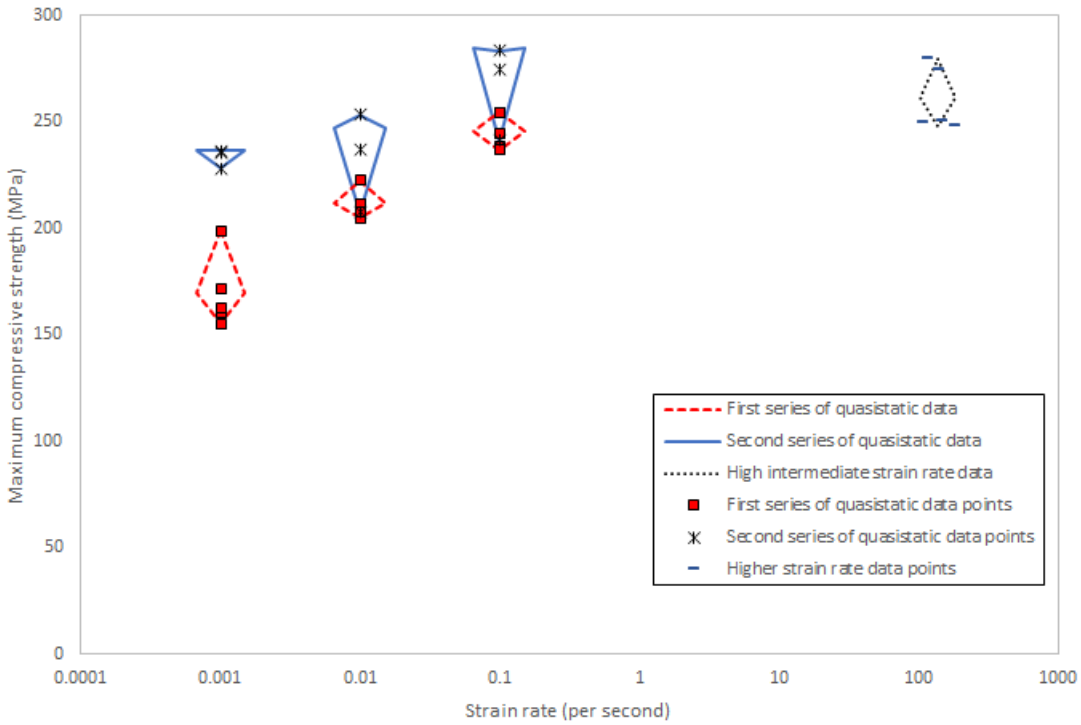

Figure 4.14: The maximum compressive strength data enclosures and data points for cortical baboon bone.

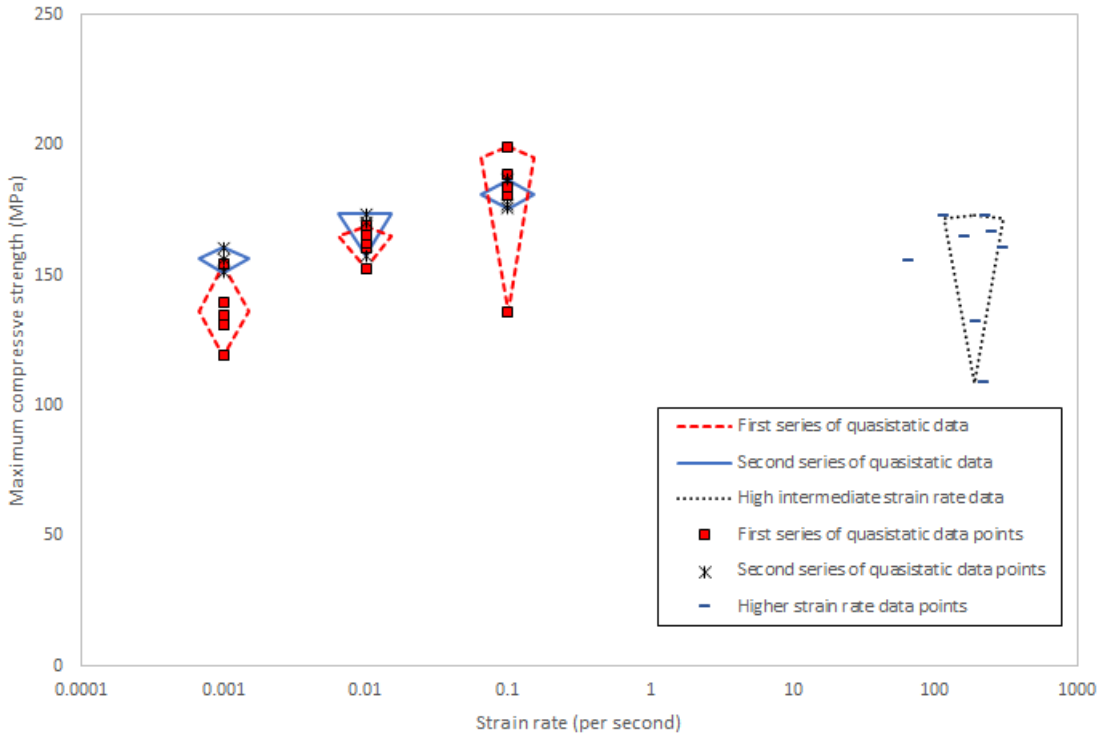

Figure 4.15: The maximum compressive strength data enclosures and data points for cortical crocodile bone.

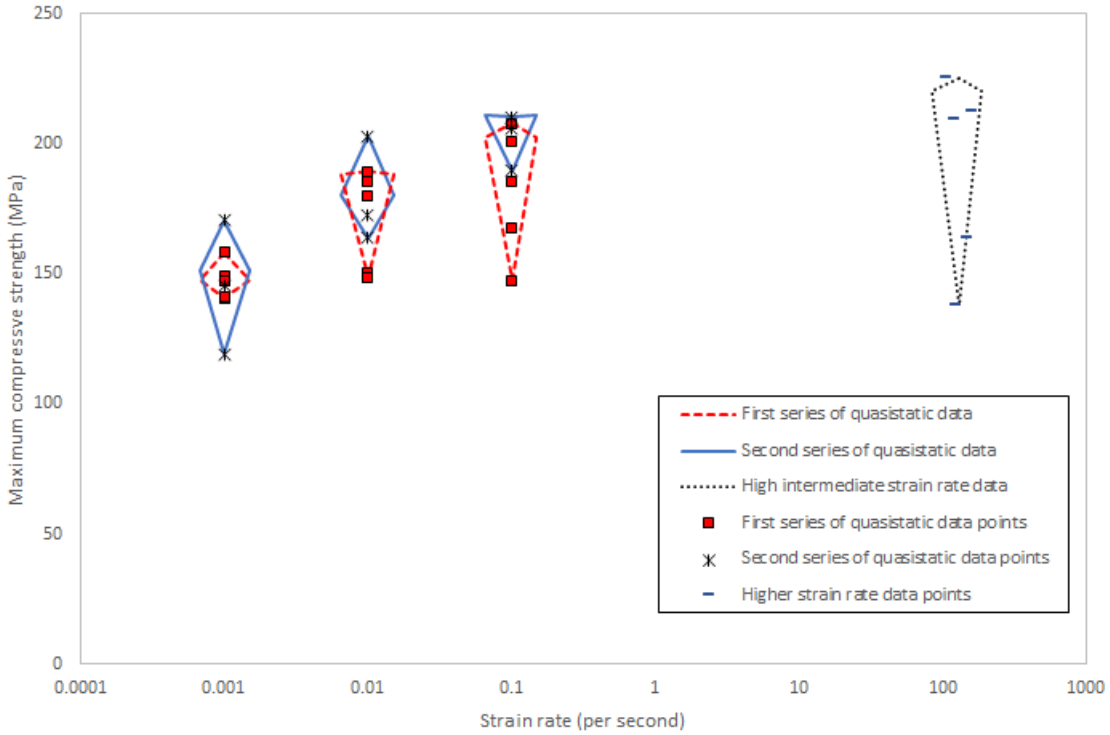

Figure 4.16: The maximum compressive strength data enclosures and data points for cortical sheep bone.

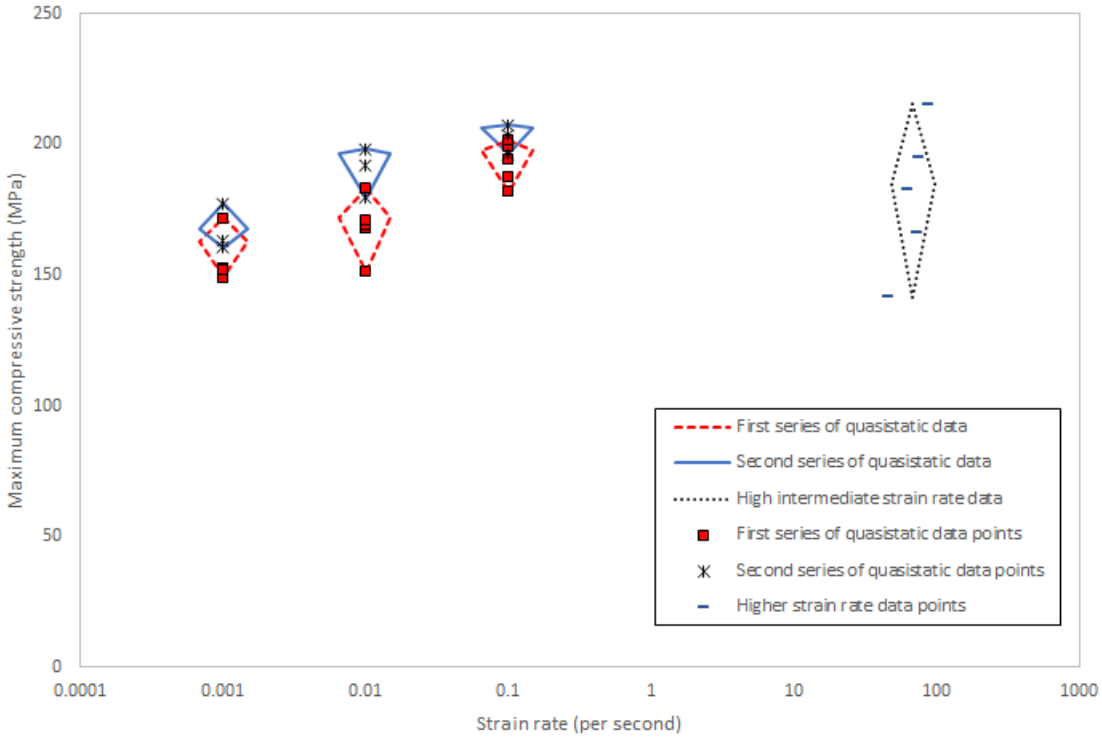

Figure 4.17: The maximum compressive strength data enclosures and data points for cortical ostrich bone.

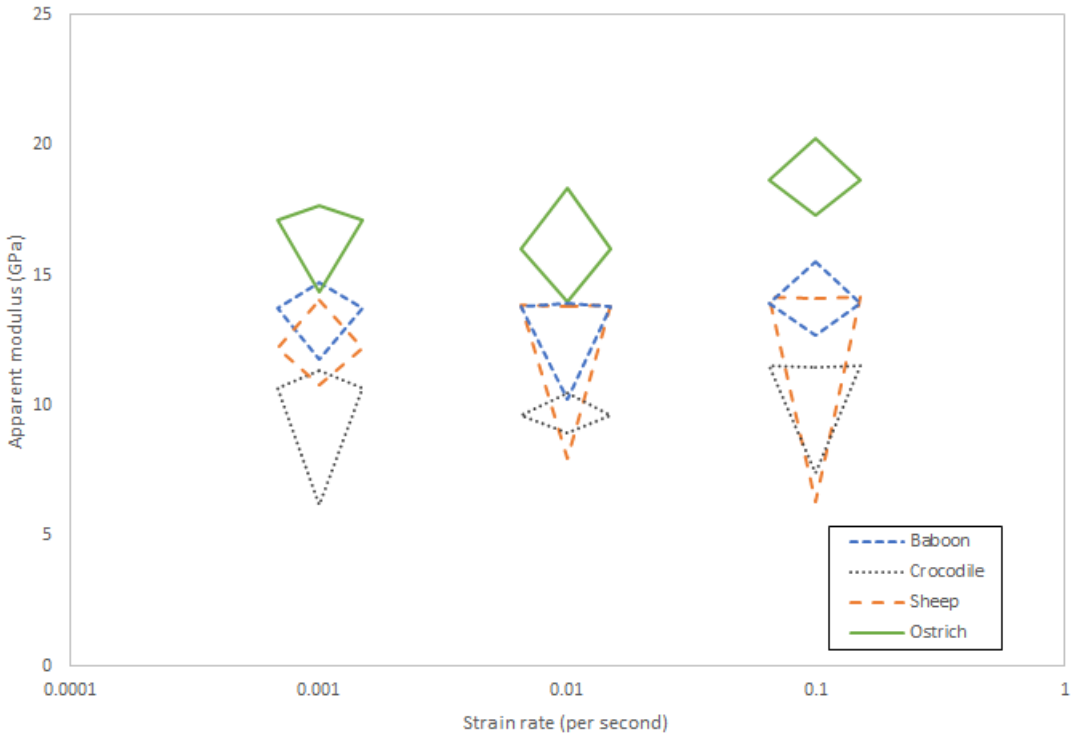

Figure 4.18: The apparent moduli across all species from the first series of quasistatic testing.

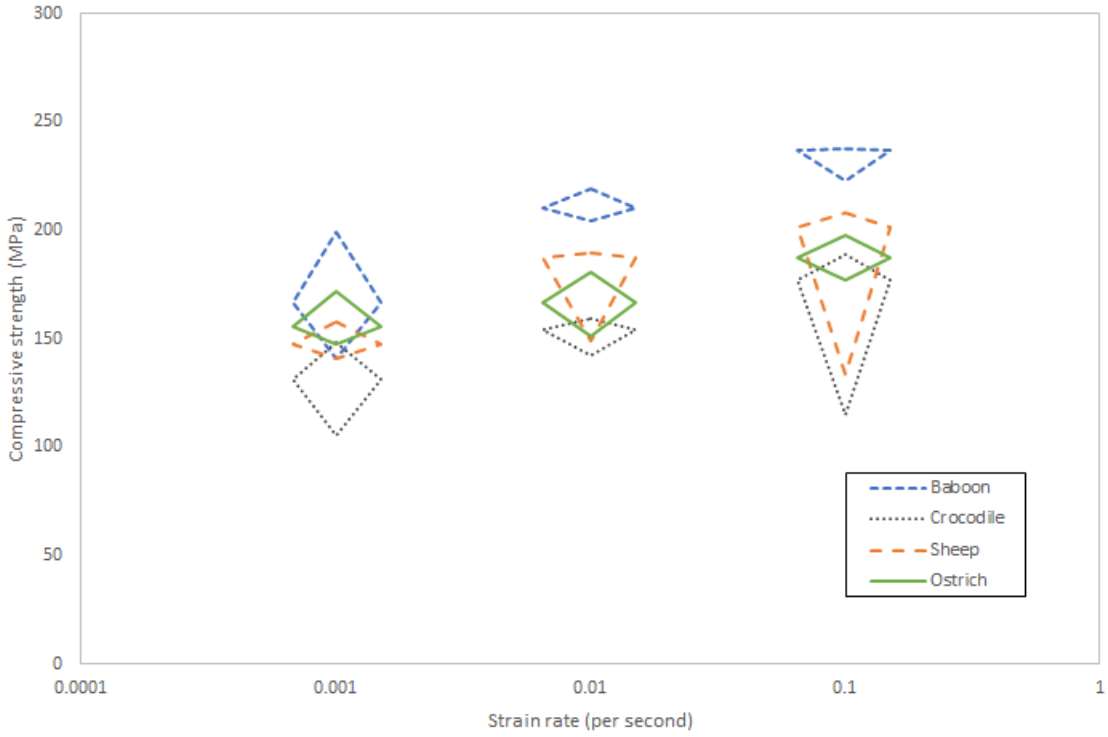

Figure 4.19: The 0.2% offset compressive yield strengths across all species from the first series of quasistatic testing.

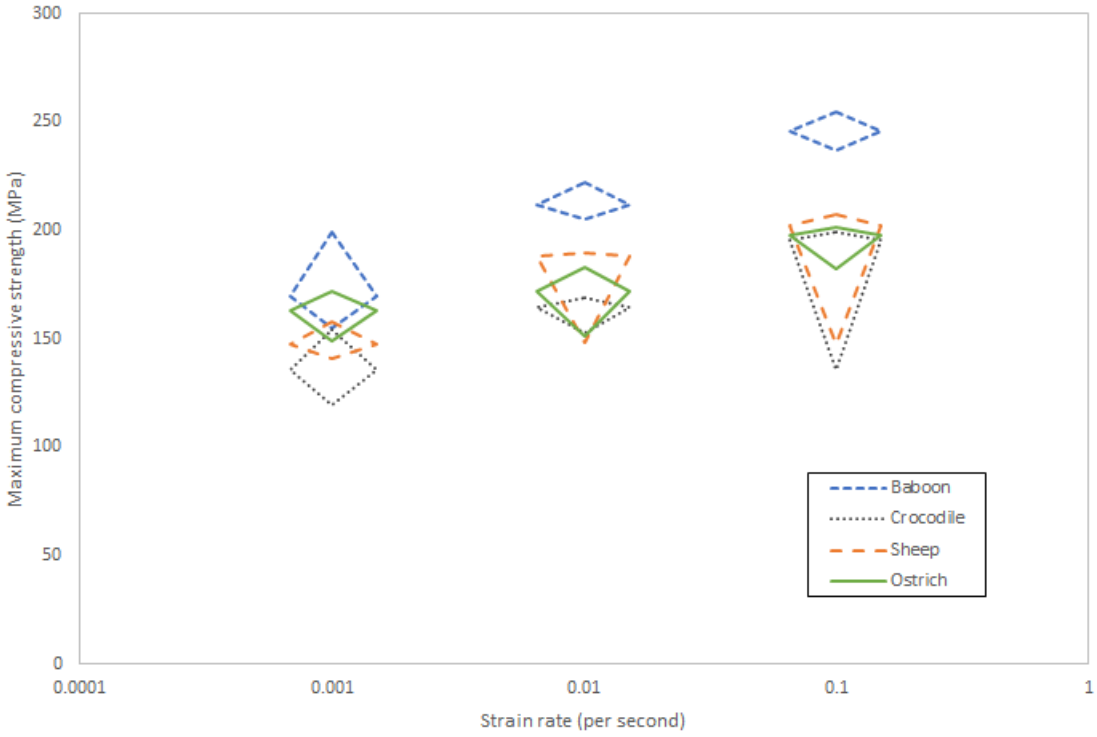

Figure 4.20: The maximum compressive strengths across all species from the first series of quasistatic testing.

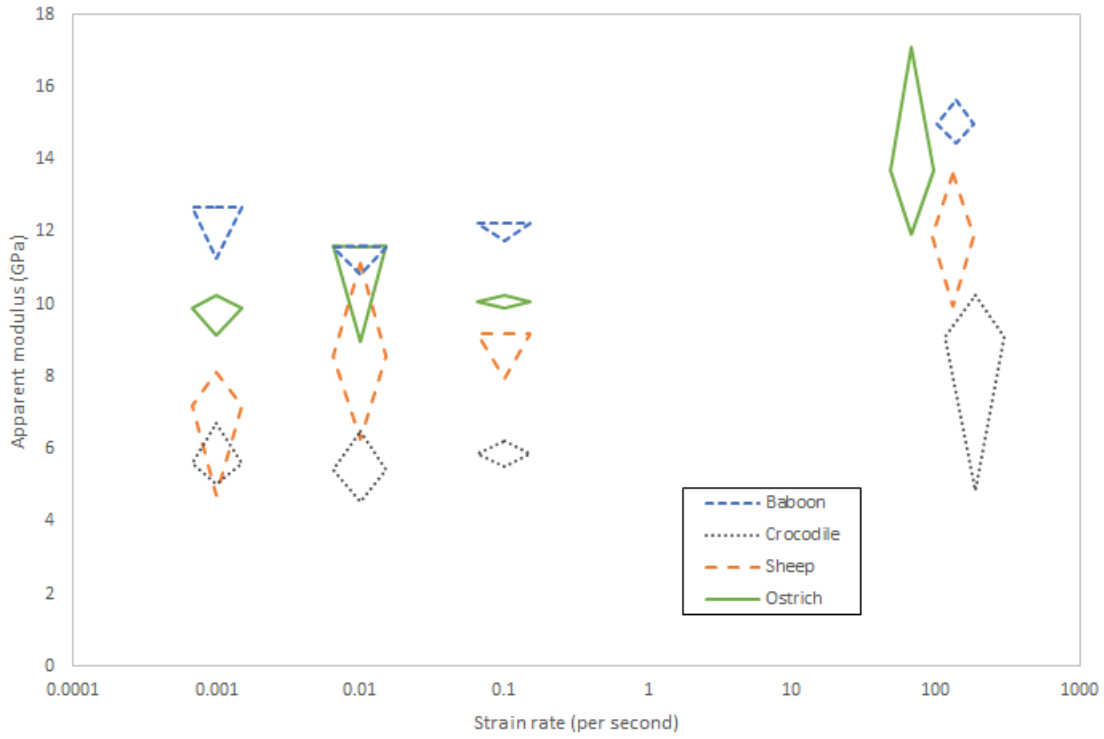

Figure 4.21: The apparent moduli across all species, for both the second series of quasistatic and the high intermediate strain rate tests.

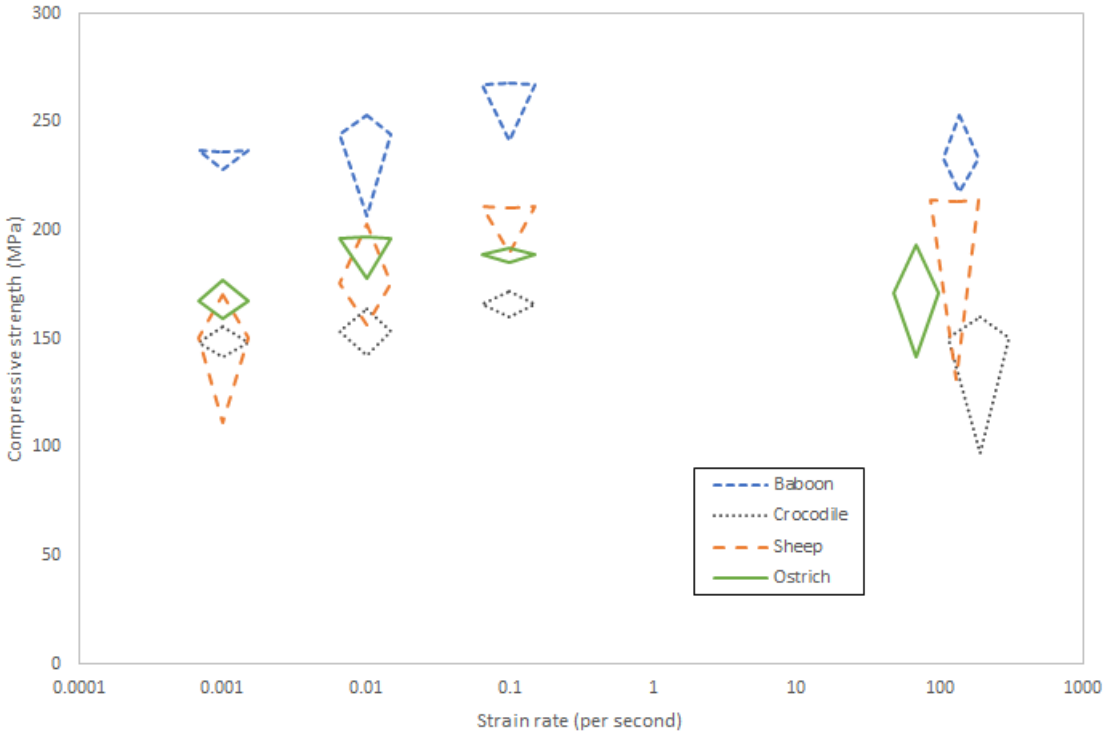

Figure 4.22: The 0.2% offset compressive yield strengths across all species, for both the second series of quasistatic and the high intermediate strain rate tests.

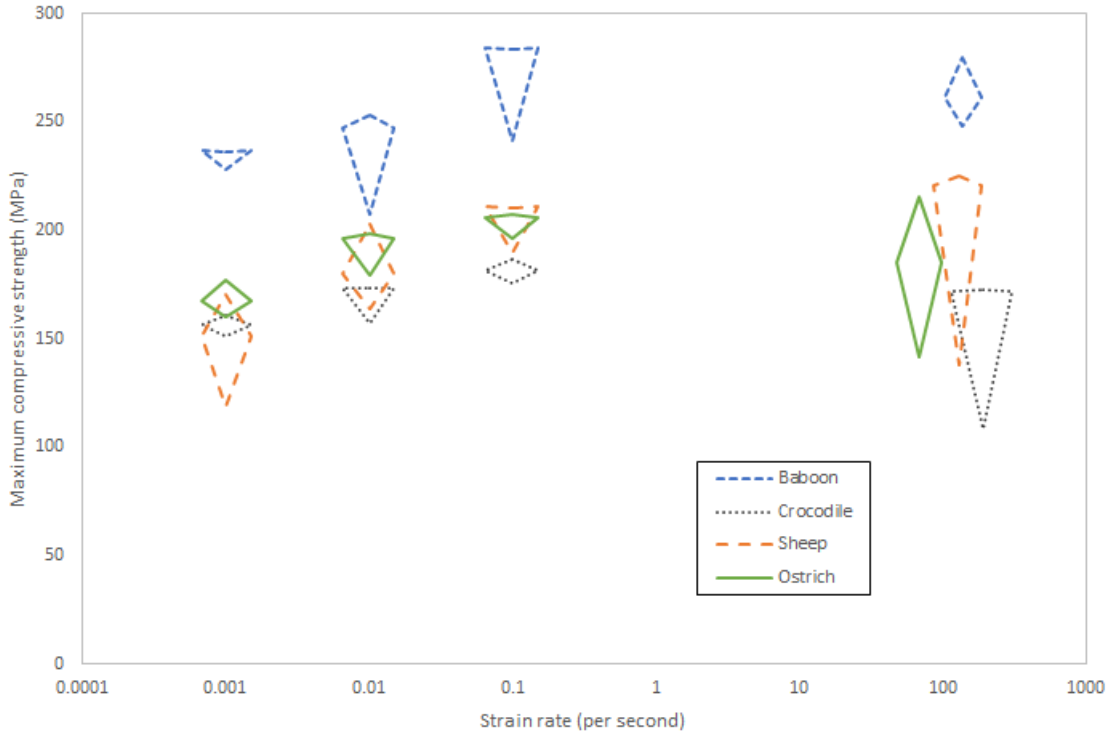

Figure 4.23: The maximum compressive strengths across all species, for both the second series of quasistatic and the high intermediate strain rate tests.

Table 4.1: Mode of apparent modulus and compressive strengths in each species, at each tested strain rate.

Species	**Strain rate tested at per second)**	**Mode of apparent modulus (GPa)**	**Mode of 0.2% offset yield strength (MPa)**	**Mode of ultimate compressive strength (MPa)**
Baboon	137.70	14.97	233.19	261.28
	old $10^{-}3$	13.73	166.50	169.94
	old $10^{-}2$	13.82	210.25	211.59
	old $10^{-}1$	13.92	236.82	245.80
	$10^{-}3$	12.68	236.66	236.69
	$10^{-}2$	11.57	244.07	247.48
	$10^{-}1$	12.23	267.11	284.60
Crocodile	188.85	9.08	150.89	172.03
	old $10^{-}3$	10.65	131.31	135.97
	old $10^{-}2$	9.61	154.30	164.86
	old $10^{-}1$	11.53	177.21	195.42
	$10^{-}3$	5.62	148.41	156.36
	$10^{-}2$	5.42	153.59	173.79
	$10^{-}1$	5.86	165.95	181.22
Sheep	130.15	11.90	214.21	220.36
	old $10^{-}3$	12.22	147.46	147.61
	old $10^{-}2$	13.862	187.73	188.03
	old $10^{-}1$	14.20	201.15	202.12
	$10^{-}3$	7.21	150.26	151.57
	$10^{-}2$	8.58	175.51	180.44
	$10^{-}1$	9.19	210.86	210.86
Ostrich	68.28	13.70	171.43	185.02
	old $10^{-}3$	17.14	155.93	163.02
	old $10^{-}2$	16.00	166.66	171.85
	old $10^{-}1$	18.68	187.30	197.91
	$10^{-}3$	9.90	167.75	167.80
	$10^{-}2$	11.63	196.58	196.68
	$10^{-}1$	10.08	188.80	206.03

Chapter 5

Discussion

This section details the comparison of the first and second series of data, with a discussion on the differences seen. This is followed by an analysis of the relationships seen between species when comparing the measured properties over the range of strain rates tested at, as well as a discussion on how the material responses changes per species as strain rate increases. Also included is a comparison of the measured values with the values found in literature.

5.1 A comparison of the first and second series of data

This section contains a comparison of the first and second series of quasistatic data, first focusing on the apparent moduli, and then the compressive strengths measured.

5.1.1 A comparison of the apparent moduli from the first and second quasistatic data series

A second series of quasistatic tests was performed to determine if there had been any ageing effects due to the required storage time of the specimens (as discussed in Section 3.2.3). In Figures 4.6 through 4.9 the apparent moduli from both the first and second series of testing are displayed, overlaid with one another. It can be seen that there is a clear, but not uniform, decrease in the apparent modulus for all species tested in the second round of testing. The crocodile, sheep and ostrich bone all displayed a fairly large decrease in apparent modulus. The baboon bone, however, showed much less of a decrease in apparent modulus. This lesser degradation suggests that the difference found in the material response is due to a change in the bone properties during storage. The baboon bone was stored for the longest period of time, being stored whole, in a freezer, for a longer period of time than the other species before being collected for this research. As it was stored for the longest time period, it makes sense that there would be less change between the first and second testing series, as the initial degradation would already have occurred before collection and testing. Furthermore, it also bolsters the confidence that differences measured were not due to the use of two separate testing machines, as if this was the case, the decrease measured would have been uniform across all tests.

There are two main suspected reasons for this decrease of apparent modulus. Firstly, it could be due to the deterioration of the whole bones from which the specimens were cut, as the first and second series of data came from two separate series of machined specimens (see Section 3.1 for details). The first series of specimens were cut at the end of February 2016, and were tested in April 2016. The second series of specimens were machined in July 2016. Both the higher intermediate strain rate tests and the second series of quasistatic tests were performed on this second series of specimens. These specimens were cut from the same shipment of bones as the first series, which had been stored frozen. These bones were whole, and not stored in any special medium, only being well wrapped in plastic bags to protect them

from any other freezer contents. It is possible that the whole bones themselves deteriorated somewhat in the five months between machining series. Also, some difference may be accounted for by the fact that they were cut from different bones than the original series, albeit from the same shipment of bone. Secondly, it could be due to deterioration of the specimens between machining and testing. Once cut, the specimens were stored frozen at -32°C, in normal saline, until they were tested at the end of August 2017 and throughout September 2017. It is possible that the specimens deteriorated during this time between cutting and testing.

Due to these differences, the first series of quasistatic data was not considered when looking at how the apparent modulus changed when moving from the quasistatic to high intermediate regimes, for any of the species tested.

5.1.2 A comparison of the compressive strength from the first and second quasistatic data series

Figures 4.10 through 4.17 show the compressive strengths, both the 0.2 % offset yield and maximum, for all species tested, again with the first and second series of data overlaid. When comparing the compressive strengths between the two series of quasistatic tests, it can be seen that there is much less of a difference than in the apparent modulus for both stresses measured. In both cases, the strength stayed the same, or displayed an increase in the second series of tests, again in a non-uniform manner. The only exceptions to this were the strengths measured at $10^{-1}s^{-1}$ in crocodile bone and at $10^{-2}s^{-1}$ in sheep bone. In both of these cases, the second series was slightly lower than the first, with a high degree of overlap between the data enclosures of the first and second series. In the cases of the crocodile bone at $10^{-2}s^{-1}$ and sheep bone at $10^{-3}s^{-1}$ (for both strengths), and ostrich bone at $10^{-1}s^{-1}$ (for the 0.2% offset strength), there appeared to be no significant difference. The remaining strain rates in crocodile, sheep and ostrich bone displayed only a minor difference. In these cases of minor difference, there was generally some overlap

between the data enclosures for the first and second series. The baboon bone stood out as having a notably higher compressive strength in the second series of tests than in the first, for all strain rates, and was the only species to display such a large difference. Unlike the other species, there was minimal overlap between the data enclosures for the first and second series of tests for baboon bone. The reason for this is currently unclear, but due to the consistent specimen preparation method, storage, and testing, it is unlikely to be an artefact of testing. Nevertheless, it would be prudent to seek confirmation of this behaviour through further testing.

Again, only the second series of quasistatic data was used in the overall comparison of all species when investigating the change in behaviour from quasistatic to high intermediate strain rates.

5.2 The assessment of the apparent moduli across all species tested

This section details the comparison of the apparent moduli of the first series of quasistatic data across all species tested, as seen in Figure 4.18. This is followed by a comparison of the measured values to the values found in literature. Lastly, a comparison of the apparent modulus data for the second data series is presented, along with a discussion of the relationships seen when moving from the quasistatic to the higher intermediate strain rate regime, across all species tested, as shown in Figure 4.21.

5.2.1 The interspecies relationships displayed in the first series of data

In both the first and second series of data, there is overlap of the apparent modulus data ranges between the species, but there is also an indication of consistent difference between the species.

In this first series of data (see Figure 4.18), the ostrich bone separates itself clearly from the other species, consistently displaying the highest apparent modulus. There is a large amount of overlap between the baboon bone and the sheep bone at all three strain rates. These two species showed the second stiffest behaviour. Crocodile bone displayed overlap with the tail of the sheep bone data enclosures for strain rates of $10^{-2}s^{-1}$ and $10^{-1}s^{-1}$. Despite this overlap, when observing the mode of each data set, there is still clear separation between the crocodile bone, and the sheep/baboon range, with crocodile bone showing the least stiff behaviour.

Of note in this first series of testing was that the baboon bone displayed a modulus lower than that of ostrich bone, and very similar to that of sheep bone. This is different to what was found in the second series of testing, where the baboon bone displayed the stiffest behaviour (see Section 5.2.3). Due to the length of time the baboon bone was stored for before being acquired, in conjunction with the amount of degradation seen in the apparent modulus of the other species versus the much smaller amount seen in baboon bone, it is speculated that the relationship between baboon response and the response of other species is more accurately portrayed by the second series of data than the first. Aside from the relation of the baboon bone modulus to other species, the order of most to least stiff displayed is the same as seen in the second series of tests, that is, with ostrich bone displaying the highest modulus, sheep bone being the next stiffest, and crocodile bone being the least stiff.

As was mentioned in Section 3.1.1, some of the baboon specimens were taken from closer to the ends of the diaphysis than the other species specimens. Only a portion of the baboon bone specimens tested in this first series of testing were from the ends of the diaphysis, and each strain rate data set had at least a few specimens

tested from the mid-diaphysis, which allowed for comparison. When the response of these end-diaphysis specimens were compared with the samples tested from the mid-diaphysis, there was no clear difference. In this case, whether the specimen came from the mid- or end-diaphysis appeared not to have a noticeable effect.

5.2.2 A comparison with the data found in literature

The following comparisons were done using the mode values for each data set, to facilitate ease of comparison between the measured data and the values found in literature.

Figures 5.1 through 5.4 show the apparent moduli from the first and second series of data in comparison to the data in the literature. In most cases, the data in the literature had no clear strain rate, or was generated using a method that does not relate to a specific strain rate. In these cases, the data was represented as a line across the range of strain rates to which it applies, or simply across the entire graph.

In the case of the baboon bone, the first series of data falls just inside the range of reported values for the second stiffest orientation of bone tested by Wang et al. [27] (seen in Figure 5.1 between the orange lines demarcating the range). In the second series of data, the quasistatic data falls within and slightly above the least stiff range reported by Wang et al. (seen in Figure 5.1 between the blue lines demarcating the range). The higher rate data falls within the second stiffest orientation of bone tested by Wang et al., although further toward the center of the range than the first series of quasistatic data. This places all of the data within the bounds of previously reported properties, but at the lower end of the range. This may be due in part to the difference in bone type tested. Wang et al. [27] investigated the properties of primate skull, which consists of flat bone, with a hard cortical shell and a thin layer of cancellous bone between. While they did harvest cortical specimens specifically, the stresses placed on skull bone and the stresses placed on a femur are different. This

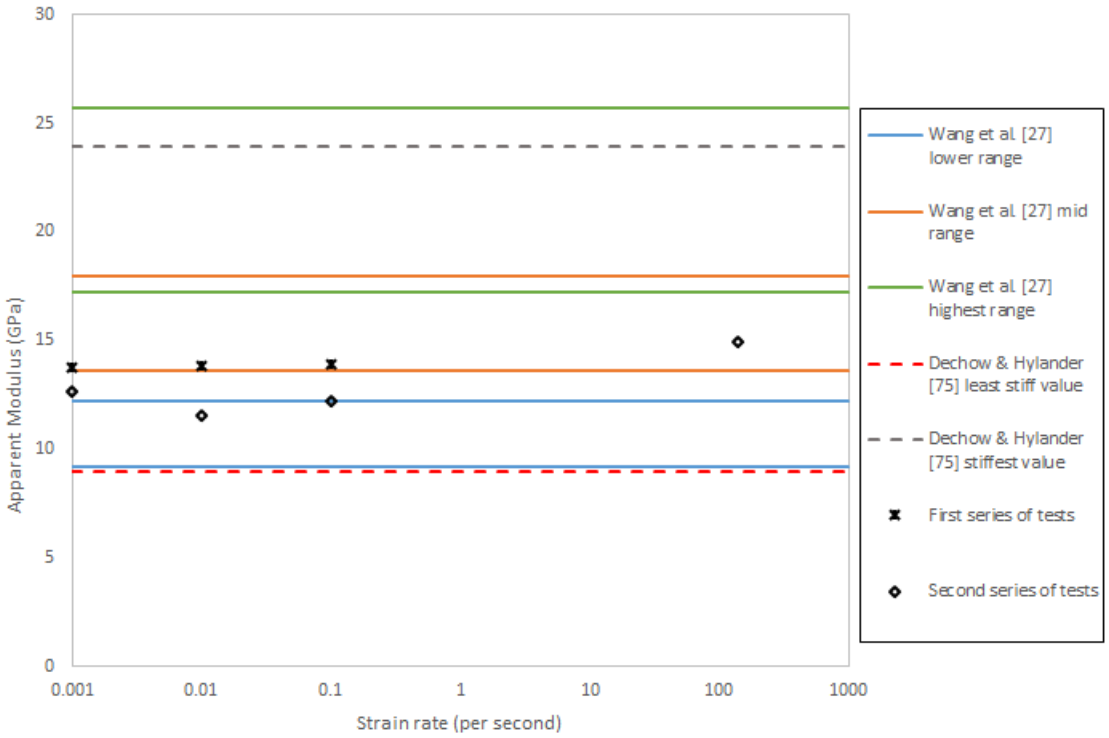

Figure 5.1: A comparison of the apparent modulus data in the literature and the first and second series of data for baboon bone.

could lead to different microstructures, different microdamage patterns, and hence, different properties. Further difference could be introduced by their testing method (ultrasonic testing), as it does not correlate with a specific strain rate. Finally, the comparison could also be affected by the degradation assumed to be present in the material from the beginning due to long storage times.

The baboon data also fell at the lower end of the range between least stiff and most stiff properties reported by Dechow and Hylander [75] (denoted in Figure 5.1 by the grey and red dashed lines). Similarly to Wang et al. [27], they tested mandible cortical specimens using ultrasonic testing. Hence, the same reasoning for why the measured properties are at the low end of the scale apply equally.

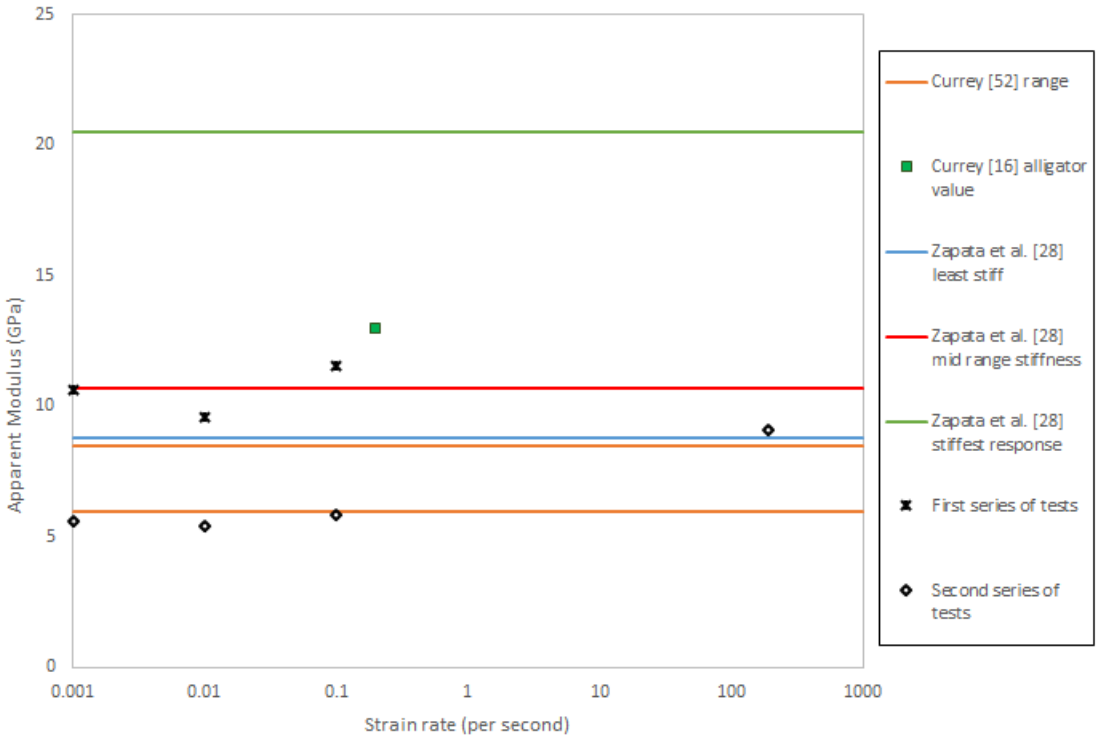

Figure 5.2: A comparison of the apparent modulus data in the literature and the first and second series of data for crocodile bone.

In the case of crocodile bone, the first series of data fell on, slightly below, and slightly above the data presented by Zapata et al. [28] for the second stiffest orientation of alligator bone they tested (seen in Figure 5.2 as the red line). Of note is that the data from the first series of tests is firmly above the range reported by Currey [52] for crocodile bone (seen as the orange lines in Figure 5.2), which is a value widely quoted in literature (see Section 2.7.2). However, the value reported by Currey [16] for alligator bone is above both the first and second series of test data.

The quasistatic range from the second series of data is just below the lower end of the range reported by Currey [52], but is still comparable, and the higher strain rate data is slightly above the upper end of the range, again still being comparable. As there was demonstrable degradation of the apparent modulus in the material

being tested, it is concerning that the measured values would agree with the most widely cited value for elastic modulus of crocodile bone in literature. This agreement suggests that either bone is far more variable than anticipated, or that there was also degradation experienced in earlier work.

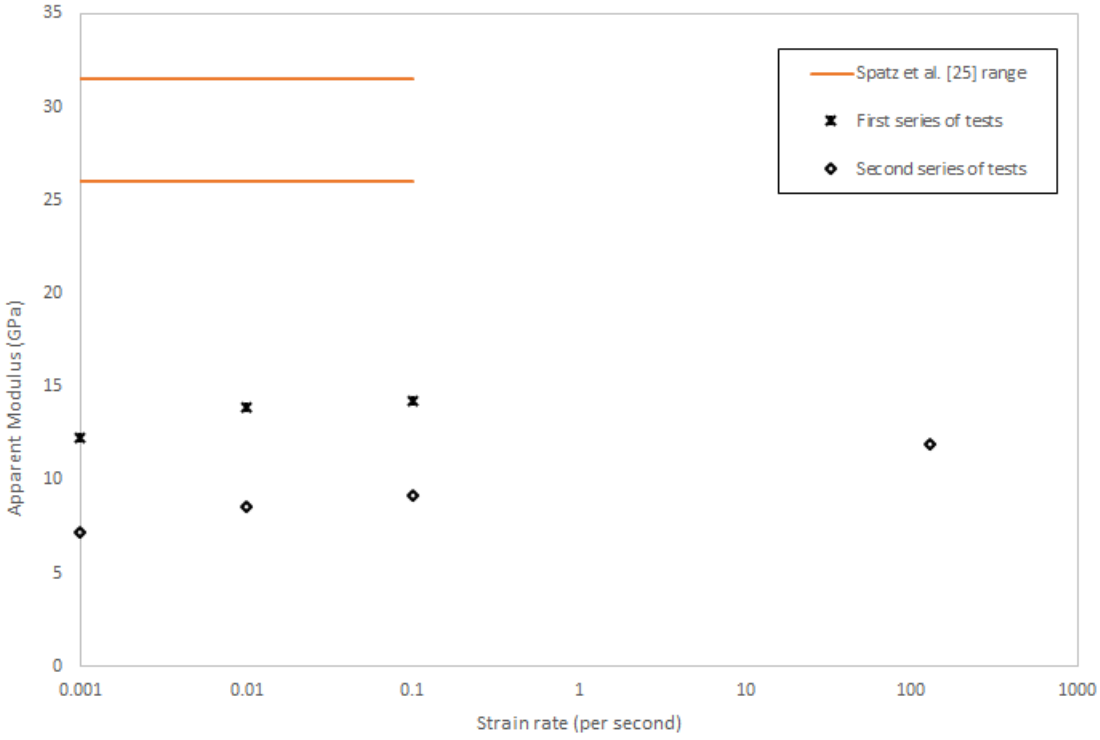

Figure 5.3: A comparison of the apparent modulus data in the literature and the first and second series of data for sheep bone.

The sheep bone shows a large difference in measured value versus literature value. Here, the apparent moduli from both the first and second series of data are significantly lower than the values reported in literature. The data from Spatz et al. [25] (seen as the orange lines in Figure 5.3) were obtained through three-point bending, with the loading being applied in the radial direction, which may account for some of the difference. Their specimens were also a much different size and shape, due to the nature of the testing, and came from multiple different long bones. The difference

between the measured values and literature values may also be contributed to by material degradation, if degradation somehow occurred in the first series of specimens before testing. Even with these considerations in mind, the difference between the measured values and literature values is still large. The data from Spatz et al. [25] is distinctly above the highest data in the review by Johnson et al. [10], as discussed in Section 2.6, which suggests that they be considered with caution.

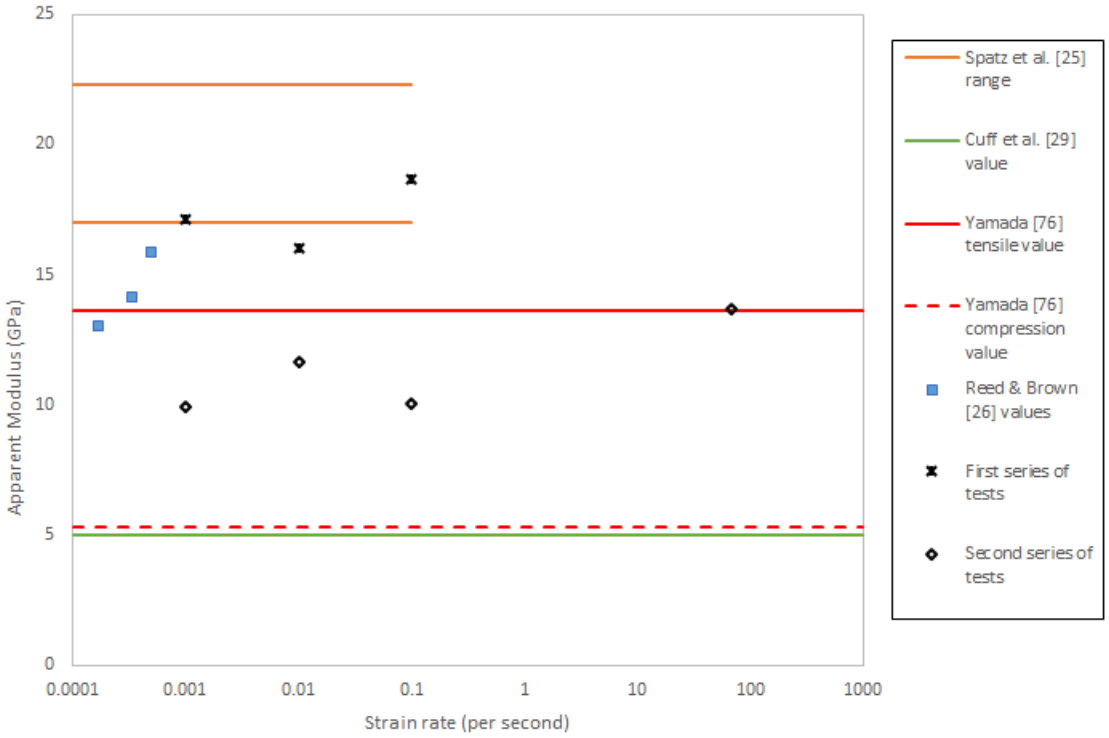

Figure 5.4: A comparison of the apparent modulus data in the literature and the first and second series of data for ostrich bone.

For ostrich bone, the first series of tests compared well with the data reported by Spatz et al. [25] (seen in Figure 5.4 as the orange lines). Two of the data points in the first series of data fell within the range reported by Spatz et al. [25], with the value at $10^{-2}s^{-1}$ being less than their reported range. The quasistatic data from the second series of data fell between the values reported by Yamada [76] for compressive

and tensile apparent modulus (seen in Figure 5.4 as the red solid and dashed lines). This is concerning, as the tests performed were compressive, and this second series of values is still notably larger than the compressive value recorded by Yamada [76]. It is also much larger than the value reported by Cuff et al. [29], although this may be attributed to by the fact that their value was obtained using nanoindentation. The values obtained by Reed and Brown [26] (seen in Figure 5.4 as the blue squares) were between the first and second series of data. Their data was all generated at a strain rate below those tested at in either the first or second series of tests.

5.2.3 The interspecies relationships displayed in the second series of data

Once again despite overlap between data ranges, there was still a clear separation of the species responses when considering the mode.

There is a large amount of overlap in the $10^{-2}s^{-1}$ tests, and in the intermediate tests, as well as between the crocodile and sheep bone tested at $10^{-3}s^{-1}$. However, there is clear separation for the values at strain rates of $10^{-1}s^{-1}$, and for baboon, ostrich, and the crocodile/sheep grouping at $10^{-3}s^{-1}$. Even in the $10^{-2}s^{-1}$ and intermediate ranges, there is a suggestion of the same differences in apparent modulus as seen in the clearly separated regions. Namely, that crocodile bone consistently displays the lowest apparent modulus, followed by sheep, which is slightly stiffer, then ostrich, which is stiffer still, and finally baboon, which displays the stiffest behaviour. That crocodile bone is consistently the least stiff raises the question of whether the semi-aquatic lifestyle of the crocodile, and the corresponding buoyancy requirements, has a significant effect on the bone properties. While beyond the scope of this research, a cursory review of some literature provides some values for both a full terrestrial reptile and some fully aquatic mammals. Currey [16] found that whale rib had an average apparent modulus of 8.4GPa, dugong bones showed a range of apparent moduli from 4.9GPa to 7.5GPa and Galapagos tortoises showed a range of apparent moduli from 11.8GPa to 13.0GPa. The apparent modulus measured for crocodile bone in the present research appears to fit this trend, being less stiff than

the terrestrial reptile and quite similar to the aquatic mammals. If the need for buoyancy does have an impact, one would expect to see a lower density in crocodile bone than the other species tested. The apparent densities were not listed for the specimens reported by Currey [16], and so are not compared here. Comparing the average apparent density across species tested in this research (see Section 3.1.2), it is evident that the crocodile bone does indeed have a slightly lower average density than the other species tested, although this difference is fairly small. This highlights an avenue of interesting future research.

When looking at each individual set of data, it could be seen that there was a large difference in the amount of scatter for each strain rate in each species. Not only is there a difference in the amount of scatter between species, but also in the amount of scatter at each strain rate within a species. It is also clear that there is consistently high scatter in the higher strain rate data. This is due to the nature of the testing performed. While the strain rate remained near constant during each higher strain rate test, the strain rate varied from test to test, adding to the scatter seen when grouped together for ease of representation. This variation of strain rate from test to test can be seen in Figures 4.6 through 4.9 when looking at the data points plotted over the enclosure for the higher strain rate data.

Overall, the baboon bone showed the least amount of scatter, as can be seen by the small, neat enclosures indicating a small amount of scatter. Ostrich bone displayed a small amount of scatter at $10^{-3}s^{-1}$ and at $10^{-1}s^{-1}$, a moderate amount at $10^{-2}s^{-1}$, and a large amount at the high intermediate strain rate. Sheep bone showed a small amount of scatter at $10^{-1}s^{-1}$, a moderate amount at $10^{-3}s^{-1}$ and the high intermediate strain rate, and a high amount at $10^{-2}s^{-1}$. Crocodile bone displayed a low degree of scatter in the quasistatic strain rates, and a high degree at the high intermediate strain rate.

An odd trend is that at a strain rate of $10^{-1}s^{-1}$, there was only a small amount of scatter regardless of which species was observed. For all species except baboon, the highest amount of scatter can be seen at the high intermediate strain rate. This may

be contributed to by the differences in individual testing strain rates, as opposed to the quasistatic strain rates, which were all the same. Another contributing factor could be that the higher rate testing is a much more aggressive testing method, which would highlight any flaws present in the material. Scatter may be increased by various factors, such as the presence of microdamage in the specimens, differences in microstructure, changes in porosity etc.. As histological analysis was outside the scope of this research, these factors were not closely assessed.

Two other factors to consider are the effects of the density of the specimens and the position around the diaphysis of the bone from which the specimens came (see Appendix A).

In the baboon bone, the highest degree of scatter was in the $10^{-3}s^{-1}$ specimens, but this was where the smallest difference in density between specimens was. In the crocodile bone, the largest difference in densities was found at the intermediate rates, and also the largest amount of scatter, but the second highest density difference (which was almost equal to the highest density difference) was present at $10^{-1}s^{-1}$, which displayed the least amount of scatter in apparent modulus for crocodile. From analysis, there was a similar lack of correlation between density difference and scatter in sheep and ostrich bone.

There does not appear to be a clear link between the amount of scatter, or the values of apparent modulus, and the difference in density between specimens. This may be due to the fact that there was a small range of measured densities versus a high scatter in the apparent modulus data. The densities were indeed very similar for all specimens measured.

When the position on the circumference of the diaphysis from which the specimen was taken was compared to the apparent modulus measured, there was no clear difference seen due to placement around the diaphysis (see Appendix A for data). This lack of effect may have been contributed to by the small sample sizes used.

Also a possible contributing factor is the lack of variation in positioning, with the majority of the samples coming from the anterior surface of the bone.

Finally, when looking at the mode of each data set, there is a distinct increase in the apparent modulus, in all species, when moving from quasistatic to high intermediate strain rates. This agrees with work done previously by van der Westhuizen [32] and Paul [12].

5.3 The assessment of the compressive strength across all species tested

This section contains the comparison of compressive strengths, both 0.2% offset yield and maximum, from the first series of testing (as shown in Figures 4.19 and 4.20), as well as a comparison of the measured data with values from literature. Also included is a comparison of the strengths from the second series of testing, and a discussion of the relationships and behaviours seen in compressive strengths when moving from the quasistatic to the high intermediate strain rate regime (as shown in Figures 4.22 and 4.23).

5.3.1 The interspecies relationships displayed in the first series of data

Once again, there is a large degree of overlap in the compressive strength data enclosures when comparing species (shown in Figures 4.19 and 4.20). There is a much higher degree of overlap in the maximum strength than in the 0.2% offset strength. There is also a suggestion of separation between species when looking at the mode of

each data set, with a much clearer separation in the 0.2% offset strength, although there are similarities in the relationships between species for both properties.

The baboon bone clearly separates itself as having the highest compressive strengths at all three quasistatic rates, for both properties. The only overlap was seen at the tail of the enclosures at $10^{-3}s^{-1}$ for both properties. For the remaining three species, despite overlap being seen at all three strain rates, crocodile bone also separated itself out, having the lowest compressive strength in the case of the 0.2% offset strength. This same relation is hinted at in the maximum compressive strength data, but much less clearly than in the offset strength. There is a high amount of overlap between the sheep and ostrich specimens, with ostrich bone showing a higher compressive strength at $10^{-3}s^{-1}$, and sheep bone showing a slightly higher compressive strength at rates of $10^{-2}s^{-1}$ and $10^{-1}s^{-1}$. Similar relationships can be seen in the second series of tests, and will be discussed further in Section 5.3.3.

5.3.2 A comparison with the data found in literature

Presented in Figures 5.5 through 5.8 are comparisons of the maximum strength mode values from the data generated, and the values found reported in literature. The maximum strengths were chosen, as the values reported in literature are generally ultimate strengths. However, in the case of crocodile bone, the 0.2% offset yield strengths are reported, as the single comparison value is a yield strength (see Figure 5.6).

Figure 5.5 shows the working stresses measured by Dechow and Hylander [75] from macaque bone. These values are vastly lower than the maximum compressive strengths measured in baboon femur, as was expected, as these were sustainable working stresses in a living subject. While this confirms that the measured stresses are not too low, not much else can be discerned from comparing these stress values.

In Figure 5.6, it can be seen that the measured yield strength in crocodile bone is significantly higher than the value reported in literature by Currey [16] for alligator

bone. This may be reasonable, as the tests by Currey [16] were performed in tension, which would produce a lower value than compression testing.

In Figure 5.7, it can be seen that, like with the apparent modulus, the measured sheep data is significantly lower than the values reported in literature by Moreno and Forriol [65].

Ostrich bone displayed a compressive strength that was markedly higher than most literature values (see Figure 5.8). The only exception was the ultimate compressive strength reported by Reed & Brown [26], which appeared to be comparable to the measured values.

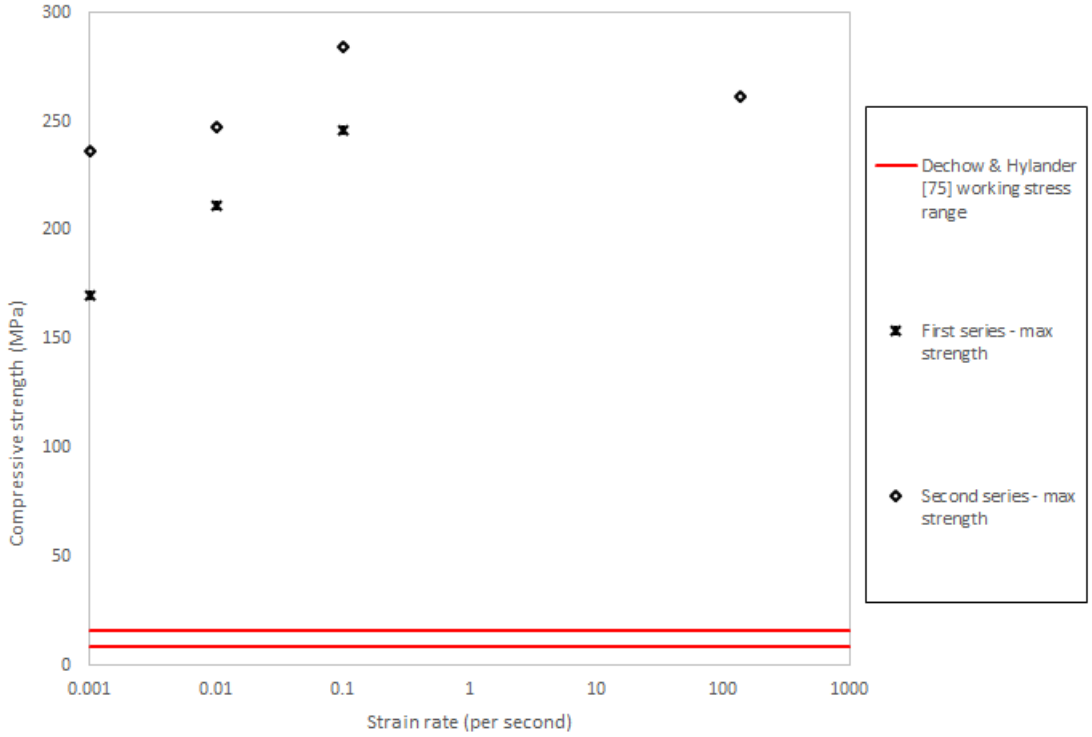

Figure 5.5: A comparison of the maximum compressive strength data in the literature and the maximum compressive strengths from the first and second series of tests for baboon bone.

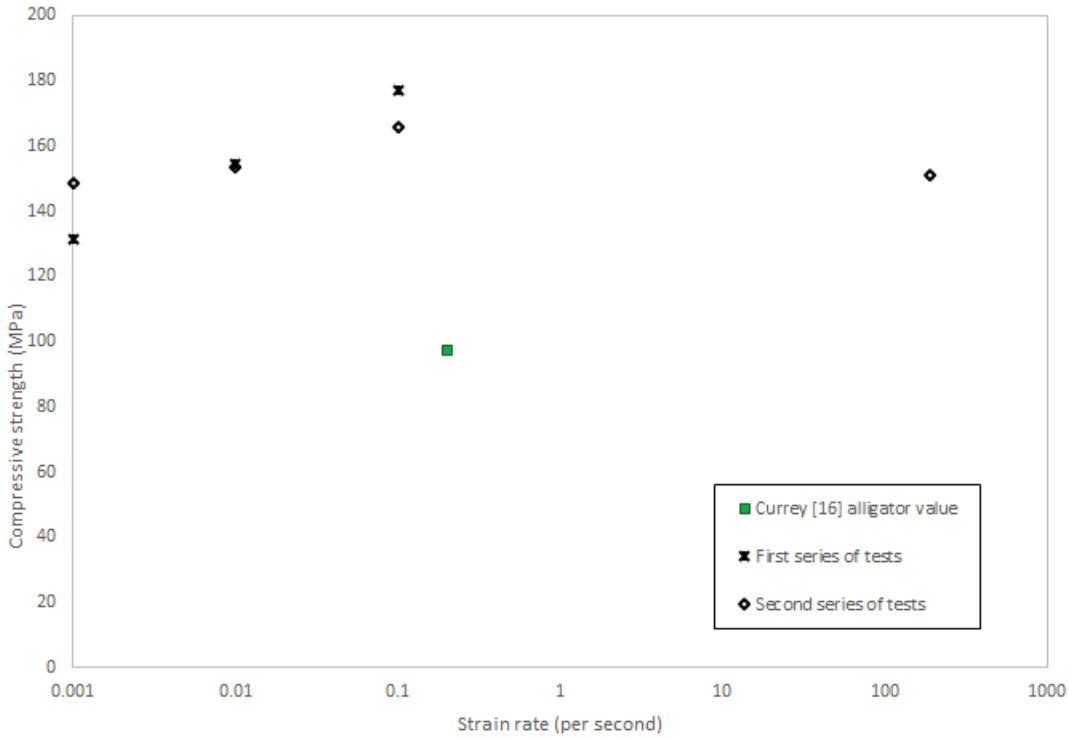

Figure 5.6: A comparison of the compressive yield strength data in the literature and the 0.2% offset yield strengths from the first and second series of tests for crocodile bone.

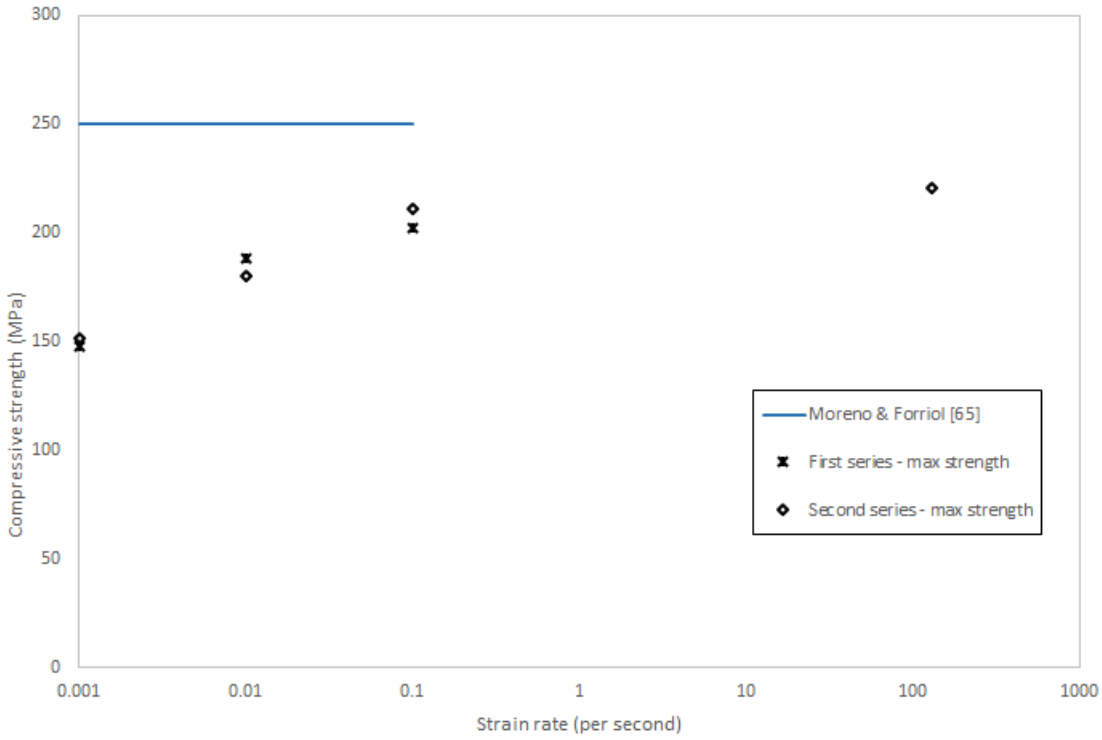

Figure 5.7: A comparison of the maximum compressive strength data in the literature and the maximum compressive strengths from the first and second series of tests for sheep bone.

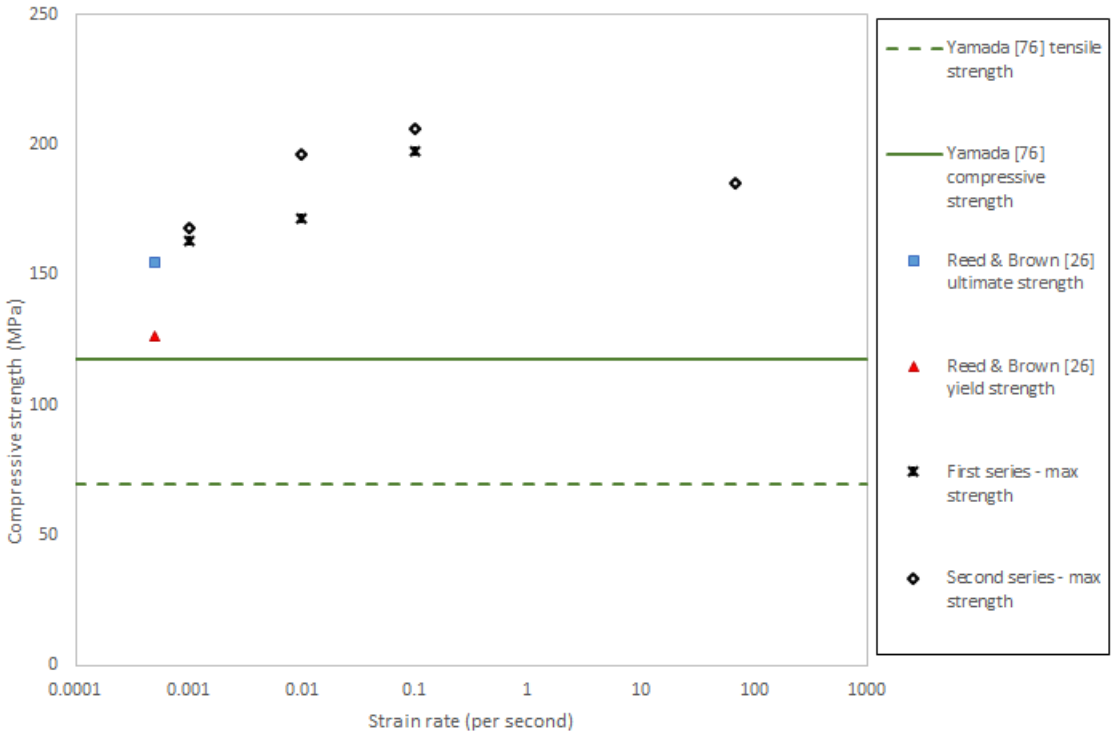

Figure 5.8: A comparison of the maximum compressive strength data in the literature and the maximum compressive strengths from the first and second series of tests for ostrich bone.

5.3.3 The interspecies relationships displayed in the second series of data

This subsection details the comparison of both the 0.2% offset yield strength and the maximum compressive strength data from the second test series for all species over all strain rates tested, as visualised in Figures 4.22 and 4.23.

When observing the compressive strength, there is far less separation between the majority of the data than is seen in the apparent modulus. While baboon bone shows a clear separation from the others species, displaying a consistently higher compressive strength (both 0.2% offset and maximum), the other three species show data with significant overlaps. The crocodile bone tends to display the lowest compressive strength. In the case of the 0.2% offset strength, at $10^{-3}s^{-1}$, sheep bone displays an equally low compressive strength. In the case of the maximum strength at $10^{-3}s^{-1}$, sheep bone actually displays a lower strength than crocodile bone, and at $10^{-2}s^{-1}$, crocodile and sheep bone show a very similar maximum strength. The sheep and ostrich bone display a large amount of overlap with one another, with the sheep bone displaying higher compressive strength at $10^{-1}s^{-1}$ and the higher strain rate, while ostrich bone displays the higher strength at $10^{-3}s^{-1}$ and $10^{-2}s^{-1}$, for both properties measured. In the quasistatic regime, these differences are fairly small, especially for the maximum strength. This high degree of overlap suggests that there is less difference in compressive strength between species (with baboon being the exception) than in apparent modulus.

Baboon bone has consistently shown the highest compressive strengths, as well as the highest apparent modulus, across all species tested. If the specimens taken were from a region of mostly avascular bone, with fewer osteons (either primary or secondary), as is highly possible in non-human primate bone (see Section 2.1.2), this would make sense. Histological analysis was outside the scope of this dissertation, and hence was not performed, so this cannot be confirmed.

5.3. THE ASSESSMENT OF THE COMPRESSIVE STRENGTH ACROSS ALL SPECIES TESTED

A great similarity was displayed between sheep and ostrich bone, with neither being consistently stronger than the other. Crocodile bone also showed great similarity, but did separate out as the weakest of the three. As the ostrich, crocodile, and sheep bone could all be expected to contain some level of fibrolamellar bone, it is reasonable to see such similarity between the specimens tested. It is speculated that the variance of the properties within a single species may be linked to the level of osteon presence within each specimen. Indeed it would make sense that there would be some baseline similarity, with the properties of the sheep and crocodile bone decreasing as an increase in osteons occurs. Future research into the histology of specimens may provide interesting and valuable information.

Notably, there is a clear increase in both compressive strengths measured when increasing the strain rate from $10^{-3}s^{-1}$ to $10^{-2}s^{-1}$, and from $10^{-2}s^{-1}$ to $10^{-1}s^{-1}$, followed by no increase, or even a slight decrease at the higher strain rates. This does not agree with previous work by van der Westhuizen [32] and Paul [12], unlike the findings on the apparent moduli. Both van der Westhuizen [32] and Paul [12] found that strength was fairly constant across the quasistatic regime, with an increase seen in the intermediate to dynamic regime. However, observing specifically van der Westhuizen's data, it can be seen that when the entire data set is observed the strength in the quasistatic regime appears fairly constant, but when only the quasistatic regime is examined it can be seen that there is a slight increase across the quasistatic regime, similar to what is seen in the new data presented here. This suggests that the difference in response between the new data and literature data, seen as strain rate increases from quasistatic to dynamic, is due to the dynamic samples failing before their full potential is reached. This failure to reach full potential may be due in part to the smallness and hence increased difficulty of manufacturing of the new specimens. This would create a situation where more asperities may be introduced into the specimens, as well as any present asperities having a greater effect on the response, leading to premature failure of the specimens. Furthermore, the difference in response could be due to the degradation of the material, as the exact extent of the degradation is unclear in the specimens tested. This could also have been attributed to by the fracturing of the specimens during the higher strain rate testing. During

the higher rate testing, the majority of the specimens were destroyed, leaving only fragments behind. The higher strain rate used provided a more aggressive testing condition than used in quasistatic testing. This would highlight any flaws in the material, and could lead to this earlier failure.

There was appreciably less scatter in the strength data in the quasistatic regime than in the apparent modulus data, especially for the maximum strength. The exceptions were the baboon bone at $10^{-2}s^{-1}$ for both strengths, and at $10^{-1}s^{-1}$ in the maximum strength, and sheep bone at $10^{-3}s^{-1}$ for both strengths and at $10^{-2}s^{-1}$ for the 0.2% offset strength. This, again suggests that strength is less variable than apparent modulus across the species tested.

There is a similar amount of scatter in the higher strain rate regions in both the apparent modulus and the maximum compressive strength. This fairly large amount of scatter at the higher strain rates makes sense, as there was more variability in the testing in that regime, as detailed in Section 5.2.3.

The same trend was seen in all species investigated, wherein the compressive strengths measured increased with each strain rate increment from $10^{-3}s^{-1}$ to $10^{-1}s^{-1}$, then levelled out at the higher strain rate.

Amongst the species tested, there was no relation seen between the position on the circumference of the bone and the strength measured (see Appendix A). There was also no relationship between density and strength found in any of the tested species (again see Appendix A). The range of densities and positions found in the specimens was small, possibly too small to see the true effect of density differences, as well as there being a very small sample size used.

Chapter 6

Conclusions & Recommendations

6.1 Conclusions

This section contains conclusions on both the equipment modified, and on the behaviours and relationships displayed in the data presented.

The CiT striker worked as intended. The strain rates produced during testing were consistently near constant. The shortening of the tube allowed for greater ease of use when used in conjunction with the tandem nested momentum trapping system, as this meant the inner momentum trap was not required to fit through the reaction mass needed for the CiT.

The adjustments made to the original momentum trapping system, namely the introduction of the tapered threads and stepped interfaces on the collars, worked as intended. The collars did not loosen drastically with every use, and did not require frequent re-tightening. However, due to the scale of the specimens, and the range of strain rates covered in the tests, the momentum trapping system was found to be too large. For correct functioning when testing small specimens at intermediate

rates, alterations to reduce the mass of the system are required.

There were distinct ageing effects noticeable in the specimens tested. There was a clear decrease in the apparent modulus measured between the first and second series of tests. There was a difference seen in all species tested, but the difference was not consistent between species. Baboon bone, which had been stored for the longest period of time prior to the first series of tests, showed the smallest decrease in apparent modulus. It is theorised that there is some amount of degradation occurring in the bones while stored whole, and as the baboon bone was stored whole for the longest period of time, initial degradation in baboon bone may have occurred before the first series of tests was run, unlike the bones tested from other species. This may explain why there was less decrease seen in the apparent modulus of baboon bone than in other species. There was less difference in the compressive strength measured between the first and second series of tests than was seen in the apparent modulus for all species except baboon. The compressive strengths remained constant or showed an increase in the second series of testing. Once again, this difference was not consistent across all species. The baboon bone showed the largest change, with a markedly higher increase across all three quasistatic rates than the other species tested.

When considering the apparent modulus, there was a clear separation between the species tested. In the second series of testing, the order of most stiff to least stiff response was consistent across all strain rates tested, namely baboon showing the stiffest behaviour, followed by ostrich, then sheep, and finally crocodile showing the most compliant behaviour. In the first series of testing, this order was slightly different, with baboon bone showing a stiffness lower than ostrich bone, comparable to sheep bone. This is again theorised to be due to pre-existing degradation in the baboon bone, as discussed in the previous paragraph. The trend of ostrich bone being stiffer than sheep bone, and sheep bone being stiffer than crocodile bone was consistent across both series of testing. The observed degradation effect suggests that the relations between baboon bone and the other species is more accurately portrayed in the second series of testing.

When considering the compressive strength, there was again a separation between the species tested. The highest strength was consistently shown by baboon bone in both the first and second series of testing. The lowest strength was seen in crocodile bone, and more clearly in the 0.2% offset yield strength than the maximum strength. The sheep and ostrich bone were fairly similar in strength response, with ostrich showing the highest strength (both 0.2% offset and maximum) at strain rates of $10^{-3}s^{-1}$ in both test series, and at $10^{-2}s^{-1}$ in the second series of tests. In the case of the maximum strength at a rate of $10^{-1}s^{-1}$ in the first series of tests, the crocodile, sheep and ostrich bone showed an equal strength. The sheep bone showed the highest strength at the remaining strain rates.

Looking at the relationship between properties and strain rate (using solely the second series of tests), strain rate dependence can be clearly seen. In the case of the apparent modulus, there are minor differences within the quasistatic range, but a clear, distinct increase when moving from the quasistatic to high intermediate strain rate regimes. This is seen across all species, and agrees with the findings in literature. When compressive strengths are considered, a small, consistent increase in strength can be seen as strain rate increases in the quasistatic regime. This is followed by no increase, or even a minor decrease at the high intermediate range. Greater apparent moduli were seen at these higher strain rates, which implies that the strain at failure decreased with the increase in strain rate. These unexpectedly low strength values may hence be a consequence of the aggressive testing methods used for the higher strain rate testing. This relationship was seen across all species tested, for both 0.2% offset yield strength and maximum compressive strength. These results do not agree with previous findings. However, previous findings were based on larger specimens, which may be less susceptible to early failure. Further research on the compressive strengths seen at the high intermediate strain rate would be valuable.

6.2 Recommendations

There are four main recommendations for future research of this nature.

The results of this work show distinct differences between the ultimate values of material responses between species. Histological analysis was beyond the scope of this research, but if performed in future research, it may yield some interesting and useful information. With accurate information on the microstructure present in the specimens, conclusions about the effects of those microstructures may be able to be drawn. This may be especially useful in the case of comparing species which may have a large amount of overlap in possible microstructures seen, such as when there is expected to be a base of fibrolamellar bone with varying amounts of osteons present. The different bone microstructures across species (as discussed in the literature review) may result in different porosities, but this would require a close examination, and possibly histological examination to determine, hence the recommendation therefore. As to whether the mechanical properties etc. would be the same for the raw material across species, the different microstructures of bone may result in differing levels of mineral content and hence differing properties, but the current research suggests it may be more similar than expected. Furthermore, it may be valuable for such histological analysis to be performed on the specimens used in this research, which have been preserved for future analysis. Investigation into the exact progress of remodelling of bone across species was also considered outside the scope of this dissertation, but may be looked at in future research.

The scale of the momentum trapping system must be reduced for use with small specimens and stress waves. The length of the trapping system is based on the length of the incident bar in use, which is required to be long to provide the correct test duration. To reduce the momentum of the trapping system, the diameters used for both the incident bar and the trapping system itself require reduction. Further consideration of the outer collar stepping is also required, to prevent the damaged experienced in the initial trials. Either more precise alignment of the inner and outer traps is required from the beginning of testing, or the outer collar must be made of

a stronger material. Titanium, such as was used for the inner collar, is one such material option.

Further studies should be performed on the effects of time between animal death, bone collection, and testing. Clear ageing effects were seen in this research, but the precise extent is currently unclear. As this has a distinct impact on the measurement of mechanical properties, it would be valuable to gain a better understanding of what is actually occurring in these specimens, and where along the process the changes in material response are occurring. Also of interest would be the performance of high intermediate strain rate testing on very fresh specimens, to observe how it compares with the data presented.

Lastly, it is recommended that the time between the collection of the bones, the cutting of the specimens, and the actual testing be reduced to a minimum when not performing studies on degradation with specimen ageing. This should reduce any deterioration of the specimens to a minimum. It is recommended that any testing apparatus to be used should be designed, built and calibrated before bone collection if possible. If this cannot be done practically, alternate storage mediums should be considered for the whole bones, and possibly for the cut specimens as well.

Bibliography

[1] "File 603 anatomy of a long bone.jpg." *https* : *//upload.wikimedia.org/wikipedia/commons/c/ca/*603*_Anatomy_of_a_Long_Bone.jpg*. Last Accessed: 04-02-2018.

[2] "The fibrolamellar smoking gun." http://reptilis.net/2007/07/04/the-fibrolamellar-smoking-gun/. Last Accessed: 05-10-2017.

[3] C. Crowder and S. Stout, *Bone histology: an anthropological perspective*. CRC Press, 2011. pg. 118.

[4] "Haversian diagram." http://www.umich.edu/ bme332/ch9bone/plywood1.jpg. Last Accessed: 05-10-2017.

[5] D. Brits, M. Steyn, E. Noelle, *et al.*, "A histomorphological analysis of human and non-human femora," *International journal of legal medicine*, vol. 128, no. 2, pp. 369–377, 2014.

[6] A. R. Tumarkin-Deratzian, "Fibrolamellar bone in wild adult alligator mississippiensis," *Journal of Herpetology*, vol. 41, no. 2, pp. 341–345, 2007.

[7] J. Castanet, K. C. Rogers, J. Cubo, and J. Jacques-Boisard, "Periosteal bone growth rates in extant ratites (ostriche and emu) implications for assessing growth in dinosaurs," *Comptes Rendus de l'Académie des sciences-Series III-Sciences de la Vie*, vol. 323, no. 6, pp. 543–550, 2000.

[8] A. A. Abdel-Wahab, K. Alam, and V. V. Silberschmidt, "Analysis of anisotropic viscoelastoplastic properties of cortical bone tissues," *Journal of the mechanical behavior of biomedical materials*, vol. 4, no. 5, pp. 807–820, 2011.

[9] "Anatomical position digram." https://www.imaios.com/en/e-Anatomy/Limbs/Planes-and-motions-diagrams. Last Accessed: 30/10/2017.

[10] T. Johnson, S. Socrate, and M. Boyce, "A viscoelastic, viscoplastic model of cortical bone valid at low and high strain rates," *Acta biomaterialia*, vol. 6, no. 10, pp. 4073–4080, 2010.

[11] T. Cloete, A. Van Der Westhuizen, S. Kok, and G. Nurick, "A tapered striker pulse shaping technique for uniform strain rate dynamic compression of bovine bone," *EDP Sciences*, vol. 1, pp. 901–907, 2009.

[12] G. Paul, "The strain rate dependent properties of bovine cortical bone," Master's thesis, University of Cape Town, 2014.

[13] M. Prot and T. J. Cloete, "A tandem momentum trap for dynamic specimen recovery during split hopkinson pressure bar testing of cancellous bone," *Journal of Dynamic Behavior of Materials*, vol. 2, no. 1, pp. 50–58, 2016.

[14] S. L. Hui, C. W. Slemenda, and C. C. Johnston Jr, "Age and bone mass as predictors of fracture in a prospective study.," *Journal of Clinical Investigation*, vol. 81, no. 6, pp. 1804–1809, 1988.

[15] Z. Wu, T. C. Ovaert, and G. L. Niebur, "Viscoelastic properties of human cortical bone tissue depend on gender and elastic modulus," *Journal of Orthopaedic Research*, vol. 30, no. 5, pp. 693–699, 2012.

[16] J. D. Currey, "Tensile yield in compact bone is determined by strain, post-yield behaviour by mineral content," *Journal of Biomechanics*, vol. 37, no. 4, pp. 549–556, 2004.

[17] J. D. Currey, "The effects of strain rate, reconstruction and mineral content on some mechanical properties of bovine bone," *Journal of Biomechanics*, vol. 8, no. 1, pp. 81–86, 1975.

[18] E. Novitskaya, P.-Y. Chen, S. Lee, A. Castro-Ceseña, G. Hirata, V. A. Lubarda, and J. McKittrick, "Anisotropy in the compressive mechanical properties of bovine cortical bone and the mineral and protein constituents," *Acta Biomaterialia*, vol. 7, no. 8, pp. 3170–3177, 2011.

[19] B. Sanborn, C. Gunnarsson, M. Foster, P. Moy, and T. Weerasooriya, "Effect of loading rate and orientation on the compressive response of human cortical bone," tech. rep., DTIC Document, 2014.

[20] K. S. Davison, K. Siminoski, J. Adachi, D. A. Hanley, D. Goltzman, A. B. Hodsman, R. Josse, S. Kaiser, W. P. Olszynski, A. Papaioannou, *et al.*, "Bone strength: the whole is greater than the sum of its parts," in *Seminars in arthritis and rheumatism*, vol. 36, pp. 22–31, Elsevier, 2006.

[21] J. D. Currey, "The many adaptations of bone," *Journal of Biomechanics*, vol. 36, no. 10, pp. 1487–1495, 2003.

[22] B. Kaye, C. Randall, D. Walsh, and P. Hansma, "The effects of freezing on the mechanical properties of bone," *The Open Bone Journal*, vol. 4, no. 1, 2012.

[23] E. H. van Haaren, B. C. van der Zwaard, A. J. van der Veen, I. C. Heyligers, P. I. Wuisman, and T. H. Smit, "Effect of long-term preservation on the mechanical properties of cortical bone in goats," *Acta orthopaedica*, vol. 79, no. 5, pp. 708–716, 2008.

[24] U. Stefan, B. Michael, and S. Werner, "Effects of three different preservation methods on the mechanical properties of human and bovine cortical bone," *Bone*, vol. 47, no. 6, pp. 1048–1053, 2010.

[25] H.-C. Spatz, E. O'Leary, and J. F. Vincent, "Young's moduli and shear moduli in cortical bone," *Proceedings of the Royal Society of London B: Biological Sciences*, vol. 263, no. 1368, pp. 287–294, 1996.

[26] K. L. Reed and T. D. Brown, "Elastic modulus and strength of emu cortical bone," *The Iowa orthopaedic journal*, vol. 21, pp. 53–57, 2001.

[27] Q. Wang, D. S. Strait, and P. C. Dechow, "A comparison of cortical elastic properties in the craniofacial skeletons of three primate species and its relevance to the study of human evolution," *Journal of Human Evolution*, vol. 51, no. 4, pp. 375–382, 2006.

[28] U. Zapata, K. Metzger, Q. Wang, R. M. Elsey, C. F. Ross, and P. C. Dechow, "Material properties of mandibular cortical bone in the american alligator, alligator mississippiensis," *Bone*, vol. 46, no. 3, pp. 860–867, 2010.

[29] A. R. Cuff, J. A. Bright, and E. J. Rayfield, "Validation experiments on finite element models of an ostrich (struthio camelus) cranium," *PeerJ*, vol. 3, p. e1294, 2015.

[30] R. Crowninshield and M. Pope, "The response of compact bone in tension at various strain rates," *Annals of Biomedical Engineering*, vol. 2, no. 2, pp. 217–225, 1974.

[31] R. R. Adharapurapu, F. Jiang, and K. S. Vecchio, "Dynamic fracture of bovine bone," *Materials Science and Engineering: C*, vol. 26, no. 8, pp. 1325–1332, 2006.

[32] A. van der Westhuizen, *The strain rate dependent properties and modelling of bovine cortical bone in compression*. PhD thesis, University of Cape Town, 2008.

[33] T. J. Cloete, G. Paul, and E. B. Ismail, "Hopkinson bar techniques for the intermediate strain rate testing of bovine cortical bone," *Philosophical Transactions of the Royal Society of London A: Mathematical, Physical and Engineering Sciences*, vol. 372, no. 2015, 2014.

[34] B. Clarke, "Normal bone anatomy and physiology," *Clinical journal of the American Society of Nephrology*, vol. 3, no. Supplement 3, pp. S131–S139, 2008.

[35] K. Padian and E.-T. Lamm, *Bone histology of fossil tetrapods: advancing methods, analysis, and interpretation*. Univ of California Press, 2013.

[36] "Bone structure." https://opentextbc.ca/anatomyandphysiology/chapter/6-3-bone-structure/. Last Accessed: 08-02-2018.

[37] "Bone formation and development." https://opentextbc.ca/anatomyandphysiology/chapter/6-4-bone-formation-and-development/. Last Accessed: 08-02-2018.

[38] M. L. Bouxsein, "Bone quality: where do we go from here?," *Osteoporosis international*, vol. 14, no. 5, pp. 118–127, 2003.

[39] S. Weiner, W. Traub, and H. D. Wagner, "Lamellar bone: structure–function relations," *Journal of structural biology*, vol. 126, no. 3, pp. 241–255, 1999.

[40] T. Wright and W. Hayes, "Tensile testing of bone over a wide range of strain rates: effects of strain rate, microstructure and density," *Medical and biological engineering*, vol. 14, no. 6, pp. 671–680, 1976.

[41] J. L. Katz, H. S. Yoon, S. Lipson, R. Maharidge, A. Meunier, and P. Christel, "The effects of remodeling on the elastic properties of bone," *Calcified Tissue International*, vol. 36, no. 1, pp. S31–S36, 1984.

[42] M. Martiniaková, B. Grosskopf, R. Omelka, K. Dammers, M. Vondrkov, and M. Bauerov, "Histological study of compact bone tissue in some mammals: a method for species determination," *International Journal of Osteoarchaeology*, vol. 17, no. 1, pp. 82–90, 2007.

[43] D. H. Enlow, *An Evaluation of the Use of Bone Histology in Forensic Medicine and Anthropology*, pp. 93–112. Berlin, Heidelberg: Springer Berlin Heidelberg, 1966.

[44] S. Gourion-Arsiquaud, J. C. Burket, L. M. Havill, E. DiCarlo, S. B. Doty, R. Mendelsohn, M. C. van der Meulen, and A. L. Boskey, "Spatial variation in osteonal bone properties relative to tissue and animal age," *Journal of Bone and Mineral Research*, vol. 24, no. 7, pp. 1271–1281, 2009.

[45] P. Augat and S. Schorlemmer, "The role of cortical bone and its microstructure in bone strength," *Age and ageing*, vol. 35, no. suppl 2, pp. ii27–ii31, 2006.

[46] E. N. Ebbesen, J. S. Thomsen, H. Beck-Nielsen, H. J. Nepper-Rasmussen, and L. Mosekilde, "Age-and gender-related differences in vertebral bone mass, density, and strength," *Journal of Bone and Mineral Research*, vol. 14, no. 8, pp. 1394–1403, 1999.

[47] R. B. Martin and P. J. Atkinson, "Age and sex-related changes in the structure and strength of the human femoral shaft," *Journal of Biomechanics*, vol. 10, no. 4, pp. 223–231, 1977.

[48] J. D. Currey, K. Brear, and P. Zioupos, "The effects of ageing and changes in mineral content in degrading the toughness of human femora," *Journal of biomechanics*, vol. 29, no. 2, pp. 257–260, 1996.

[49] D. Carter and W. C. Hayes, "Compact bone fatigue damage i residual strength and stiffness," *Journal of Biomechanics*, vol. 10, no. 5, pp. 325–337, 1977.

[50] J.-P. Berteau, C. Baron, M. Pithioux, F. Launay, P. Chabrand, and P. Lasaygues, "In vitro ultrasonic and mechanic characterization of the modulus of elasticity of children cortical bone," *Ultrasonics*, vol. 54, no. 5, pp. 1270–1276, 2014.

[51] T. Crenshaw, E. Peo, A. Lewis, B. Moser, and D. Olson, "Influence of age, sex and calcium and phosphorus levels on the mechanical properties of various bones in swine," *Journal of Animal Science*, vol. 52, no. 6, pp. 1319–1329, 1981.

[52] J. Currey, "Comparative mechanical properties and histology of bone," *American Zoologist*, vol. 24, no. 1, pp. 5–12, 1984.

[53] P. Lucksanasombool, W. Higgs, R. Higgs, and M. Swain, "Fracture toughness of bovine bone: influence of orientation and storage media," *Biomaterials*, vol. 22, no. 23, pp. 3127–3132, 2001.

[54] D. T. Reilly and A. H. Burstein, "The elastic and ultimate properties of compact bone tissue," *Journal of biomechanics*, vol. 8, no. 6, pp. 393–405, 1975.

[55] R. Allena and C. Cluzel, "Identification of anisotropic tensile strength of cortical bone using brazilian test," *Journal of the mechanical behavior of biomedical materials*, vol. 38, pp. 134–142, 2014.

[56] B. An, Y. Liu, D. Arola, and D. Zhang, "Fracture toughening mechanism of cortical bone: An experimental and numerical approach," *Journal of the mechanical behavior of biomedical materials*, vol. 4, no. 7, pp. 983–992, 2011.

[57] Q. Grimal, S. Haupert, D. Mitton, L. Vastel, and P. Laugier, "Assessment of cortical bone elasticity and strength: mechanical testing and ultrasound provide complementary data," *Medical engineering & physics*, vol. 31, no. 9, pp. 1140–1147, 2009.

[58] F. G. Evans and M. Lebow, "Regional differences in some of the physical properties of the human femur," *Journal of applied physiology*, vol. 3, no. 9, pp. 563–572, 1951.

[59] V. Ebacher, C. Tang, H. McKay, T. R. Oxland, P. Guy, and R. Wang, "Strain redistribution and cracking behavior of human bone during bending," *Bone*, vol. 40, no. 5, pp. 1265–1275, 2007.

[60] M. M. Barak, J. D. Currey, S. Weiner, and R. Shahar, "Are tensile and compressive youngs moduli of compact bone different?," *Journal of the mechanical behavior of biomedical materials*, vol. 2, no. 1, pp. 51–60, 2009.

[61] D. B. Burr, M. B. Schaffler, and R. G. Frederickson, "Composition of the cement line and its possible mechanical role as a local interface in human compact bone," *Journal of Biomechanics*, vol. 21, no. 11, pp. 939–945, 1988.

[62] J. D. Currey, "The effect of porosity and mineral content on the young's modulus of elasticity of compact bone," *Journal of Biomechanics*, vol. 21, no. 2, pp. 131–139, 1988.

[63] J. C. Goh, E. J. Ang, and K. Bose, "Effect of preservation medium on the mechanical properties of cat bones," *Acta Orthopaedica Scandinavica*, vol. 60, no. 4, pp. 465–467, 1989.

[64] C. Öhman, E. DallAra, M. Baleani, S. V. S. Jan, and M. Viceconti, "The effects of embalming using a 4% formalin solution on the compressive mechanical properties of human cortical bone," *Clinical biomechanics*, vol. 23, no. 10, pp. 1294–1298, 2008.

[65] J. Moreno and F. Forriol, "Effects of preservation on the mechanical strength and chemical composition of cortical bone: an experimental study in sheep femora," *Biomaterials*, vol. 23, no. 12, pp. 2615–2619, 2002.

[66] D. Hasson and R. Armstrong, "A ductile-to-brittle transition in bone?," *Journal of Materials Science*, vol. 9, no. 7, pp. 1165–1170, 1974.

[67] E. D. Sedlin and C. Hirsch, "Factors affecting the determination of the physical properties of femoral cortical bone," *Acta Orthopaedica Scandinavica*, vol. 37, no. 1, pp. 29–48, 1966.

[68] J. Smith and R. Walmsley, "Factors affecting the elasticity of bone," *Journal of anatomy*, vol. 93, no. Pt 4, pp. 503–523, 1959.

[69] A. A. Abdel-Wahab, A. R. Maligno, and V. V. Silberschmidt, "Micro-scale modelling of bovine cortical bone fracture: Analysis of crack propagation and microstructure using x-fem," *Computational Materials Science*, vol. 52, no. 1, pp. 128–135, 2012.

[70] V. Ebacher, P. Guy, T. R. Oxland, and R. Wang, "Sub-lamellar microcracking and roles of canaliculi in human cortical bone," *Acta biomaterialia*, vol. 8, no. 3, pp. 1093–1100, 2012.

[71] D. R. Carter and W. C. Hayes, "Bone compressive strength: the influence of density and strain rate," *Science*, vol. 194, no. 1, pp. 174–1176, 1976.

[72] G. Evans, J. Behiri, L. Vaughan, and W. Bonfield, "The response of equine cortical bone to loading at strain rates experienced in vivo by the galloping horse," *Equine Veterinary Journal*, vol. 24, no. 2, pp. 125–128, 1992.

[73] J. McElhaney and E. F. Byars, "Dynamic response of biological materials," ASME, 1965.

[74] R. M. Kulin, F. Jiang, and K. S. Vecchio, "Effects of age and loading rate on equine cortical bone failure," *Journal of the Mechanical Behavior of Biomedical Materials*, vol. 4, no. 1, pp. 57–75, 2011.

[75] P. C. Dechow and W. L. Hylander, "Elastic properties and masticatory bone stress in the macaque mandible," *American journal of physical anthropology*, vol. 112, no. 4, pp. 553–574, 2000.

[76] H. Yamada and F. G. Evans, *Strength of biological materials*. Williams & Wilkins, 1970.

[77] A. Casinos and J. Cubo, "Avian long bones, flight and bipedalism," *Comparative Biochemistry and Physiology Part A: Molecular & Integrative Physiology*, vol. 131, no. 1, pp. 159–167, 2001.

[78] M. F. Spotts, *Impact*, ch. 18. Prentice-Hall, 1964.

[79] G. T. Gray, H. Kuhn, and D. Medlin, "Classic split-hopkinson pressure bar technique," *ASM Handbook. Volume 8: Mechanical Testing and Evaluation, ASM International, Materials Park, OH 44073*, pp. 462–476, 2000.

[80] R. J. Aristizabal, "Estimating the parameters of the three-parameter lognormal distribution," *FIU Electronic Theses and Dissertations*, vol. 575, 2012.

Appendix A

All measured data

Displayed here is the data collected for each specimen used, namely the apparent modulus, the 0.2% offset yield strength and the maximum compressive strength. For the second series of specimens, the density, and the position from which the specimen was taken were also noted.

First, the data pertaining to the first series of tests is presented, followed by the data pertaining to the second series of tests.

Specimen	Strain rate (per second)	Apparent modulus (GPa)	0.2% Offset yield strength (MPa)	Maximum compressive strength (MPa)
Ba7	0.001	14.00	199.0	199.0
Ba16	0.001	11.78	141.1	155.2
Ba23	0.001	14.71	160.4	160.4
Ba44	0.001	12.08	162.2	162.7
Ba51	0.001	13.69	171.3	171.3
Ba5	0.01	12.83	209.1	211.6
Ba19	0.01	12.45	204.6	204.9
Ba35	0.01	13.92	219.5	222.4
Ba46	0.01	13.73	210.7	211.6
Ba50	0.01	10.25	205.3	207.5
Ba8	0.1	13.32	233.3	244.2
Ba10	0.1	12.70	228.4	238.7
Ba20	0.1	13.62	222.9	236.9
Ba34	0.1	15.51	237.5	254.3
Ba48	0.1	14.44	237.6	254.5

Figure A.1: The baboon bone data pertaining to the first series of tests.

Specimen	Strain rate (per second)	Apparent modulus (GPa)	0.2% Offset yield strength (MPa)	Maximum compressive strength (MPa)
Cr2	0.001	11.34	148.5	154.2
Cr9	0.001	10.03	126.8	130.8
Cr25	0.001	10.16	135.2	139.8
Cr35	0.001	6.19	105.3	119.3
Cr46	0.001	9.03	125.1	134.5
Cr1	0.01	9.69	159.4	168.9
Cr11	0.01	9.39	142.6	152.7
Cr22	0.01	10.48	151.1	160.5
Cr34	0.01	8.96	150	162.2
Cr47	0.01	9.52	156.5	165.5
Cr3	0.1	11.48	188.7	199.3
Cr17	0.1	11.42	168	180.8
Cr26	0.1	10.97	160.1	183.5
Cr33	0.1	7.42	114.8	135.9
Cr41	0.1	8.80	168.4	188.4

Figure A.2: The crocodile bone data pertaining to the first series of tests.

Specimen	Strain rate (per second)	Apparent modulus (GPa)	0.2% Offset yield strength (MPa)	Maximum compressive strength (MPa)
La1	0.001	12.58	149.3	149.3
La6	0.001	10.82	140.6	140.6
La23	0.001	11.17	141.4	141.4
La30	0.001	14.04	158.2	158.2
La50	0.001	12.40	147.5	147.5
La3	0.01	12.55	179.9	179.9
La12	0.01	7.95	149.6	150.3
La26	0.01	11.91	148.7	148.7
La31	0.01	13.82	185.4	185.4
La45	0.01	13.67	189.4	189.4
La5	0.1	6.33	133.5	147.5
La18	0.1	13.62	207.8	207.8
La24	0.1	13.71	185.7	185.8
La40	0.1	14.13	200.7	201.0
La49	0.1	9.38	166.3	167.7

Figure A.3: The sheep bone data pertaining to the first series of tests.

Specimen	Strain rate (per second)	Apparent modulus (GPa)	0.2% Offset yield strength (MPa)	Maximum compressive strength (MPa)
Os4	0.001	17.65	171.8	171.8
Os17	0.001	15.98	152.9	152.9
Os27	0.001	16.24	152.6	152.6
Os36	0.001	14.33	147.3	149.1
Os41	0.001	17.34	150.3	152.1
Os2	0.01	18.37	180.5	183.2
Os13	0.01	13.99	165.4	168.2
Os28	0.01	15.48	151.1	151.2
Os37	0.01	16.58	165.3	169.4
Os42	0.01	15.01	167.9	171.0
Os3	0.1	20.23	190.7	199.2
Os16	0.1	17.31	177.5	182.0
Os26	0.1	18.75	181.9	187.6
Os39	0.1	19.32	188.2	194.6
Os48	0.1	17.74	198	201.5

Figure A.4: The ostrich bone data pertaining to the first series of tests.

Specimen	Strain rate (per second)	Apparent modulus (GPa)	0.2% Offset yield strength (MPa)	Maximum compressive strength (MPa)	Density (g/cm^3)	Area of bone from which sample taken
Ba98	181.57	14.47	217.4	248.2	2.08207	Anterior
Ba110	106.17	15.31	227.8	250.1	2.08100	Anterior
Ba97	146.72	14.59	225.2	250.9	2.06244	Anterior
Ba114	137.77	15.65	253.3	274.8	2.18121	Anterior
Ba113	116.29	14.70	239.4	279.7	2.20817	Anterior
Ba108	0.1	12.22	267.5	274.7	2.10798	Anterior
Ba102	0.1	12.19	268.1	283.5	2.13400	Anterior
Ba115	0.1	11.77	241.5	241.5	2.08932	Anterior
Ba99	0.01	11.63	235.1	236.9	2.05755	Anterior
Ba117	0.01	11.37	206.7	207.6	2.08477	Anterior
Ba122	0.01	10.84	253.5	253.5	2.13195	Anterior
Ba123	0.001	12.52	236.5	236.5	2.10423	Anterior
Ba104	0.001	11.27	228.3	228.3	2.12397	Anterior
Ba100	0.001	12.66	235.4	235.4	2.10365	Anterior

Figure A.5: The baboon bone data pertaining to the second series of tests.

Specimen	Strain rate (per second)	Apparent modulus (GPa)	0.2% Offset yield strength (MPa)	Maximum compressive strength (MPa)	Density (g/cm^3)	Area of bone from which sample taken
Cr95	159.77	8.42	134.7	164.7	2.03167	Anterior
Cr68	114.18	10.24	160.1	172.7	1.97805	Posterior
Cr87	64.48	7.49	143.2	155.4	1.95811	Anterior
Cr96	221.68	9.78	146	172.8	1.99396	Anterior
Cr97	246.72	7.71	154.9	166.6	1.93645	Anterior
Cr88	296.87	8.75	142.8	160.5	1.97339	Anterior
Cr61	189.72	8.55	112.4	131.9	1.94336	Posterior
Cr63	217.37	4.87	97.2	108.6	1.91695	Posterior
Cr80	0.1	6.22	164	177.3	1.98759	Anterior
Cr81	0.1	5.51	160.5	175.5	2.07256	Anterior
Cr76	0.1	5.85	171.7	186.7	1.97172	Posterior
Cr72	0.01	5.09	142.6	157.5	1.91492	Posterior
Cr73	0.01	6.47	152.8	170.1	1.99572	Posterior
Cr91	0.01	4.56	163.9	173.4	1.98869	Anterior
Cr99	0.001	5.05	144.6	156.1	1.91987	Anterior
Cr85	0.001	5.03	141.8	151.2	1.93763	Anterior
Cr78	0.001	6.71	155.9	160.6	1.96531	Posterior

Figure A.6: The crocodile bone data pertaining to the second series of tests.

Specimen	Strain rate (per second)	Apparent modulus (GPa)	0.2% Offset yield strength (MPa)	Maximum compressive strength (MPa)	Density (g/cm^3)	Area of bone from which sample taken
La113	146.35	9.95	154.5	164.0	1.93092	Posterior
La71	120.05	11.75	206.1	209.4	2.03862	Anterior
La73	105.36	13.60	213.4	225.3	2.02765	Anterior
La88	157.91	13.60	209.9	212.8	2.02783	Anterior
La101	121.06	10.55	131.7	138.0	1.89431	Anterior
La83	0.1	9.17	189.5	189.5	2.06034	Anterior
La70	0.1	7.97	206.0	206.0	2.04001	Anterior
La67	0.1	8.99	210.3	210.3	2.03844	Anterior
La72	0.01	11.15	202.7	202.7	2.04202	Anterior
La97	0.01	8.30	156.2	163.6	1.97062	Anterior
La98	0.01	6.25	166.6	172.4	1.96801	Anterior
La103	0.001	4.74	111.3	119.0	1.89686	Anterior
La99	0.001	6.70	144.1	145.3	2.02082	Anterior
La82	0.001	8.13	170.6	170.6	2.05085	Anterior

Figure A.7: The sheep bone data pertaining to the second series of tests.

Specimen	Strain rate (per second)	Apparent modulus (GPa)	0.2% Offset yield strength (MPa)	Maximum compressive strength (MPa)	Density (g/cm^3)	Area of bone from which sample taken
Os89	72.90	12.74	148.0	166.2	1.98420	Anterior
Os93	73.64	17.10	187.7	194.8	2.02616	Anterior
Os72	62.31	13.90	164.9	182.4	1.99734	Anterior
Os104	87.24	12.84	193.7	215.4	2.03480	Anterior
Os81	45.32	11.94	141.6	141.6	2.01908	Anterior
Os73	0.1	9.89	188.6	203.5	1.98526	Anterior
Os65	0.1	10.27	192.1	207.5	1.97031	Anterior
Os119	0.1	10.06	185.6	196.4	2.03166	Posterior
Os97	0.01	11.08	197.4	198.2	1.99938	Anterior
Os116	0.01	11.56	191.3	191.7	1.98956	Posterior
Os102	0.01	8.96	177.6	179.4	2.04098	Anterior
Os110	0.001	10.25	177.2	177.2	2.02071	Anterior
Os91	0.001	9.13	162.8	162.9	2.02045	Anterior
Os74	0.001	9.38	159.4	160.5	2.11132	Anterior

Figure A.8: The ostrich bone data pertaining to the second series of tests.

Appendix B

Demonstration of the validity of the use of a lognormal distribution for small sample sizes

In the research presented, there were cases in which the mode appeared outside the range of data measured. This is not considered to be an error, but consistent with the properties of lognormal distribution. To illustrate this, displayed here is an example of a randomly generated set of skewed data, which is analysed using the same three-parameter lognormal distribution as in the research. The randomly generated data is then reassessed with an ever decreasing number of data points from the original data set, and compared to the original analysis to show that even with very few data points, a lognormal distribution is more representative of the data than a normal distribution.

First, the entire randomly generated set of skew data (consisting of 500 data points) was assessed using both a normal fit and a lognormal fit, shown in Figure B.1. Clearly, the lognormal fit represents the data much more accurately. The mode was calculated the same way as was done in the research and noted down for comparison with each following analysis. The first twenty data points were taken from the

set, and the analysis was repeated, shown in Figure B.2. As before, the lognormal distribution represents the data better than a normal distribution could. The mode was calculated and compared to the mode calculated with the full set of data, and was found to be only 2.7% different. The same process was followed using only five data points (see Figure B.3) and the difference from the initial mode was found to be only 1.5% different, and still the better representation of the data than a normal analysis. Finally, this analysis was repeated on only three data points (Figure B.4), the mode was found to be only 1.8% different, with the lognormal distribution still showing the more accurate representation of the data than the normal distribution. Consequently, even when using a small sample size, for a skewed data distribution, the lognormal distribution provides a more useful representation of the data than the normal distribution.

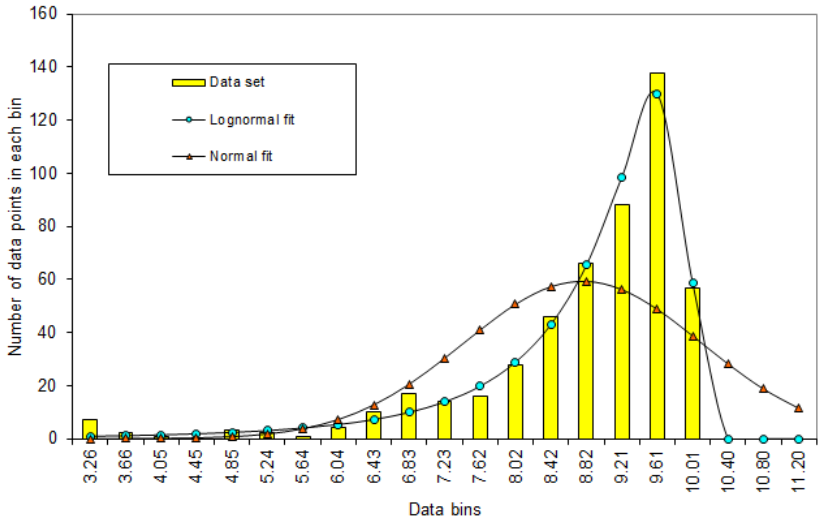

Figure B.1: A graph displaying the full set of randomly generated data, separated into bins, with a normal and lognormal distribution plotted on top of the data.

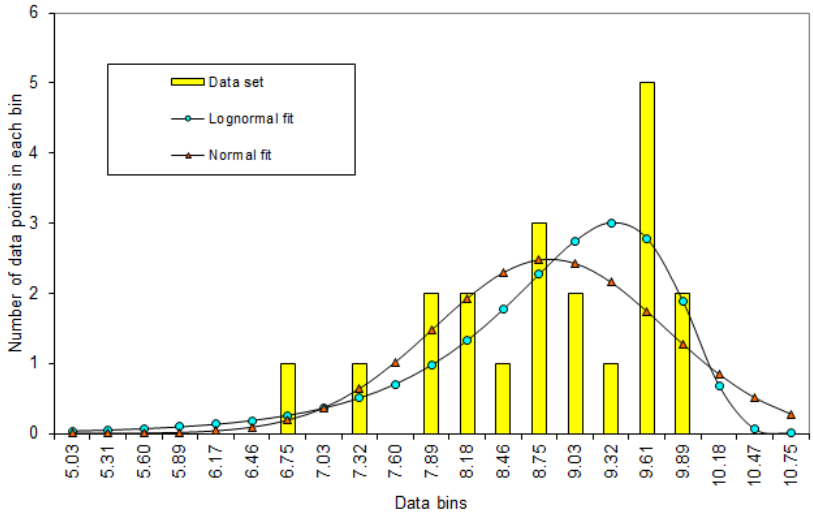

Figure B.2: A graph displaying the first 20 data points from the randomly generated set, separated into bins, with a normal and lognormal distribution plotted on top of the data.

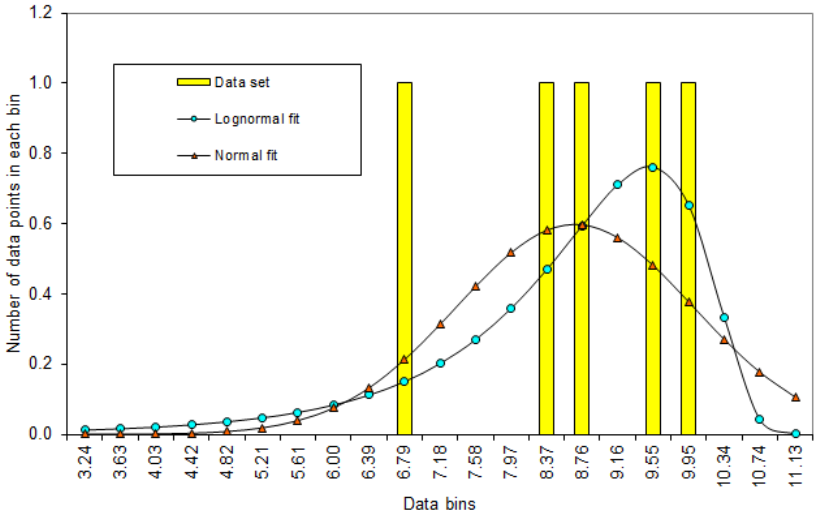

Figure B.3: A graph displaying the first 5 data points from the randomly generated set, separated into bins, with a normal and lognormal distribution plotted on top of the data.

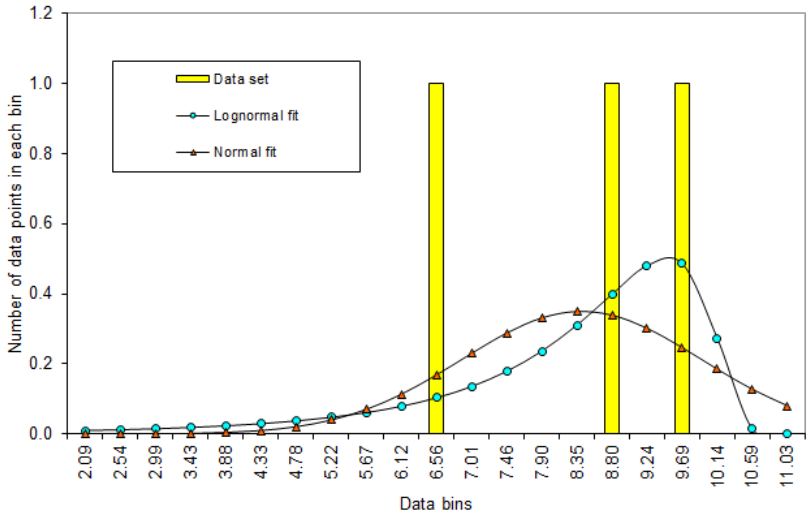

Figure B.4: A graph displaying the first 3 data points from the randomly generated set, separated into bins, with a normal and lognormal distribution plotted on top of the data.